Hydrocarbon Source Potential of Upper Eocene and Oligo-Miocene ("Maykop") Rocks in Georgia

Anindita S. Samsu, BSc

Univ.-Prof. Mag.rer.nat. Dr.mont. Reinhard F. Sachsenhofer

Chair of Petroleum Geology

University of Leoben

A thesis submitted for the degree of

Master of Science

December 2014

Affidavit

I declare in lieu of oath, that I wrote this thesis and performed the associated research myself, using only literature cited in this volume.

Eidesstattliche Erklärung

Ich erkläre an Eides statt, dass ich die vorliegende Masterarbeit selbständig und ohne fremde Hilfe verfasst, andere als die angegebenen Quellen und Hilfsmittel nicht benutzt und die den benutzten Quellen wörtlich und inhaltlich entnommenen Stellen als solche erkenntlich gemacht habe.

Leoben, December 2014

Anindita S. Samsu

Acknowledgments

First and foremost, I would like to thank my supervisor, Reinhard Sachsenhofer, for his invaluable guidance throughout the process of writing this thesis.

Secondly, I would like to extend my gratitude to CanArgo Georgia Ltd. for providing me with the data which made this project possible. I also owe my thanks to Wolfgang Nachtmann for all his support and for seeing this project through. A heartfelt thank you goes to Anna Adamyan for her motivation and for dedicating her time and effort to assist me in all aspects of this project.

I would like to express my gratitude to Stjepan Ćorić for providing me with results of the nannoplankton analysis, which became an integral part of this work.

Special thanks goes to Achim Bechtel and Reinhard Gratzer for sharing with me their knowledge on biomarkers and guiding me through the laboratory work and to Doris Groß for showing me the works and always being ready to lend a helping hand. A big thank you goes to Sabine Feuchter for her patience in helping me with the sample preparation.

A sincere thank you to my colleagues and friends at the Chair of Petroleum Geology for all the support, motivating words, and eagerness to help whenever I needed it. We are all in this together.

Last but not least, I owe a world of thanks to my husband, Joel, and my friends and family, near and far, for being the people I can always count on.

Abstract

The most prolific source rock in the eastern Georgian portion of the Kura Basin occurs within the so-called "Maykop Formation" which is traditionally assigned to the Oligocene–Early Miocene. Most of the existing literature on Maykop shales concentrate on the South Caspian Basin and the Azerbaijani portion of the Kura Basin, while age and stratigraphic data for the Georgian sector is scarce. For this reason, the present study aims to (1) investigate the source potential of the Maykop Formation and the underlying Upper Eocene succession specific to the Near-Tbilisi area and (2) establish a new stratigraphic division for the Upper Eocene to Lower Miocene interval.

For estimation of source potential and determination of depositional environments, drill cuttings samples from three existing wells northeast of Tbilisi (Norio-72, Ninotsminda-97, and Manavi-12) were selected for elemental analysis using the LECO and Eltra methods, Rock-Eval pyrolysis, organic petrology, biomarker analysis, and carbonate isotopy. Age assignment of the samples was carried out with calcareous nannoplankton data provided by S. Ćorić. In addition, biomarker analysis on oil samples from the Ninotsminda field and Manavi-12 well enabled source-oil correlation. 1-D thermal maturation modeling allowed estimation of eroded thickness, paleo-heat flow, and the onset of hydrocarbon generation.

Although most samples were contaminated by oil-based mud, important results could still be obtained. A revised stratigraphy dates samples to Eocene and Oligocene. Bulk geochemical parameters and biomarkers indicate deposition in dysoxic environments. The organic matter input came from a mixed marine and terrestrial source, resulting in type III-II kerogen in Oligocene rocks and type II-III kerogen in Eocene rocks. Relatively low values for vitrinite reflectance and T_{max} show that the studied intervals are immature to marginal mature. Oils from Eocene and Cretaceous reservoirs of the Ninotsminda field and Manavi-12 well form one oil family and were most likely generated from Eocene source rocks. On the other hand, asphaltene-rich oil from the Oligocene reservoir of the Ninotsminda field forms a separate oil family. 1-D thermal models created using data from the Norio-72 and Ninotsminda-97 wells suggest that the two areas experienced different amounts of uplift. The original thickness of the combined Oligocene and Miocene rocks was significantly higher in the Norio area compared to the Ninotsminda area. However, erosion at Norio was minimal (0 to 500 m), while sediments up to 2000 m thick were eroded at Ninotsminda. Due to a relatively low heat flow (approximately 45 mW/m^2), significant hydrocarbon generation

could have occurred only at a maximum burial depth exceeding 5500 m. Time plots of maturity and transformation ratio calibrated against vitrinite reflectance data imply that hydrocarbon generation from the studied interval began in the Late Miocene at Norio and did not occur at all at Ninotsminda.

Results of this study suggest that, following the nomenclature of Peters (1986), the upper part of the Oligocene holds poor hydrocarbon potential, while the lower part holds fair gas and oil potential. The Eocene succession shows very good generative potential for gas and oil.

Kurzfassung

Die sogenannte „Maykop Formation“ gilt als das wichtigste Muttergestein im ostgeorgischen Teil des Kura Beckens und wird in der Literatur dem Oligozän—Untermiozän zugeordnet. Während bereits existierende Studien zu den „Maykop Shales“ den Schwerpunkt auf das Kaspische Becken und den azerbaijanischen Teil des Kura Beckens setzen, sind nur wenige Daten zur Stratigraphie des georgischen Teils vorhanden. Mit der vorliegenden Studie wird das Muttergesteinspotential der Maykop-Formation (Oligozän–Untermiozän) und des Obereozäns untersucht und eine biostratigraphische Unterteilung der Schichtfolge des Obereozäns bis Untermiozäns versucht.

Das Muttergesteinspotential und die Ablagerungsbedingungen der untersuchten Einheiten konnten anhand von Bohrkleinproben aus drei Bohrungen (Norio-72, Ninotsminda-97 und Manavi-12), welche nordöstlich von Tiflis abgeteuft wurden, bestimmt werden. Um dies zu erreichen wurden Elementaranalysen mit den LECO und Eltra Methoden, Rock-Eval Pyrolyse, organische Petrologie, Biomarkeranalyse sowie Karbonatisotopie eingesetzt. Daten von kalkigem Nannoplankton wurden von S. Ćorić zur Verfügung gestellt und dienten der Alterszuordnung der Proben. Des Weiteren wurden Biomarkerdaten benutzt um Öle aus dem Ninotsminda-97 Ölfeld und der Manavi-12 Bohrung mit Muttergesteinen zu korrelieren. Ein eindimensionales thermisches Reifemodell wurde erstellt, um die erodierte Mächtigkeit der Beckensedimente, den Wärmefluss und den Beginn der Kohlenwasserstoffgenerierung abzuschätzen.

Nach der überarbeiteten Stratigraphie wurde den Proben ein Alter von Eozän bis Oligozän zugewiesen. Anhand von geochemischen Parametern und Biomarkern konnte festgestellt werden, dass die Sedimente unter dysoxischen Bedingungen abgelagert wurden. Eine Mischung aus marinen und terrestrischen organischem Material bildete Typ III-II Kerogen in Proben aus dem Oligozän und Typ II-III Kerogen in den Eozänproben. Relativ niedrige Werte für Vitrinitreflexion und T_{max} zeigen, dass die untersuchten Intervalle keine, beziehungsweise geringe Reife aufweisen. Korrelationen mittels Biomarkern weisen darauf hin, dass Öle aus Eozän- sowie Kreide-Speichergesteinen des Ninotsminda Ölfeldes und der Manavi-12 Bohrung der gleichen Ölfamilie zugeordnet werden können und von Eozänmuttergesteinen generiert wurden. Öl aus dem oligozänen Speichergestein des Ninotsminda Feldes, welches einen signifikanten Anteil an Asphaltenen beinhaltet, repräsentiert

eine zweite Ölfamilie. Mithilfe von eindimensionalen thermischen Reifemodellen, für deren Erstellung Daten aus den Norio-72 und Ninotsminda-97 Bohrungen verwendet wurden, konnte die ursprüngliche Mächtigkeit des Oligozäns und des Miozäns abgeschätzt werden. Die zwei Bereiche unterscheiden sich deutlich in deren Hebung. Die erodierte Mächtigkeit bei Norio war minimal (0 bis 500 m). Hingegen wurden bei Ninotsminda bis zu 2000 m mächtige Sedimente abgetragen. Aufgrund des geringen regionalen Wärmeflusses (circa 45 mW/m^2) erfolgte die Kohlenwasserstoffgenese erst ab einer Versenkungstiefe von 5500 m.

Die Ergebnisse dieser Studie zeigen, dass der obere Teil des Oligozäns nach der Nomenklatur von Peters (1986) ein geringes („poor“) Kohlenwasserstoffpotential aufweist, wobei der untere Teil mittelmäßiges („fair“) Potential für Gas- und Ölgenese vorweisen kann. Gesteine aus dem Eozän hingegen zeigen sehr hohes („very good“) Potential für Gas- und Ölbildung.

Contents

1 Introduction 1

2 Geological Setting 4

2.1 Evolution of the Kura Basin 6

2.2 Stratigraphy 8

2.3 Hydrocarbon Shows and Discoveries 11

3 Samples 14

3.1 Norio-72 15

3.2 Ninotsminda-97 17

3.3 Manavi-12 17

3.4 Oil Samples 18

3.5 Drilling Mud 18

4 Methods 20

4.1 Sample Preparation 20

4.2 Elemental Analysis (TC, TOC, S) 20

4.2.1 LECO 21

4.2.2 Eltra 22

4.3 Rock-Eval Pyrolysis 22

4.4 Vitrinite Reflectance 24

4.5 Semi-Quantitative Maceral Analysis 25

4.6 Calcareous Nannoplankton 26

4.7 Gas Chromatography-Mass Spectroscopy 26

4.8 X-Ray Diffraction Analysis 30

4.9 Isotope Geochemistry of Carbonates 31

4.10 Maturity Modeling 31

5 Results **33**
5.1 Norio-72 . . . 33
5.1.1 Stratigraphy . . . 33
5.1.2 Carbonate Content . . . 35
5.1.3 Bulk Geochemical Parameters and Vitrinite Reflectance . . . 35
5.1.4 Biomarker Proxies . . . 38
5.1.5 Maceral Composition . . . 39
5.2 Ninotsminda-97 . . . 41
5.2.1 Stratigraphy . . . 41
5.2.2 Bulk Geochemical Parameters and Vitrinite Reflectance . . . 42
5.2.3 Biomarker Proxies . . . 43
5.2.4 Maceral Composition . . . 44
5.3 Manavi-12 . . . 44
5.3.1 Stratigraphy . . . 44
5.3.2 Bulk Geochemical Parameters and Vitrinite Reflectance . . . 44
5.3.3 Biomarker Proxies . . . 46
5.3.4 Maceral Composition . . . 46
5.4 Oil Samples . . . 48
5.5 Depositional Environment and Source Input . . . 48
5.6 Maturity Modeling . . . 54

6 Conclusions **61**

Bibliography **63**

List of Figures **I**

List of Tables **III**

List of Appendices **IV**

1. Introduction

The largest oil discoveries in Georgia are located in the Kura Basin, a NW-SE elongated basin within the Transcaucasian intermontane depression. It is bound to the north by the Greater Caucasus Mountains and to the south by the Adjara-Trialeti fold-belt of the Lesser Caucasus Mountains (Fig. 1.1). Organic-rich Oligocene and Lower Miocene rocks known as the "Maykop Shale" are considered to be the main contributing source rocks in the region.

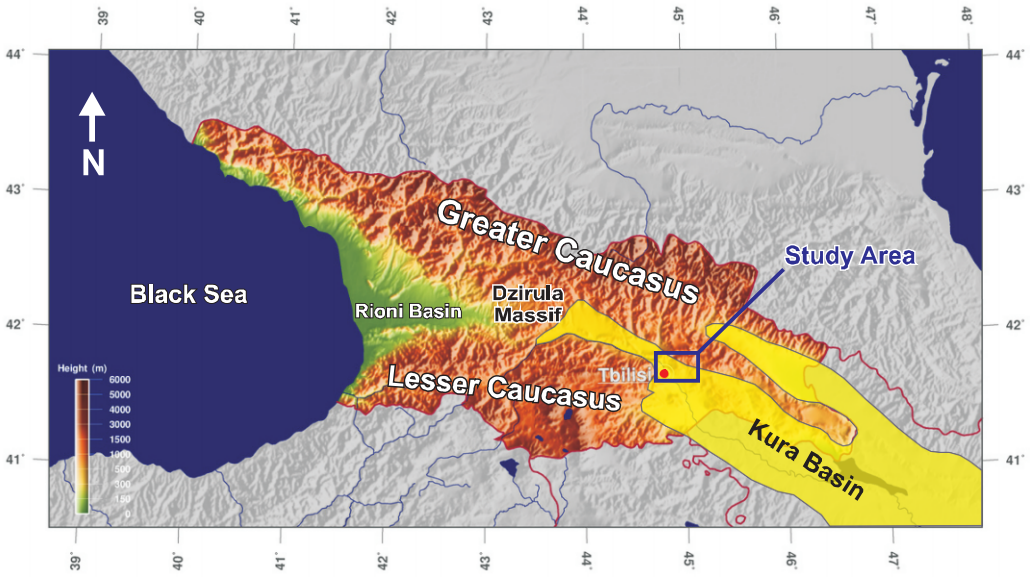

Figure 1.1: Relief map of Georgia (modified from Ginkgo Maps, October 2014). The locations of the Kura Basin and the study area are indicated.

In the Kura and Rioni basins of the Transcaucasian intermontane depression, the term "Maykop" is most often used in describing the Oligocene–Lower Miocene successions (also "Maykopian series" or "Maykop Formation"; Gamkrelidze, 1964; Popov et al., 2004), which consist of alternating gypsiferous clays and sandstones. Outcrops of these sediments appear in the western part of the pre-Caucasus foredeep. This term has also been attributed to a facies type (Popov et al., 2004), which has been characterized by Adamia et al. (2011) as brown, agrillaceous-sandy, gypsiferous, carbonate-poor rocks deposited in the semi-closed

basins of the Paratethys. In the present study, the term "Maykop" is used the traditional way and designated to the sediments belonging to the Oligocene–Lower Miocene interval.

In general, literature on the geology of Georgia is scarce, with much of them dating back to the former USSR period. Several studies on the Maykop Shale of the Eastern Paratethys (Fig. 1.2) have been published, although most of them focus on the South Caspian Basin and the Azerbaijani portion of the Kura depression. The present study aims to characterize the source potential of the Maykop and its underlying Upper Eocene succession occurring in the Near-Tbilisi area of the Kura Basin. In the context of this particular study, there are uncertainties regarding the lower boundary of the Maykop interval, whereby in the wider scope the upper boundary of the succession is also ambiguous. Moreover, the Eocene/Oligocene boundary, marking the beginning of the deposition of organic-rich sediments under stagnant water conditions, is still subject to debate (Popov et al., 1993; Schulz et al., 2002).

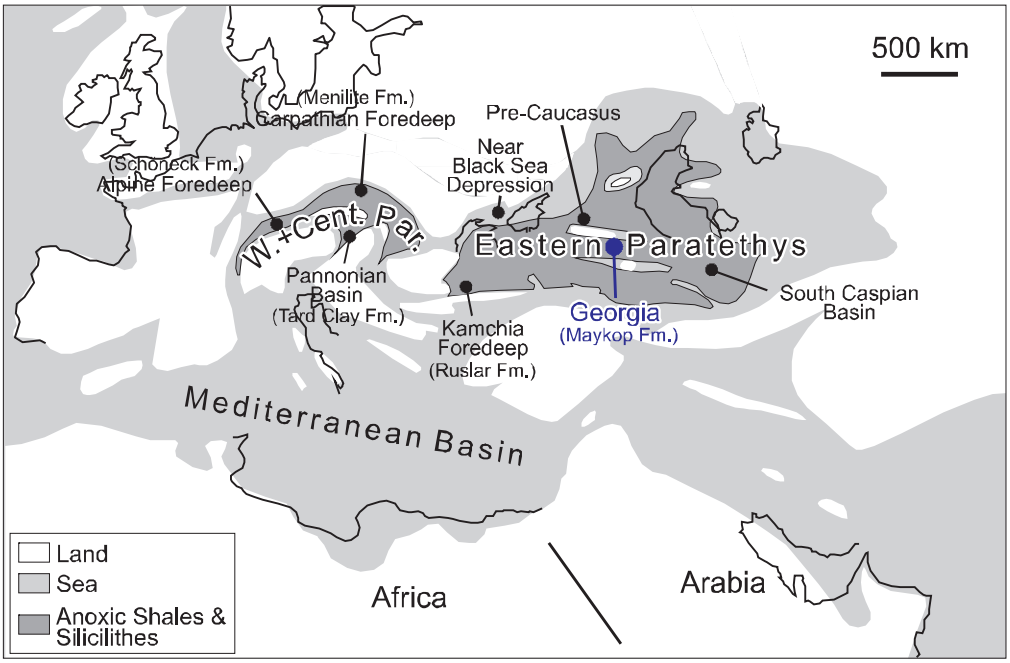

Figure 1.2: Paleogeographic map of the Paratethys at the Eocene/Oligocene transition (simplified from Popov et al., 2004).

Data and samples used in this investigation were provided by CanArgo Georgia Ltd. The wells from which samples were obtained are located east of Tbilisi and penetrate large anticline structures belonging to the Adjara-Trialet fold-belt (see below). Vertical variations in hydrocarbon source potential of the postulated Maykop sediments in the Near-Tbilisi area were investigated (Fig. 1.1). In addition, the Upper Eocene succession was evaluated in order to determine its importance as source rocks in the region. To accomplish these objectives,

221 drill cuttings samples were analyzed with the Eltra or LECO methods for determination of their bulk geochemical parameters as well as with Rock-Eval pyrolysis. In order to identify the Eocene/Oligocene boundary, calcareous nannoplankton analysis enabled age assignment of the samples. Using organic petrology and biomarker data obtained through Gas Chromatography-Mass Spectroscopy (GC-MS), thermal maturity profiles were created to estimate former heat flow scenarios, eroded sediment thicknesses, and the onset of hydrocarbon generation in the Norio and Ninotsminda areas. Biomarkers also enabled oil-source correlation and determination of the depositional environment of the Upper Eocene–Lower Miocene rocks.

During the course of the study, it was discovered that all of the cuttings samples were heavily contaminated by oil-based mud (OBM), making the application of standard organic geochemical techniques and interpretations impossible. Great effort was placed into removing the contaminant from the samples, testing different methods of pre-analysis sample preparation, and applying advanced techniques to recognize and eliminate the effect of contamination in Rock-Eval signals. However, none of the attempts led to complete removal of the contaminant, although important results could still be obtained. Additionally, it became evident that the stratigraphy of the drilled sections had to be revised and that Upper Eocene rocks contain more organic matter than Oligocene rocks.

The next chapter describes the geological setting of the study area. Especially due to the previously mentioned contamination of the analyzed samples, Chapter 3 is dedicated to describing sample conditions and lithology. The analysis methods used in this investigation are explained in Chapter 4, while results are presented in Chapter 5. The Appendices encompass a complete list and photo documentation of the cuttings samples, calcareous nannoplankton, GC-MS chromatograms, vitrinite reflectance and maceral analysis results, carbonate isotopy results, and thermal model input parameters.

2. Geological Setting

Georgia is located within the Caucasus region of the Alpine-Carpathian-Himalayan orogenic belt, where the Eurasian plate is converging with the African-Arabian plate (Adamia, 1991; Adamia et al., 2011). The geological evolution of this area is largely affected by its position within a continent-continent collisional setting. A detailed geological description of the Caucasus is presented in Adamia et al. (2011).

Throughout the Mesozoic, the Caucasus was part of the Tethys Ocean and its bordering Eurasian and Gondwana/African-Apulian-Arabian margins (Adamia et al., 2011). Beginning in the Jurassic, subduction of the Tethyan seafloor led to the development of calc-alkaline arc volcanism (Eppelbaum and Khesin, 2012). As a result, a system of island-arcs and extensional intra-arc and back-arc basins existed in this active margin setting. As part of the Alpine tectonic cycle, narrowing of the Tethys began in the Late Mesozoic, while the syn- and post-collisional intervals starting in the Oligocene were accompanied by inversion of the basins. Convergence led to the formation of the fold-thrust belts of the Greater and Lesser Caucasus and the Transcaucasian intermontane depression in between, which gave shape to present-day Georgia. Following the closure of Tethys (Miocene, ~20 Ma), northwards shifting of the subduction zone and the indentation of the Arabian block into Eurasia separated the Black Sea from the South Caspian Sea, where oceanic crust remained.

Due to uplift and a eustatic sea-level drop, previously marine basins eventually became semi-isolated euxinic basins, forming what became the Paratethys (Popov et al., 1993; Adamia et al., 2011). In the Oligocene, sub-basins of the Paratethys hosted the deposition of organic-rich source rocks (Fig. 1.2). According to paleogeographic reconstructions, this realm has been subdivided into the Central Paratethys, which contains the Menilite Formation of the Carpathian Foreland and the Schöneck Formation of the Northern Alpine Foreland Basin, and the Eastern Paratethys, which hosts the Maykop Formation and its equivalent Ruslar Formation in Bulgaria (Fig. 2.1; Köster et al., 1998; Schulz et al., 2002; Popov et al., 2004; Sachsenhofer et al., 2009). In Georgia, Maykop sediments were deposited in the Kura Basin and Rioni Basin of the Transcaucasian intermontane depression.

Figure 2.1: Stratigraphic correlation of the Paratethys (Upper Eocene–Lower Miocene) and main events in the Eastern Paratethys (Popov et al., 2001).

This chapter discusses the tectonic and geodynamic evolution of the Kura Basin in more detail (Section 2.1). Furthermore, Section 2.2 is dedicated to the stratigraphy of the Kura Basin. Lastly, existing hydrocarbon shows and fields in Georgia are discussed in Section 2.3.

2.1 Evolution of the Kura Basin

The Kura Basin is an inter-arc feature, formed as a result of the Alpine-Himalayan compression (Yükler et al., 2000). Previous studies have attempted to reconstruct the complex tectonic processes occurring within the active plate margin, associated with periods of basin closure and rejuvenation (Fig. 2.2; Adamia, 1991). The development of hydrocarbon fields in the Near-Tbilisi area has provided data necessary for understanding the geological history of the Kura Basin. The structural evolution could be inferred from well and seismic data as well as surface geological maps (Patton, 1993).

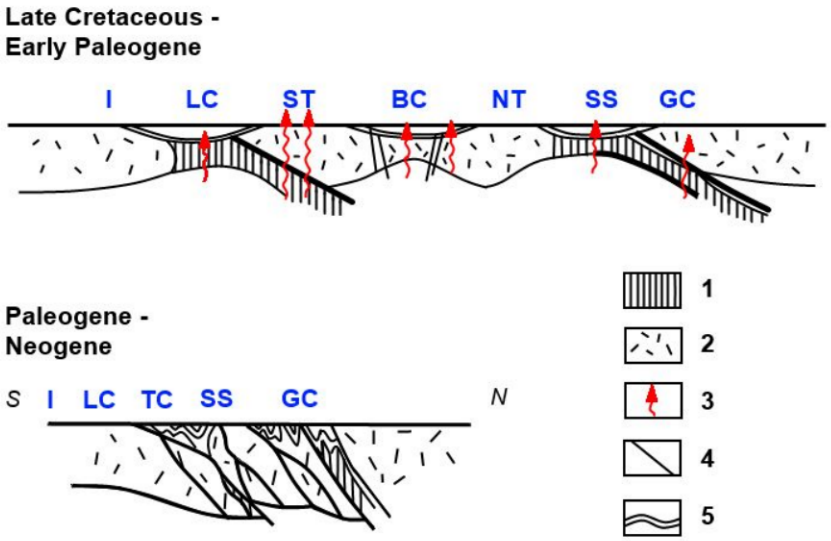

Figure 2.2: Geodynamic evolution of the Transcaucasus intermontane depression (modified after Adamia, 1991; Patton, 1993); I = Iranian Platform; LC = Lesser Caucasus (Paleotethys); ST, NT = southern and northern segment of Transcaucasian island arc; BC = Black Sea-Caspian inter-arc (Adjara-Trialeti rift basin); SS = Marginal sea of Greater Caucasus (Main Range); TC = Transcaucasian island arc; GC = Greater Caucasus; 1 = oceanic crust; 2 = continental crust; 3 = volcanism; 4 = faults; 5 = Mesozoic/Cenozoic sediments.

Prior to the Alpine collision, the Near-Tbilisi region was located in an intra-arc setting within the eastern end of the Adjara-Trialeti rift basin (Fig. 2.2). The Adjara-Trialeti foldbelt, now the northernmost tectonic unit of the Lesser Caucasus, was formed during the Styrian tectonic phase in the Middle Miocene. A system of E-W trending anticlines was created as a result, forming hydrocarbon structural traps (Fig. 2.3). In the north, folding of

the Greater Caucasus occurred later in the Early Pliocene. Compression and the associated thrusting gave form to an accretion prism below the Kura Basin, while deformation on the northern and southern flanks of the Greater Caucasus main range took place (Fig. 2.4; Philip et al., 1989). Detachment occurred within the plastic Maykop shales. Thrust and strike-slip faults dominate in this compressional setting (Adamia et al., 2011).

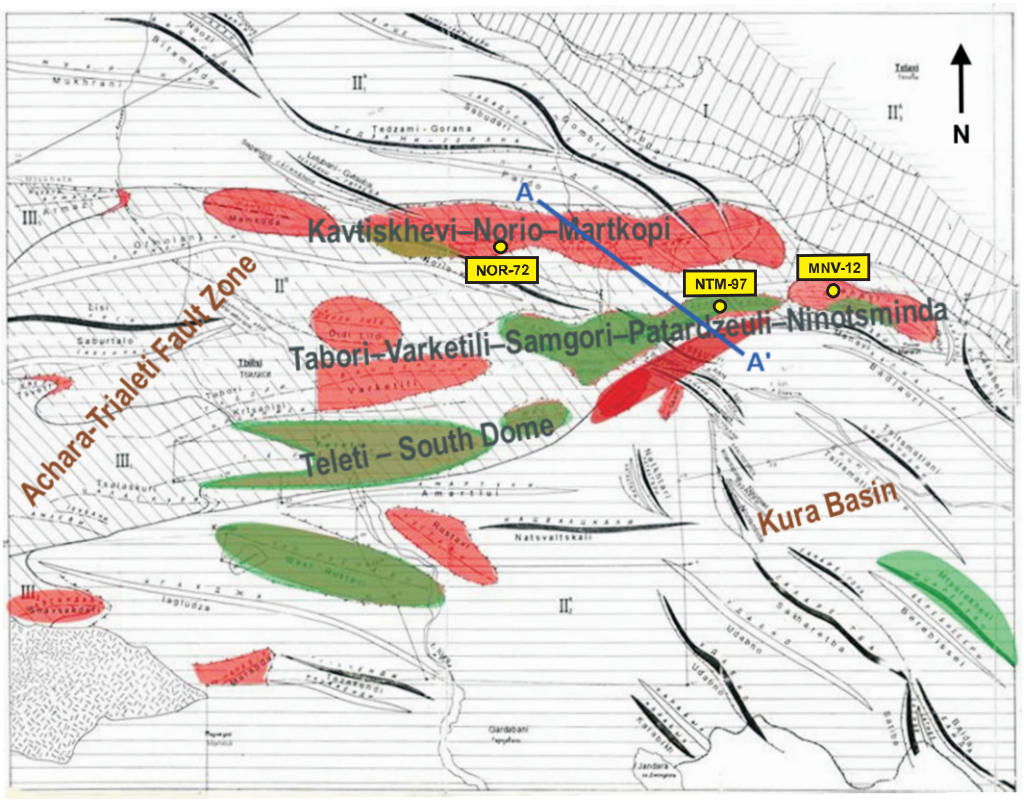

Figure 2.3: Map of the E-W trending anticlines of the Adjara-Trialeti fold-belt on which the hydrocarbon accumulations of the East-Tbilisi region are located (CanArgo, 2013). The three wells from which the investigated cuttings samples originate are marked. The cross section (A-A') is shown in Fig. 2.4.

Well data from the Samgori field (Near-Tbilisi area, south of the study area) shows that the dominant thrust fault does not cut through Akchagilian (Pliocene) sediments, while folding associated with the thrusting is evident in rocks as young as Upper Miocene (Patton, 1993: Fig. 2.4). Therefore, the main thrusting and accompanying folding occurred in the Late Miocene–Early Pliocene, which is consistent with the findings of Mgeladze et al. (1989).

Sedimentation of the source rocks in the Kura Basin was controlled by the evolution of the Paratethys as well as climate conditions. Isolation of the Paratethys, deepening of the basin due to active sea-floor spreading, and mesophilic, humid climatic conditions

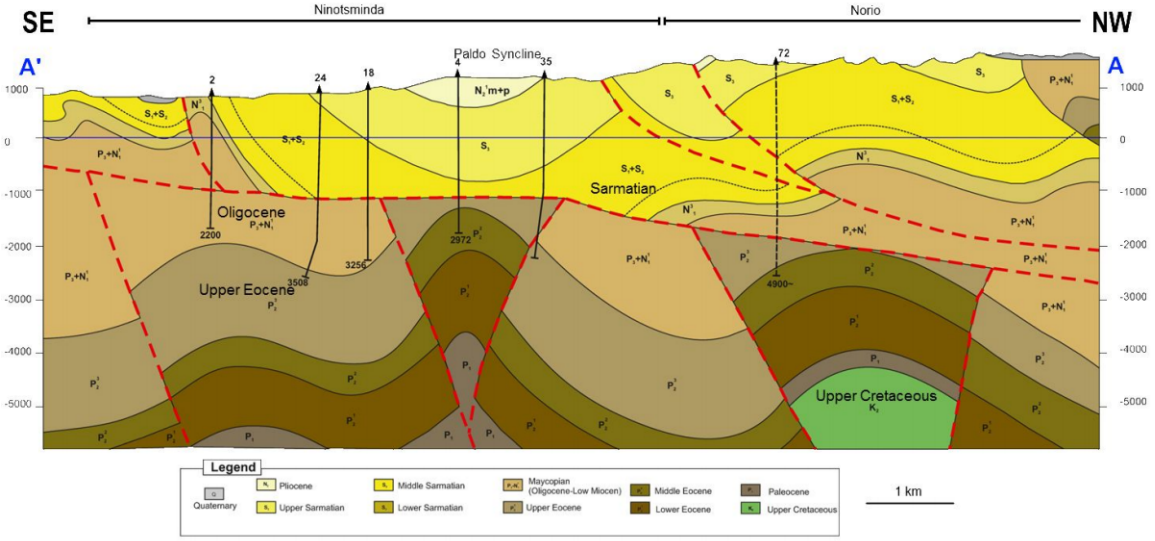

Figure 2.4: Structural cross section of the Ninotsminda and Norio fields (CanArgo, 2013). The location of the cross section is indicated on the map in Fig. 2.3.

led to thermohaline water stratification and a dominantly estuarine water circulation pattern. This resulted in recurrent periods of stagnation and the deposition of dysoxic to oxic sediments of the "maykopian and menilitic facies" (Popov et al., 2004). Uninterrupted sedimentation in the Late Eocene–Early Miocene took place.

In the Near-Tbilisi area, molasse sediments overlie folded Cretaceous–Paleogene sequences belonging to the eastern end of the Adjara-Trialeti tectonic unit.

2.2 Stratigraphy

In Georgia, the Transcaucasian intermontane depression is superimposed onto the rigid Georgian Massif and the Adjara-Trialeti fold-belt. The area encompasses two NW-SE trending basins forming the Rioni-Kura intermontane rift (Adamia, 1991; Adamia et al., 2011), separated by the Dzirula massif consisting of uplifted crystalline Precambrian–Paleozoic basement and its sedimentary Late Paleozoic–Cretaceous cover.

The stratigraphy of the Kura Basin has been determined based on well and outcrop data (Fig. 2.5; Patton, 1993) as well as geophysical data (CanArgo, 2013). The Mesozoic–Cenozoic sedimentary succession in the Near-Tbilisi area comprises a total thickness of 12 km.

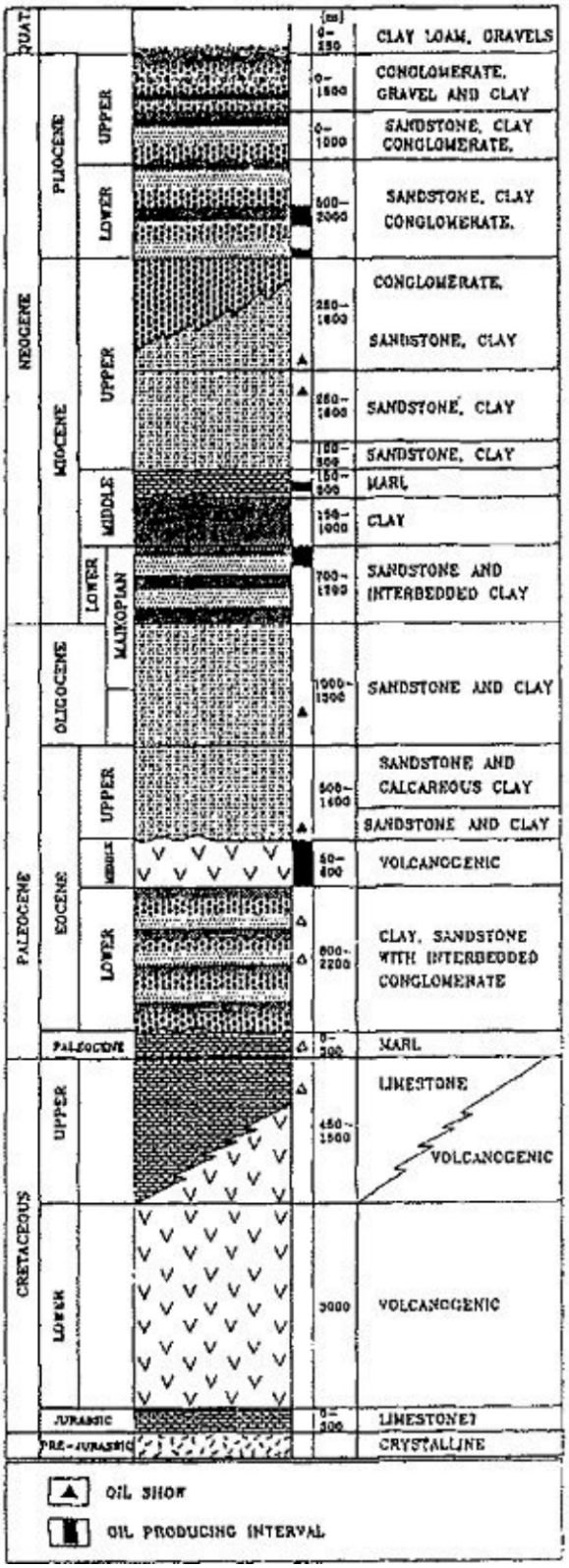

Figure 2.5: Stratigraphic column of the Kura Basin (modified after Georgian Oil, 1990; Patton, 1993)

Pre-Mesozoic

The Upper Precambrian crystalline basement, represented by the Dzirula Massif which separates the Kura Basin from the Rioni Basin in the west, is made up of schists, paragneisses, and amphibolites. This complex is overlain by the thrusted and metamorphosed Lower or Middle Paleozoic ophiolitic mélange. Both units are intruded by Late Paleozoic granites and overlain by Late Visćan–Early Sephukovian tuffs (Khain and Koronovsky, 1997).

Mesozoic

The Paleozoic succession is unconformably overlain by the Mesozoic and Cenozoic basement cover (Khain and Koronovsky, 1997) beginning with Triassic–Jurassic terrigenous and carbonate deposits, porphyrites, and fine-grained siliciclastics. Outcrops of the volcaniclastic-rich Cretaceous (Albian to Campanian–Maastrichtian) succession are present in the Trialeti Range of the Adjara-Trialeti fold belt, which partly borders the Kura Basin in the southwest. The Albian–Turonian interval contains tuffs, tuff breccias, and augite-labradorite porphyrites, while the post-Turonian succession consists of silty limestones and marls with rare silty tuffs and conglomerate interbeds.

Paleocene–Eocene

Cenozoic sediments encompass the Paleocene to Pliocene. Paleocene–Lower Eocene rocks are characterized by marls in the lower part and sandstones, calcareous clays, and conglomerate interbeds in the upper part. The Middle Eocene interval is rich in volcaniclastic sediments.

The Upper Eocene–Maykop terrigenous turbidite interval is 3 to 5.5 km thick and constitutes a deep marine facies in the eastern part. In the west, evidence of a shallow marine facies includes an increased grain size and inter-formational erosion surfaces. The Upper Eocene consists of sandy clays with marl interbeds in the lower part and alternating clays and sandstones in the upper part.

In the western and central part of the Near-Tbilisi region, the Upper Eocene conformably overlies the Middle Eocene. The eastern segment (Patardzeuli-Ninotsminda-Manavi Zone) is more complex due to regional thrust faults cutting into the upper section of the Upper Eocene and Maykop, reducing the combined thickness of these intervals to a total of 300 to 330 m.

Oligocene–Lower Miocene (Maykop)

The Oligocene–Lower Miocene interval, usually referred to as the Maykop Formation, is made up of sandy clays with occasional fine-pebble conglomerate interbeds in the lower part and sandstone with clay interbeds in the upper part. In these organic-rich rocks, an abundance of pyrite in relation to iron oxides suggests that sedimentation occurred under reducing conditions (Guliyev et al., 2003). The Maykop is thickest in the southern and northern parts of the Near-Tbilisi region (2800 to 3200 m) and thins towards the center.

The Lower Oligocene, characterized by grayish-brownish clays, sandstones, siltstones, and rare dolomitized limestones and marl interbeds, is more sandy than the Middle and Upper Oligocene sediments. Sandstone contents and the amount of plant remains increase towards the west. An abundance of reworked effusive rock fragments is present. Middle and Upper Oligocene sediments are made up of brown jarosite-gypsum-bearing (Maykop-type) clays with rare sandstone interbeds and low organic content.

The Sakaraulian (Lower Miocene; Fig. 2.1), which overlies the Oligocene, comprises light-colored, grayish-yellowish, organic-rich, quartz-arkose-sandstones as well as brownish, jarosite-gypsum-bearing clays with low organic content. This formation is conformably overlain by the Kozahurian (Middle Miocene), which consists of Maykop-type clays with rare sandstone and siltstone beds.

2.3 Hydrocarbon Shows and Discoveries

Modern oil exploration in Georgia began in 1930, when the government-owned Georgian Oil was founded (Patton, 1993). The major oil discoveries in eastern Georgia are located at the contact between the Adjara-Trialeti fold-belt and the Kura Basin (Fig. 2.6). A system of anticlines and faults exists, providing numerous structural hydrocarbon traps. Among the hydrocarbon fields in this zone are Samgori-Patardzeuli, Ninotsminda, Teleti, South Dome, Rustavi, West Rustavi, Norio/Martkopi, and Manavi. Three anticline series with E-W trending axes, at which the main producing fields are located, are present in the Near-Tbilisi region (listed from north to south; see Fig. 2.3):

Kavtiskhevi-Armazi-Norio-Martkopi-Manavi

Tabori-Varketili-Samgori-Patardzeuli-Ninotsminda

Amlevi-Teleti-South Dome

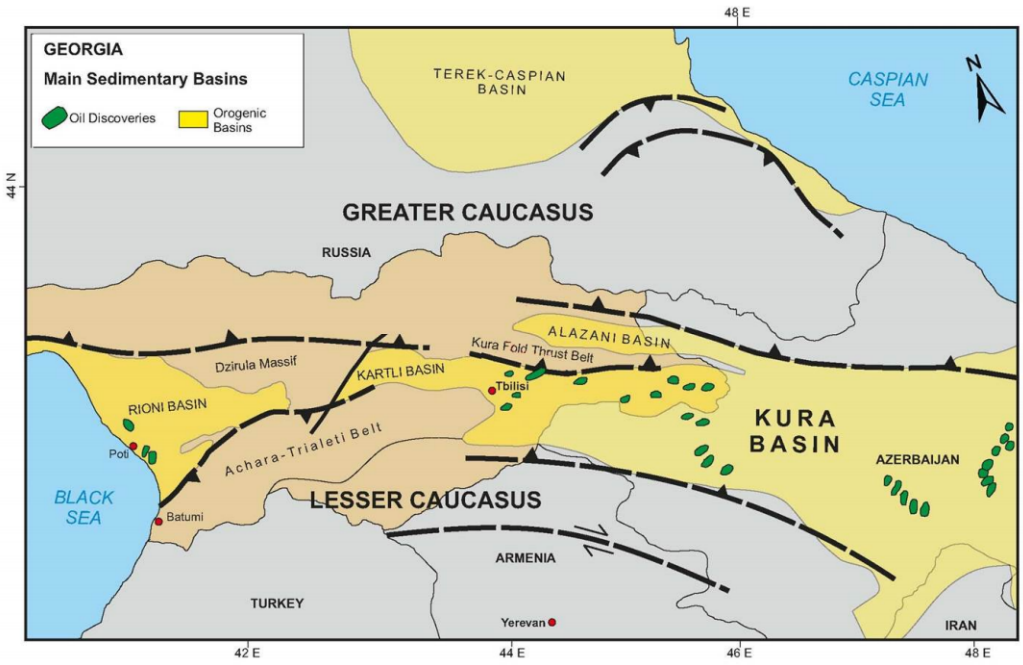

Figure 2.6: Map of the sedimentary basins and oil fields in Georgia (CanArgo, 2013).

In addition to trapping, the faults played an important role in hydrocarbon accumulation, as they provided secondary migration paths. Hence, the identification of major fault zones is crucial for locating hydrocarbon-bearing zones. Other migration pathways include sandy-silty beds.

According to literature, the main hydrocarbon source in the Kura Basin is the Oligocene–Lower Miocene (Maykop) shale. These shales contain between 1 and 10% TOC and are characterized by type II-III kerogen (Yükler et al., 2000). In the Near-Tbilisi area, the Oligocene may have entered the oil window sometime during the second half of the Middle Miocene (CanArgo, 2013). The Upper Eocene, also a potential source rock, entered the oil window towards the end of the Oligocene.

As reservoirs, the Upper Eocene and Maykop have proved to be oil-bearing. Reservoir units in the Upper Eocene consist of fine to medium-grained, hard sandstones, some of which are fractured. The thickness of the sandstone units reach several tens of meters in some places. Based on core data, total porosity is estimated between 9.9 and 18.5%, and the average porosity is 14.0%. Within the Maykop, quartz-arkose and quartz sandstones of the Lower Miocene (Sakaraulo) with thicknesses of up to 6 m contribute to oil production. Core data shows that the total porosity of the sandstones varies between 8.2 and 28.0%.

General descriptions of the Upper Eocene and Maykop in this chapter are mostly based on internal reports. For the present study, drill cuttings samples from the aforementioned intervals from the Norio, Ninotsminda, and Manavi fields are described in detail in the next chapter, while the rest of this work focuses on the organic geochemical parameters of these potential source rocks.

3. Samples

Second to core samples, drill cuttings provide the most complete record of the subsurface. Cuttings samples taken from three wells east of Tbilisi (Norio-72, Ninotsminda-97, and Manavi-12; see Fig. 3.1) and oil samples from the Ninotsminda field and Manavi-12 well were the main sources of data for this study. This chapter focuses on describing the lithology and conditions of the studied samples.

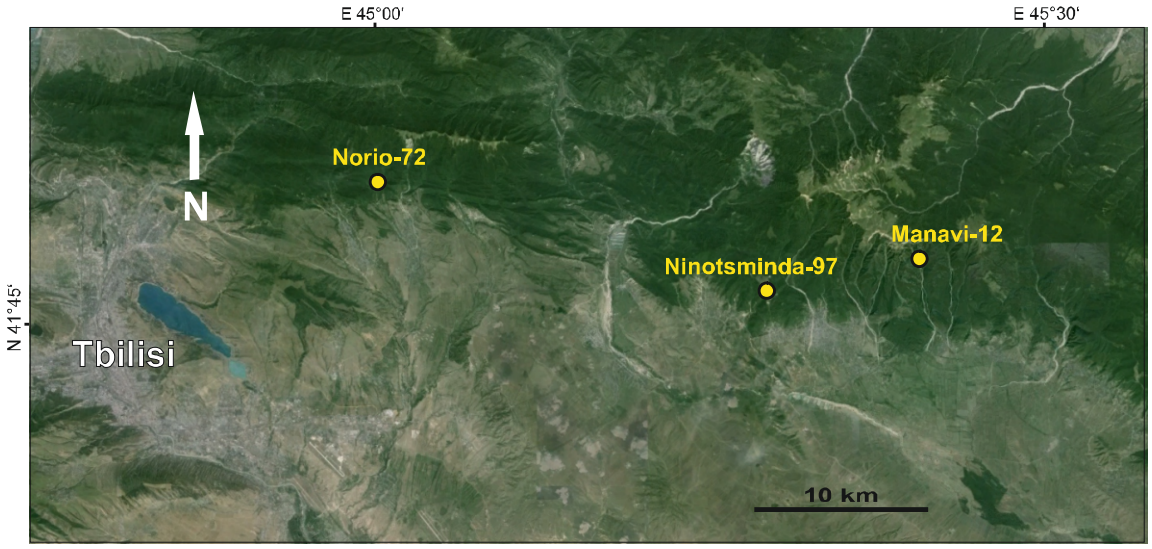

Figure 3.1: Map of the Near-Tbilisi study area, showing the locations of the Norio-72, Ninotsminda-97, and Manavi-12 wells (modified from Google Earth, May 2014).

A total of 304 drill cuttings and five oil samples were provided by CanArgo Georgia Ltd. The first sample set was received on October 12, 2013, while the second set was received on December 16, 2013. Ultimately, 221 samples were selected for analysis (see Table 3.1), whereby the analysis methods applied on each sample are specified in Appendix A.

Most of the delivered samples were dry and packed either inside sealed, labeled brown paper envelopes or cloth bags with sample tags. Only the wet, unwashed samples from

Norio-72 from depths of 4510 to 4891 m were packed in cloth bags with an inner plastic lining.

Well	Depth	No. of Samples	Date Received	Description
Norio-72	3625 to 4510 m	160 (126)	Oct 12, 2014	washed
	4510 to 4891 m	37 (35)	Dec 16, 2014	unwashed
Ninotsminda-97	2330 to 2560 m	27 (23)	Oct 12, 2014	washed
Manavi-12	3749 to 3821 m	15 (0)	Dec 16, 2014	washed
	3821 to 3980 m	52 (37)	Oct 12, 2014	washed
	3980 to 4050 m	13 (0)	Dec 16, 2014	washed

Table 3.1: Drill cuttings samples provided by CanArgo. Numbers in parentheses represent the number of samples from a given depth interval which were selected for analysis.

Various mud additives were used in all three wells. Ninotsminda-97 supplied the "cleanest" samples, as the interval of interest was drilled entirely with KCL polymer mud. On the other hand, Manavi-12 and some of the Norio-72 samples were contaminated with oil (diesel oil and oil from Eocene reservoirs) which had been added to the drilling mud. Additional contaminants such as rubber, iron splitters, plastic, wood, and insects were present in the cuttings. For documentation, each sample was photographed using a digital single-lens reflex camera (see Appendix B). Representative samples from each well are shown in Fig. 3.2.

3.1 Norio-72

The Norio-72 exploration well (also Martkopi-72) is the deepest well in the CanArgo concession. It was chosen as a key well because the available samples cover the greatest depth interval. Cuttings samples were taken every 5 m between depths of 3625 and 4510 m and every 3 m between depths of 4510 and 4841 m. A mud log (4298 to 4900 m) and wireline log (2925 to 4450 m: gamma ray, spontaneous potential, caliper, resistivity, neutron-gamma) were also provided by CanArgo. Some of the samples are highly contaminated due to the use of OBM for drilling the sections below a depth of 4510 m.

Samples from the lower section (below 4510 m) are characterized by dark gray, flake-like chips with uniform thickness and diameters reaching 1 cm. One side of each chip is polished and the other side is marked by mm-wide striations (see Fig. 3.3). This texture often results from the removal of chips by shearing action by a polycrystalline diamond compact (PDC) bit, commonly used for drilling shale formations in combination with OBM (Preslar and McDermaid, 1984; Graves, 1986).

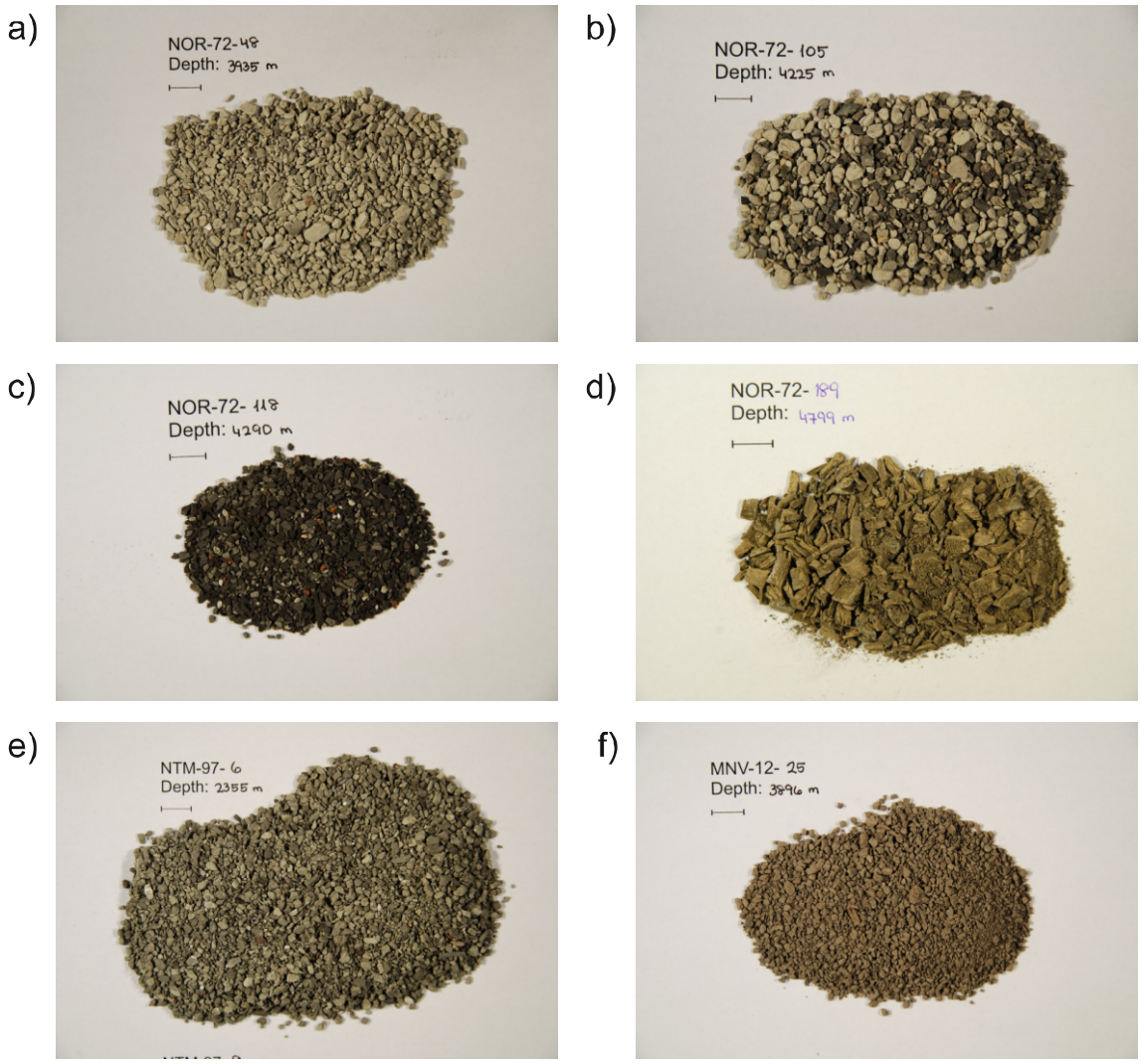

Figure 3.2: Photos of representative cuttings samples (length of scale bar is 1 cm): (a) predominantly light gray sample (NOR-72-48); (b) mixture of light gray, gray, and dark gray grains (NOR-72-105); (c) predominantly dark gray sample (NOR-72-148); (d) dark gray, oil-contaminated chips (NOR-72-189); (e) representative cuttings from the Ninotsminda-97 well (NTM-97-6); and (f) representative cuttings with brown coating from the Manavi-12 well (MNV-12-25).

Each sample from the upper section (3625 to 4510 m) consists of a mixture of light, medium, and dark gray grains. Darker gray samples contain higher percentages of clayey and silty material which are rich in organic matter, whereas lighter gray samples are typically more sandy. A high percentage of quartz and feldspar in these light gray samples was confirmed by x-ray diffractometry. The grains are generally sub-rounded and soft enough to be destroyed with a fingernail. Light gray and medium gray grains react with HCl while dark gray grains do not. Medium gray grains contain swelling clay minerals. The samples

generally become darker towards the bottom of the section. Sub-angular dark gray grains are dominant below a depth of 4280 m.

Several coaly grains were found in samples NOR-72-26 (3825 to 3840 m) and NOR-72-28 (3835 to 3840 m). These were hand-picked for vitrinite reflectance measurements. Aggregates of grains bound together by dry drilling mud as well as reddish-yellow grains occurring as accessories were removed prior to analysis.

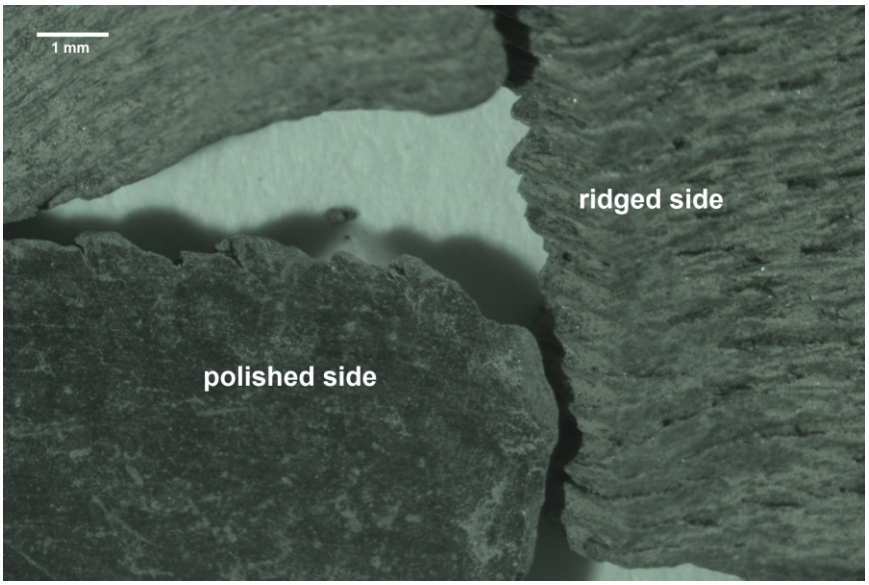

Figure 3.3: Stereomicroscope photograph of cuttings from sample NOR-72-185 (4757 to 4760 m). One side of each grain is polished while the other side is characterized by uniform ridges. Each grain is slightly curved.

3.2 Ninotsminda-97

Ninotsminda-97 is a production well and is also the source of the shallowest samples in this study (2330 to 2560 m). Samples were taken at intervals of 5 m and consist of mixtures of grains with different shades of gray (light gray, medium gray, and dark gray). Brownish-gray aggregates are present as accessories. In general, the grains react with HCl. Coal grains in samples NTM-97-9 (2370 to 2375 m) and NTM-97-21 (2525 to 2530 m) were picked for vitrinite reflectance measurements.

3.3 Manavi-12

The Manavi-12 exploration well is one of the deepest wells in the CanArgo concession. Samples from this well are characterized by a strong hydrocarbon scent. They contain gray

grains with a brown powdery coating. Sample intervals vary between 2 m (3938 to 3960 m; 3980 to 4050 m), 3 m (3749 to 3938 m) and 5 m (3960 to 3980 m).

Samples from the second sample delivery (above 3821 m; below 3970 m) were contaminated by either thin, clear strands of unknown material which adhere to the grains or 0.5 mm-wide strips of cellophane. These objects could neither be successfully removed by hand-picking nor with organic solvents (e.g., chloroform). For this reason, these samples were not suitable for analysis.

3.4 Oil Samples

Four oil samples from wells in the Ninotsminda field were provided by CanArgo in October 2013. Three of the samples (G-NTM-21, G-NTM-59, and G-NTM-98) are from Eocene reservoirs. One sample (G-NTM-78) came from an Oligocene reservoir. Information about the locations of these wells is missing.

One oil sample from Manavi-12 (G-MNV-12) was provided at a late stage in the project (April 2014). The origin of the oil is near the oil-water contact in a Cretaceous carbonate reservoir. According to reports from CanArgo, oil from this reservoir was never produced.

3.5 Drilling Mud

Information on drilling mud and their chemical additives, which was provided by CanArgo, is summarized in this section because of its adverse effect on analytical results. OBM was used in Norio-72 and Manavi-12 to prevent swelling while drilling through clayey formations. Table 3.2 summarizes the types of drilling muds used in the three wells at various depth intervals.

Well	**Depth Interval**	**Mud**
Norio-72	3625 to 4571 m	KCL
	4400 to 4867 m	OBM
	4867 to 4900 m	KCL
Ninotsminda-97	2330 to 2560 m	KCL
Manavi-12	1912 to 4100 m	OBM
	4100 to 5100 m	WBM

Table 3.2: Drilling muds used in Norio-72, Ninotsminda-97, and Manavi-12 at various depth intervals. KCL = potassium chloride; OBM = oil-based mud; WBM = water-based mud.

In Norio-72, the following additives were added to the KCL polymer mud: baryte, Duo-Vis, sodium bicarbonate C110, sodium acid pyrophosphate (SAPP), citric acid C126, calcium carbonate ($CaCO_3$), Milpark MD, Alcomer 120L, M-I CIDE, soda ash, lime, gypsum, Kelzan XCD, calcium lignosulphonate, Unical, Staflo Exlo, Staflo Regular, Alcomer 110RD, Defoam-X^{TM}, Soltex , MIL-PAC LV, MIL-PAC R, GLYDRILL MC, xanthan gum, and caustic soda. Additives for OBM include baryte, M-I SEAL (fine and medium blends), calcium carbonate, lime, mica flakes (fine and medium grades), Soltex , calcium chloride ($CaCl_2$), CARBO-MUL HT, CARBO-TEC , CARBO-GEL , and CARBO-TROL .

In Ninotsminda-97, additives for KCL polymer mud include POLYPAC UL, calcium carbonate, Drispac regular, SPERSENE CFL (chrome-free lignosulfonate), baryte, caustic soda, xanthan gum, D-SPERSE, TACKLE, M-I CIDE, and M-I PAC.

In Manavi-12, the following additives were added to the OBM: diesel, baryte, $CaCO_3$, cellophane, lime, MI-X-II (cellulose fiber), mica flakes (medium and coarse grades), $CaCl_2$, CARBO-MUL , CARBO-GEL , OMNI-TEC , CARBO-TROL , and gilsonite. Additives for the water-based mud (WBM) include baryte, Duo-Vis, xanthan gum, soda bicarbonate, KCL, $CaCO_3$, Milpark MD, caustic soda, M-I CIDE, soda ash, lime, calcium lignosulfate, Defoam-X^{TM}, MI-X-II (cellulose fiber), mica (fine, medium, and coarse grades), citric acid, PIPE-LAX (additive in diesel oil or OBM for freeing differentially stuck pipes), and MIL-PAC .

4. Methods

Accomplishing the objectives mentioned in Chapter 1 required the application of several standard methods for source rock investigations, which are explained in this chapter. Section 4.1 outlines the pre-analysis sample preparation procedure for the drill cuttings. The succeeding sections briefly explain the theory behind the applied analysis methods and the associated measurement procedures. The table in Appendix B specifies the methods with which each cuttings sample was analyzed.

4.1 Sample Preparation

For documentation, individual cuttings samples were photographed and observed with a Leica MZ6 stereomicroscope. Contaminants such as rubber, iron splitters, plastic, wood, and insects were removed using a magnet and a pair of tweezers. A representative portion of each sample was dried and powdered for analysis.

One set of samples (NOR-72-161 to NOR-72-197) which had been stored in plastic-lined cloth bags were covered in OBM and therefore required special handling. In order to remove the OBM impregnation, a tablespoonful of each sample was placed inside a tea filter and dipped two to three times into a beaker filled with chloroform. The sample-filled filters were then dried overnight before the samples were removed and crushed. It is important to note that the impregnating material could not be completely removed, as the samples still retained their hydrocarbon-characteristic odor.

4.2 Elemental Analysis (TC, TOC, S)

The effectiveness of a source rock is dependent on the quantity, quality, and maturity of the organic matter it contains (Peters et al., 2005b). The total organic carbon (TOC) content, which can be obtained using the LECO and Eltra methods, is a measure for the quantity of organic matter and therefore the organic richness of a rock sample. Because

it directly affects the generative potential of a hydrocarbon source rock, it is typically the first screening parameter used in source rock analysis. Fair siliciclastic source rocks are characterized by a minimum TOC of 0.5 wt.% (Peters and Moldowan, 1993). Combined with Rock-Eval parameters (S_1 and S_2; see Section 4.3), TOC provides a quick insight into the amount of hydrocarbons which can be generated (Table 4.1).

Potential	**TOC** [wt.%]	**S_1*** [mg HC/g rock]	**S_2***	**Bitumen** [ppm]	**Hydrocarbons** [ppm]
Poor	<0.5	<0.5	<2.5	<500	<300
Fair	0.5–1	0.5–1	2.5–5	500–1000	300–600
Good	1–2	1–2	5–10	1000–2000	600–1200
Very good	2–4	2–4	10–20	2000–4000	1200–2400
Excellent	>4	>4	>20	>4000	>2400

Table 4.1: Quantity-based generative potential of immature source rocks (Peters and Cassa, 1994). *Rock-Eval parameters (see below).

For the present investigation, two instruments with similar measuring principles, a LECO CS-300 and an Eltra Helios Double Dual Range C/S Analyzer, were used for determining TOC, total carbon (TC), and sulfur (S) contents in the rock samples. For TOC measurements, samples needed to be acidified beforehand.

In both instruments, analysis involved combustion of the rock sample in a pure oxygen atmosphere. Any carbon and sulfur present was converted to CO_2 and SO_2 respectively, which flowed through an infra-red detection cell. The mass of the released gases was converted to %C and %S based on the dry sample weight. Details on the LECO and Eltra measurement procedures are explained in the subsections below.

4.2.1 LECO

Prior to measurements using the LECO method, 80 mg of each powdered sample was pre-treated with 500 µL of alcohol. For TOC measurements, the samples were pre-treated twice with 500 µL of alcohol and 200 µL of concentrated HCl.

The instrument was calibrated with carbon (501-937) and sulfur (502-449) standards. Tungsten and iron chips were added as accelerators for sample ignition. The samples were burned in a pure oxygen atmosphere at 1500°C.

4.2.2 Eltra

For the Eltra method, 100 to 120 mg of each sample was burned in a pure oxygen atmosphere at approximately 1350°C. Samples used for TOC measurements were pre-treated twice with 500 µL of distilled water followed by 1500 µL of 50% phosphoric acid on a heater at roughly 95°C.

The first run of TOC measurements showed that oil-contaminated, hydrophobic samples (NOR-72-161 to NOR-72-197; MNV-12-1 to MNV-12-49) yielded unrealistically high TOC contents, most probably due to incomplete carbonate removal. In a second run, these samples were treated in an ultrasonic bath at 35°C for up to ten minutes before water and phosphoric acid were added in order to ensure that the acid was able to infiltrate the entire sample.

The instrument was calibrated with a calcium carbonate standard (#90810) for the low carbon detector and a coal standard (#92511-3020 Lot: 20130708A) for the sulfur detector.

Parameters Derived from Elemental Analysis

Subtracting TOC from TC yields the total inorganic carbon (TIC) content, which is derived from mineral matter as opposed to biogenic matter. This parameter is used to calculate the calcite equivalent percentage $\text{calcite}_{\text{eq}}$ via the equation below. It is not to be confused with the total ion current chromatogram (also TIC), mentioned in Section 4.7.

$$calcite_{eq} = TIC \times 8.34 \tag{4.1}$$

In non-marine sediments, the low concentration of sulfate is a limiting factor for the formation of sulfides, i.e., pyrite. On the other hand, an abundance of sulfate is present in marine sediments, where the major control on pyrite formation is the amount of decomposable organic matter. For this reason, the TOC/S ratio can be useful for distinguishing between marine and freshwater sediments (Berner, 1984).

4.3 Rock-Eval Pyrolysis

Rock-Eval pyrolysis enables determination of the generative potential (Table 4.1), kerogen type or source rock quality, and maturation stage of the samples. In this study, pyrolysis was carried out in a Rock-Eval 2+ analyzer (Vinci Technologies) in combination with the RockPlus software. Roughly 90 mg of each sample was analyzed, and every sample was measured in duplicate.

During the first stage of pyrolysis, the sample was heated up to 300°C in an inert helium atmosphere. The temperature was then kept constant for three minutes while free and adsorbed hydrocarbons (usually bitumen) were released and measured by a flame ionization detector (FID) to give the S_1 peak [mg HC/g rock]. In the second stage, the sample was heated further up to 550°C at a rate of 25°C per minute. Kerogen capable of generating petroleum and heavy extractable compounds such as resins and asphaltenes were converted into hydrocarbons through thermal cracking. These hydrocarbons were quantified by the FID to give the S_2 peak [mg HC/g rock]. The temperature at which the maximum S_2 occurred was recorded as T_{max}. CO_2 and CO released from kerogen during heating contributed to the S_3 peak and was not taken into account in this study.

Parameters Derived from Rock-Eval Pyrolysis

Several parameters which are essential for the evaluation of hydrocarbon source potential can be derived from the results of Rock-Eval pyrolysis. The hydrogen index (HI) is an indicator of whether a source rock is likely to be oil or gas prone (Table 4.2) and can be calculated using the equation below (Espitalié et al., 1977):

$$HI\,[mg\,HC/g\,TOC] = \frac{S_2 \times 100}{TOC} \tag{4.2}$$

Kerogen Type	**HI** [mg HC/g TOC]	**Expelled Product***
I	>600	Oil
II	300–600	Oil
II/III	200–300	Oil/gas
III	50–200	Gas
IV	<50	None

Table 4.2: Quality of potential source rocks (Peters and Cassa, 1991): *at peak maturity.

The sum of S_1 and S_2 gives the hydrocarbon generation potential. The production index (PI), which is the ratio between free hydrocarbons and potential hydrocarbons (generated during the heating process), can be calculated using the equation below (Espitalié et al., 1977):

$$PI = \frac{S_1}{S_1 + S_2} \tag{4.3}$$

PI increases first and foremost with increasing maturity and the associated hydrocarbon generation, although contamination from OBM or migrated hydrocarbons affecting the S_1 parameter could also lead to elevated values. After peak maturity, further increase in

maturity eventually causes a decrease in PI as free hydrocarbons begin to migrate out of the source rock, meaning that a low PI could also be a sign of overmature source rocks.

T_{max} is a maturity parameter. As the stage of maturity increases, higher thermal energy is required to generate hydrocarbons from kerogen (Killops and Killops, 1997). PI and T_{max} can be compared with vitrinite reflectance (see next section) for determining the maturation stage of a rock sample (Table 4.3).

4.4 Vitrinite Reflectance

In addition to Rock-Eval pyrolysis, another possibility for determining the thermal maturity of a sample is by measuring the reflectance of vitrinite macerals (Tissot and Welte, 1984; Mukhopadhyay and Dow, 1994). Under an incident light microscope, vitrinite reflectance increases progressively with thermal maturation. Two types of samples were prepared for this analysis: (1) picked coal grains ($\leq$1.5 mm diameter) and (2) whole rock samples.

An extensive procedure for the preparation of polished blocks was completed prior to microscopy. The first step involved embedding the selected samples in epoxy resin. For the coal polished blocks, grinding and polishing followed in seven steps using silicon carbide powder (graining: 220, 600, and 1200), diamond suspensions (9 µm, 3 µm, and 1 µm), and oxide polishing suspension colloidal silica (OPS; 0.05 µm). Instead of water, ethylene glycol was used with the polishing wheel in order to prevent damage to the coal samples.

For whole rock samples, silicon carbide powder (graining: 220, 600, 1200, 3000, 5000, and 12000) and OPS (0.05 µm) were used for grinding and polishing. In order to minimize damage to the clay-rich samples, the polished blocks were prepared manually in a dry state. The polishing wheel and ethylene glycol were used only for the last polishing step with OPS.

Mean random vitrinite reflectance (R_r) was measured on the polished block samples using an incident light Leica MPV microscope equipped with an oil immersion objective with 100x magnification. Measurement procedures followed established methods (Taylor et al., 1998). The intensity of reflected light with a wavelength of 546 nm was measured with a photomultiplier. An yttrium aluminum garnet standard (YAG, R_r = 0.899%) and gadolinium gallium garnet standard (GGG, R_r = 1.699%) were used for calibration.

Table 4.3 summarizes three maturation parameters and their approximate corresponding values to the bottom and top of the zone of oil generation. According to Peters et al. (2005b),

the relationship between vitrinite reflectance (VR) and T_{max} is based on the following equation, which is not recommended for T_{max} values below 420°C:

$$VR = 0.018 \times T_{max} - 7.16 \tag{4.4}$$

Maturity Level	PI [-]	T_{max} [°C]	R_r [%]
Top of oil window	0.1	435 to 445	0.6
Bottom of oil window	0.4	470	1.4

Table 4.3: Geochemical and optical parameters describing thermal maturation levels (Peters, 1986).

4.5 Semi-Quantitative Maceral Analysis

The origins of different maceral groups are described in Taylor et al. (1998). Vitrinite is derived from terrestrial organic matter (e.g., higher plants), liptinite from lipid-rich plant material (e.g., algae, pollen, spores, resin, cork, and cuticles), and inertinite from oxidized material (e.g., charcoal). The relative reflectivity, fluorescence and hydrocarbon potential characteristic of each maceral group is shown in Table 4.4.

Maceral Group	Reflectivity	Fluorescence	HC Potential
Vitrinite	middle	none or weak	gas
Liptinite	dark	strong	oil and gas
Inertinite	bright	none	none

Table 4.4: Reflectivity, fluorescence, and hydrocarbon potential of maceral groups (Taylor et al., 1998).

Organic petrology enabled quantification of the maceral composition of 30 selected whole rock samples. For this analysis, representative cuttings samples were prepared using the same procedure as for vitrinite reflectance measurements (see Section 4.4). The analysis was performed using an incident light Leica MPV microscope with reflected white and fluorescent light and oil immersion objectives (50x and 100x magnification). The amounts of vitrinite, liptinite, and inertinite inside the samples were roughly estimated.

4.6 Calcareous Nannoplankton

In order to obtain biostratigraphic age control for the studied successions, 52 samples were analyzed by S. Ćorić (Geological Survey of Austria) for their calcareous nannoplankton content. Age assignments were conducted based on the stratigraphic chart in Fig. 2.1. Smear slides of samples were prepared using standard procedures (Perch-Nielsen, 1985) and examined under a LEICA DMLP light microscope (crossed and parallel polarization) with 1000x magnification.

4.7 Gas Chromatography-Mass Spectroscopy

Gas Chromatography-Mass Spectroscopy (GC-MS) is a sophisticated method for obtaining biomarker data from rock samples. The analysis was performed on 24 rock extracts and five oil samples.

Prior to measurement, representative portions of selected rock samples were powdered and extracted using dichloromethane for one hour at 75°C and 50 bar in a Dionex ASE 200 accelerated solvent extractor. The extracts were then evaporated to 0.5 mL using a Zymark TurboVap 500 closed cell concentrator. Asphaltenes were precipitated from a hexane-dichloromethane solution (80:1 ratio) and separated by centrifugation using a Labofuge 200. The hexane-soluble fractions were split into saturated (aliphatic) hydrocarbons, unsaturated (aromatic) hydrocarbons, and NSO (nitrogen, sulfur, and oxygen) compounds using medium pressure liquid chromatography (MPLC) with a Köhnen-Willsch MPLC instrument (Radke et al., 1980).

To obtain biomarker data, the aliphatic and aromatic hydrocarbons were analyzed using a gas chromatograph equipped with a DB-5 fused silica column (30 m × 0.25 mm, 0.25 µm film thickness) and coupled with a Thermo Fischer ISQ quadrupole mass spectrometer. For analysis, the oven temperature gradient was programmed from 70 to 300°C at a rate of 4°C per minute. This was followed by an isothermal period of 15 minutes. Helium was used as a carrier gas. The sample was injected with an injector temperature of 275°C. The spectrometer was operated in the electron ionization (EI) mode over a mass/charge (m/z) scanning range between 50 and 650 with 0.7 s per scan.

The GC-MS data were processed in an Xcalibur data system. Individual components were identified on the basis of retention time in the total ion current (TIC) chromatogram and by comparison of the mass spectra with published data. Relative percentages and absolute concentrations of various compound groups in the aliphatic and aromatic hydrocarbon

fractions were calculated using their peaks in the gas chromatograms and their relation to the peaks of the internal standards (deuteriated *n*-tetracosane and 1,1-binaphthyl). The concentrations were normalized to the TOC content. Examples of chromatograms for the aliphatic and aromatic fractions of sample NTM-97-16 (2465 to 2470 m depth) are shown in Fig. 4.1. The most important peaks which were quantified are indicated.

Because samples from Manavi-12 were suspected of being contaminated by OBM, a special test was performed on one of the samples (MNV-12-47) to investigate both hydrocarbons in the contaminating mud and the "indigenous bitumen". The sample was placed inside a filter bag and soaked in chloroform in order to dissolve the organic compounds adhering to the grains. Afterwards, the sample was taken out of the filter bag, left to dry, pulverized, and extracted. The chloroform solution with the dissolved organic compounds was left overnight so that the chloroform evaporated and only the "mud" or "contamination" remained. This "contamination" sample (MNV-12-47m) and the extract from the washed sample (MNV-12-47w) were measured with GC-MS.

Organic Geochemical Parameters

Descriptions of organic geochemical parameters incorporated in this study follow Peters et al. (2005a).

Pristane/*n*-C_{17} and phytane/*n*-C_{18} ratios increase significantly with biodegradation and decrease with thermal maturity.

Pristane/phytane (Pr/Ph) ratios: Pristane and phytane molecules can be derived from various sources, and their ratios can give an insight into the conditions of source rock deposition. The most abundant source of pristane (C_{19}) and phytane (C_{20}) is the phytyl side chain of chlorophyll "a" in phototrophic organisms and bacteriochlorophyll "a" and "b" in purple sulfur bacteria. Reducing or anoxic conditions in sediments promote cleavage of the phytyl side chain to yield phytol, which undergoes reduction to phytane and a rest. Oxic conditions promote the competing conversion of phytol to pristene and then reduction to pristane.

According to Didyk et al. (1978), Pr/Ph ratios below 1.0 indicate anaerobic conditions during early diagenesis. Values between 1.0 and 3.0 were interpreted as reflecting dysaerobic environments.

There are, however, various other sources of pristane and phytane, which reduces the usefulness of the Pr/Ph ratio as a redox indicator (ten Haven et al., 1987). For example, phytanyl ether lipids in archaebacteria (e.g., methanogens and halophiles)

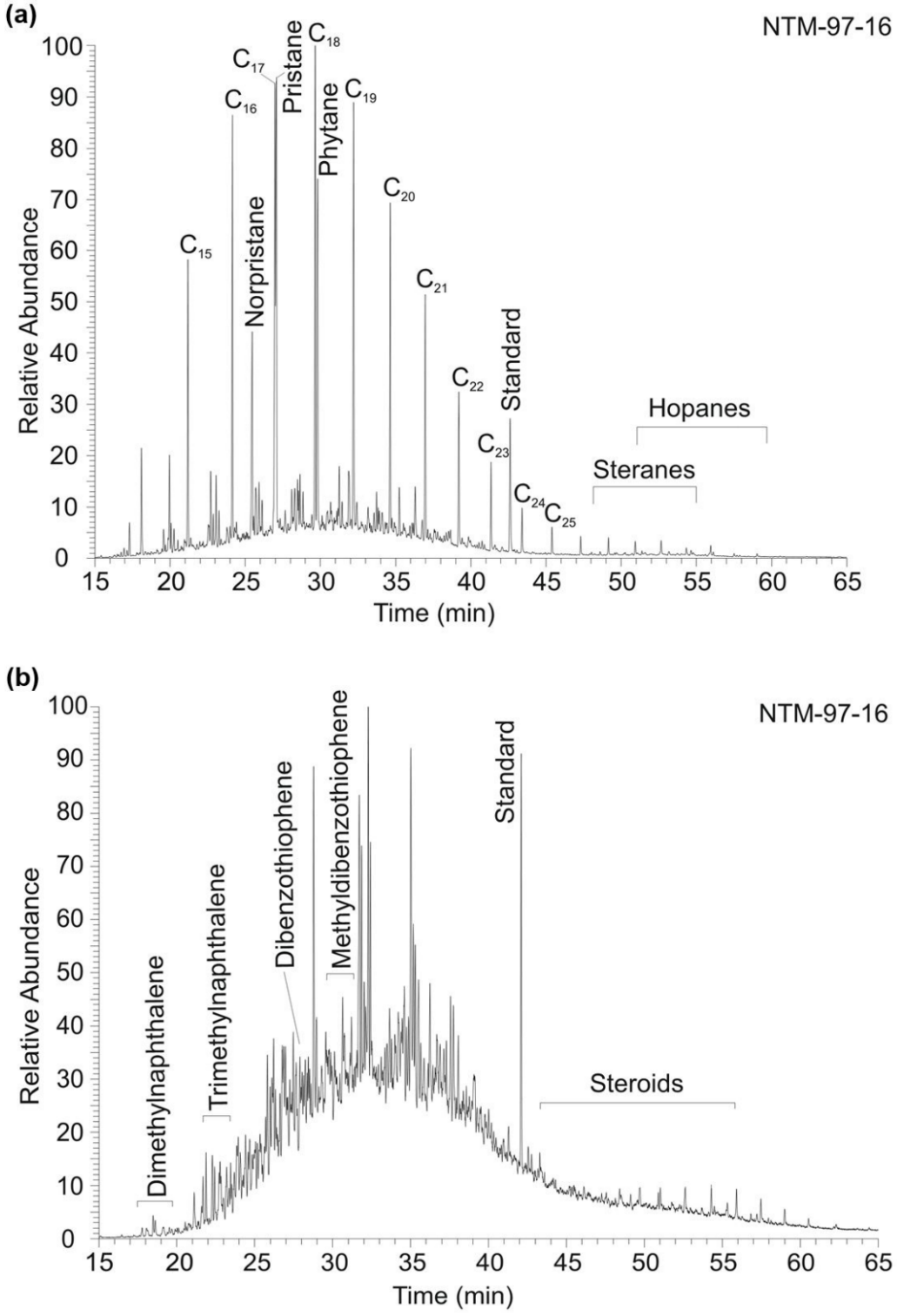

Figure 4.1: Chromatograms of the (a) aliphatic and (b) aromatic fractions of sample NTM-97-16 (2465 to 2470 m). The labeled peaks were quantified.

are potential sources of phytane (Volkman and Maxwell, 1986; Teixidor et al., 1993), and tocopherols (E vitamins; Goossens et al., 1984) and zooplankton can be significant sources of pristane.

In hypersaline environments, halophilic bacteria are important, as they contain more phytanyl lipids than methanogens. Therefore, low Pr/Ph ratios (<1) characteristic of hypersaline environments are controlled by the salinity-dependent growth rate of halophiles rather than the degree of anoxicity (ten Haven et al., 1987).

Oleanane index (oleanane/C_{30}-hopane ratio) is a marker for source input and geologic age. Oleananes are produced by angiosperms (flowering land plants), which usually indicate a Cretaceous or younger (<100 Ma) source input. Although rare, there is evidence of oleanane occurrence in pre-Cretaceous rocks (Moldowan et al., 1994; Peters et al., 1999). According to Murray et al. (1997), oleananes are best preserved in deltaic rocks influenced by marine waters during early diagenesis.

C_{27}-diasterane/C_{27}-sterane ratios are used to distinguish between oils from carbonate and clastic source rocks (Mello et al., 1988). Low diasterane/sterane ratios point towards anoxic clay-poor or carbonate source rocks, whereas high ratios indicate oxic clay-rich source rocks. According to Rubinstein et al. (1975), clay-rich source rocks facilitate the conversion of sterols to diasterenes, both precursors of diasteranes. Acidic and oxic conditions contribute to diasterene formation during diagenesis, which is ultimately reduced to diasterane.

High diasterane/sterane ratios could be the result of high thermal maturity (Seifert and Moldowan, 1978) and/or biodegradation (Seifert and Moldowan, 1979). Therefore, this ratio should only be used to characterize the depositional environments of samples with similar levels of thermal maturity.

C_{28}/C_{29} sterane ratios in marine source rocks and petroleum increase through geologic time (Grantham and Wakefield, 1988). This relationship may be associated with the increased diversification of phytoplankton assemblages in the Jurassic and Cretaceous periods. C_{28}/C_{29} sterane ratios are greater than 0.7 for Upper Jurassic–Miocene oils.

Dibenzothiophene/phenanthrene (DBT/P) ratios can be plotted against Pr/Ph ratios in order to distinguish between oils derived from different depositional environments (Hughes et al., 1995). High DBT/P ratios could be an indicator of oils originating from marine carbonate source rocks, while low ratios may indicate terrestrial or marine shale source rocks. Oils from carbonate source rocks generally tend to have higher sulfur contents, which is why high DBT/P ratios are also associated with high sulfur contents.

(20S)/(20S+20R) isomerization ratios (also expressed as 20S/20R) of C_{29} steranes increase with thermal maturity. Equilibrium of this isomerization reaction lies between 0.52 and 0.55 (Seifert and Moldowan, 1986).

($\alpha\beta\beta$)/($\alpha\beta\beta$+$\alpha\alpha\alpha$) isomerization ratios (also expressed as $\beta\beta/\alpha\alpha$) of C_{29} steranes increase with thermal maturity. The isomerization reaction reaches equilibrium between 0.67 and 0.71 (Seifert and Moldowan, 1986). The ratio is more effective at higher maturity levels than (20S)/(20S+20R) and is independent of source input.

C_{27}, C_{28}, and C_{29} steranes are commonly plotted in a triangular diagram to infer the source input and to perform oil-oil or source-oil correlations. C_{29} steranes indicate a terrestrial source, while C_{27} and C_{28} steranes originate from phytoplankton.

Methylphenanthrene Index (MPI-1): The distribution of phenanthrene and 1-, 2-, 3-, and 9-methylphenanthrene isomers is used to calculate MPI-1, a thermal maturity indicator. This index can be calibrated with vitrinite reflectance for shales and coals containing organic matter which result in type III kerogen (Radke and Welte, 1983). Therefore, MPI-1 obtained for a rock extract allows estimation of vitrinite reflectance if the rock sample lacks vitrinite. In addition, the MPI-1 obtained from an oil sample is useful for estimating the vitrinite reflectance of its source rock at the time of oil generation. Because MPI-1 increases and then decreases again with increasing thermal maturity, it is possible that the same ratios occur in samples of different maturity levels. Furthermore, it is also influenced by the source input and lithology of the source rock (Peters et al., 2005a).

4.8 X-Ray Diffraction Analysis

In the scope of the present study, x-ray diffraction (XRD) analysis enabled a first look into the mineral composition of five selected cuttings samples from the Norio-72 well. Interpretation results were mainly used for correlation with the Norio-72 mud log provided by CanArgo.

The analysis was carried out on a Philips PW 1830/40 device using Cu-Kα-radiation (1.54 Å, 35 kV, 35 mA). Scans with a step size of 0.02° were run between 2 and 67°2θ in the air-dry state (random powder mount and oriented powder mount) after heating to 350 and 550°. Qualitative interpretation was carried out using the dataset of Brindley and Brown (1980) and Moore and Reynolds (1997).

4.9 Isotope Geochemistry of Carbonates

In addition to biomarkers, stable carbon and oxygen isotopes in carbonates provide an insight into changes in the environmental conditions under which source rocks were deposited. In a marine setting, temperature, water column stratification, biological productivity, and the effects of diagenesis may control the $\delta^{13}C/\delta^{12}C$ and $\delta^{18}O/\delta^{16}O$ isotope ratios of carbonates. Furthermore, isotopic compositions are influenced by evaporation and freshwater influx.

For the present investigation, carbon and oxygen isotope measurements were carried out on samples with the highest TIC contents from the Norio-72 and Ninotsminda-97 wells. The pulverized samples were heated with 100% H_3PO_4 at 70°C in an online system (Gasbench II with carbonate option). Analysis was performed using a ThermoFisher DELTA V isotope ratio mass spectrometer. Carbon and oxygen isotope compositions were reported relative to the V-PDB (Vienna PeeDee Belemnite) standard for both $\delta^{13}C$ and $\delta^{18}O$. The reproducibility exceeded 0.2 .

4.10 Maturity Modeling

Thermal maturity modeling aims to predict the thermal history of rocks and the associated temperature change-induced hydrocarbon generation and cracking (Waples, 1994). Over time, one-dimensional models along the z axis have evolved into more complex two or three-dimensional models. Different types of thermal modeling are useful in studying the thermal history of sedimentary basins, the evolution of a petroleum system, and the type of hydrocarbon fluids which may have been generated.

Creating thermal maturity models served as a supplement to maturity investigations of the studied source rock intervals with Rock-Eval pyrolysis and biomarker analysis (see previous sections). For the present study, a 1-D basin system modeling software (PetroMod of IES, Schlumberger) was used to reconstruct paleo-heat flow and the timing of hydrocarbon generation for the Norio-72 and Ninotsminda-97 wells. These two wells were chosen because (1) samples from Norio-72 represent the greatest depth interval and (2) Ninotsminda-97 is least affected by contamination of OBM. As temperature data was not available, the models presented in this work merely serve as reconstructions of two possible "cold" ($40\,mW/m^2$) and "hot" ($50\,mW/m^2$) paleo-heat flow scenarios and the associated timing and duration of hydrocarbon generation. A constant heat flow is assumed to have existed since the Eocene.

Input parameters for the burial history curve and the thermal model were obtained from literature as well as laboratory analysis results from this study. According to Patton (1993), a geothermal gradient of 28°C/km is typical of the region. Sediment thicknesses obtained from literature (Samgori field; Patton, 1993), biostratigraphic data from calcareous nannoplankton, and lithology data from the provided mud logs were incorporated as input values for the burial history curves for all of the possible scenarios. Thermal models were calibrated on thermal indicators, i.e., vitrinite reflectance and biomarker (sterane and hopane isomerization) data.

5. Results

Results from the executed analyses provided a basis for determining the stratigraphy and ultimately for evaluating the source potential of the Upper Eocene and postulated Maykop interval in the study area. A compilation of raw data obtained during this study is included in the Appendices.

5.1 Norio-72

5.1.1 Stratigraphy

Descriptions on the wireline and mud logs from CanArgo show that at least two strongly differing stratigraphic schemes exist for the Norio-72 well (Fig. 5.1). According to the wireline log (2925 to 4450 m), the top of the Middle Miocene occurs at approximately 3475 m. The Maykop (Oligocene–Lower Miocene) extends from around 3650 m to 4400 m and is made up of alternating layers of white to light gray sandstones and light gray to gray clays. Evidence for the age assignment of these intervals is unavailable. In order to obtain a clear stratigraphic division and to determine the true Eocene/Oligocene boundary in this well, 28 samples representing the depth interval between 3625 and 4891 m were investigated for calcareous nannoplankton. Detailed descriptions of the nannoplankton assemblages are included in Appendix C.

According to the wireline log, samples between 3625 and 3745 m are attributed to the uppermost Oligocene and lowermost Miocene. However, taxa observed in the samples (NOR-72-1: *Sphenolithus cf. capricornutus*, nannoplankton zones NP25-NN1; NOR-72-9: *Sphenolithus dissimilis*, upper NP24-NN2) do not include Miocene nannoflora. For this reason, this entire depth interval was re-assigned solely to the Upper Oligocene (Chattian).

Samples between 3790 and 4250 m contain taxa with a last occurrence at the NP21/22 boundary, whereas typical Eocene forms are largely missing. This indicates that this depth

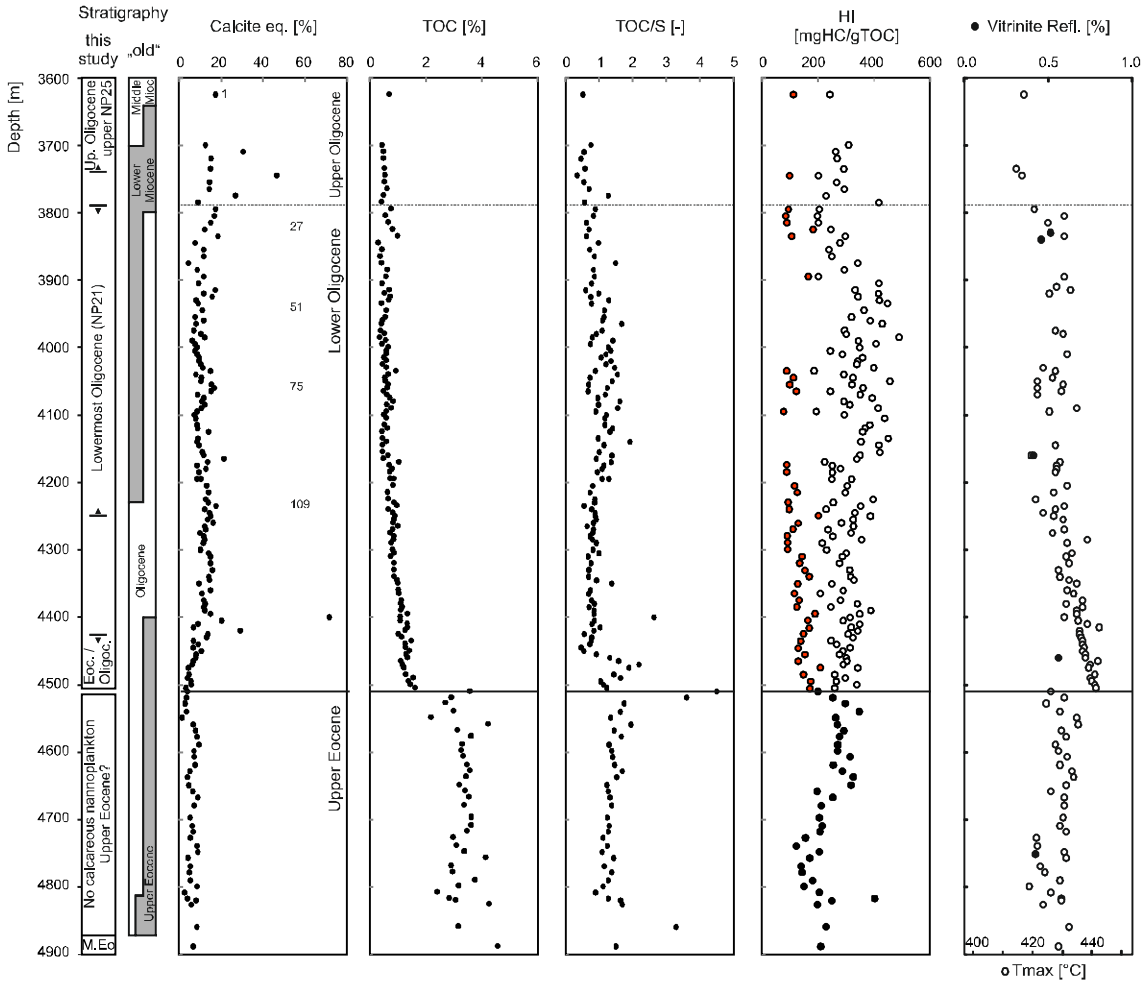

Figure 5.1: Stratigraphy and depth plots of bulk geochemical parameters and vitrinite reflectance in Norio-72. Corrected HI values in Oligocene units are shown by red symbols; uncorrected values are shown by open symbols. See text for further explanation. The relation between vitrinite reflectance and T_{max} is described in Eq. 4.4 in Section 4.4.

interval belongs to the lowermost Oligocene (Rupelian: Pshekian; see Fig. 2.1). Consequently, sediments with a middle Oligocene age (lower part of NP24 to NP22) are either very thin (between 3745 and 3790 m) or missing.

Nannoplankton assemblages from samples between 4345 and 4505 m (NOR-72-129 to NOR-72-159) do not allow precise stratigraphic attributions, but support an Eocene to earliest Oligocene age. Samples NOR-72-165 (4549 to 4553 m) to NOR-72-197 (4888 to 4891 m) contain coaly material, but calcareous nannoplankton are missing. Similar organic-rich sediments in Ninotsminda-97 were dated to the Late Eocene (see below). For this reason, and because a Middle Eocene age is generally accepted for the underlying volcaniclastic sediments, a Late Eocene age (Priabonian: Beloglinian) is likely for the studied interval below

4510 m depth. In this report, a depth of 3790 m is accepted as the boundary between the Upper and Lower Oligocene, whereas a depth of 4500 m is adopted as the boundary between the Lower Oligocene and the Upper Eocene.

To obtain a broad description of the lithology of the Oligocene, three representative samples from Norio-72 (NOR-72-30, 3845 to 3850 m, light gray; NOR-72-38, 3885 to 3890 m, medium gray; NOR-72-138, 4395 to 4400 m, dark gray) were chosen for XRD analysis. A qualitative interpretation was carried out to determine the mineralogical composition of the samples. The intensity of the quartz and calcite peaks in NOR-72-30 were higher compared to the other two samples, which was anticipated because lighter-colored samples were associated with sandier lithologies. The identified minerals in these samples include quartz, feldspar (plagioclase and orthoclase), calcite, dolomite, illite, montmorillonite, muscovite, chlorite, glauconite, and pyrite. This is in accordance with the presence of alternating layers of sandy and silty to clayey layers indicated in the wireline and mud logs. A quantitative interpretation of the mineralogical composition is beyond the scope of this work.

5.1.2 Carbonate Content

The mud log provided by CanArgo for Norio-72 is supplemented with a calcimetry log depicting the amount of calcite and dolomite in the drilled formations. The method with which these values were obtained is unknown. Between depths of 4298 and 4400 m, the calcite content in the mud log hovers around 5%, and the calcite+dolomite content ranges between 5 and 15%. There are three major spikes in the curves at 4316 m, 4360 m, and 4400 m, where calcite content reaches up to 20% and calcite+dolomite up to 38%.

These carbonate contents can be compared to measured TIC contents from the LECO and Eltra methods (see Appendix D). Elevated TIC contents occur at 3710 m, 3745 m, 3775 m, and 4400 m. Below 4400 m, the calcite content remains relatively low and constant at values mostly below 5%, while the calcite+dolomite curve is constant at around 5%. Elevated carbonate contents occur at around 4418 m, 4472 m, and 4684 m, which are do not occur in the LECO and Eltra data for these depths. Apart from the carbonate spike at 4400 m, there is incongruence between the carbonate contents from the elemental analysis and the mud log.

5.1.3 Bulk Geochemical Parameters and Vitrinite Reflectance

Bulk geochemical parameters are listed in Appendix D. Vertical profiles of $calcite_{eq}$, TOC, TOC/S, HI, and PI based on elemental analysis and Rock-Eval pyrolysis data are shown

in Fig. 5.1. Furthermore, average parameters for the Oligocene and Eocene successions are summarized in Table 5.1.

Unit	Depth [m]	TOC [%]	TOC/S [-]	HI [mg HC/g TOC]	PI [-]
Oligocene	3625-4510	0.30-1.61 (0.78)	0.35-2.63 (0.99)	77-208 (128)	0.26
Eocene	4510-4891	2.19-4.56 (3.33)	0.89-1.50 (1.59)	122-402 (237)	0.62

Table 5.1: Summary of bulk geochemical parameters for Norio-72. Average values are shown in parentheses. HI data for the Oligocene are based on corrected S_2 values.

With the exception of thin layers with increased carbonate contents, $calcite_{eq}$ contents in Oligocene rocks are typically around 10 to 15%. $Calcite_{eq}$ decreases downwards to 2% between 4400 and 4555 m across the Oligocene/Eocene boundary. Slightly lower values (5 to 10%) prevail in most of the Upper Eocene succession. In general, the observed trend fits well with the calcite and dolomite contents documented in the calcimetry column of the mud log (4300 to 4891 m; December 2005). However, the calcimetry data also indicates a thin horizon with elevated carbonate contents within the Eocene succession at 4694 m, which does not occur in the $calcite_{eq}$ depth profile.

TOC contents of Upper Oligocene rocks are in the order of 0.5%. Slightly higher values (0.6 to 1.0%) occur over a small interval in the uppermost part of the Lower Oligocene succession (3790 to 3840 m). In the rest of the Lower Oligocene, TOC increases regularly with depth from 0.3 to 1.6%. TOC contents in Eocene sediments are significantly higher (average 3.3%) and show a subtle increase with depth. There is a sudden increase in TOC at the postulated Oligocene/Eocene boundary. It is important to note that this boundary coincides with sample sets delivered in October 2013 (Oligocene; dry samples) and December 2013 (Eocene; oil-drenched samples; see Section 3.1). Thus, an effect of different sample treatment or contamination cannot be completely excluded.

S contents vary significantly in Oligocene rocks (0.4 to 1.6%). Similar to TOC, S increases with depth in the lower part of the Oligocene succession (0.7 to 2.7%) but are relatively low (0.5 to 1.4%) in its lowermost part (3845 to 4120 m). S contents in Eocene sediments are about 0.5% and show a general increase with depth (0.8 to 3.0%).

The resulting TOC/S ratios are significantly below 2.8, characteristic for sediments deposited in oxygen-deficient environments (Berner and Raiswell, 1983). In general, the TOC/S ratios in the Oligocene sediments vary between 0.5 and 1.5. There is a significant downward increase in TOC/S ratios from 0.5 to 2.0 in a narrow depth interval (4450 to

4475 m) in the lowermost part of the Oligocene succession. With the exception of several outliers, TOC/S ratios in the Eocene succession decrease with depth from 2.0 to 1.0.

Many of the Rock-Eval traces for the Oligocene rocks (above 4510 m) show bimodal S_2 peaks, resulting in two T_{max} values (see Fig. 5.2). The higher peak (415 to 442°C) represents hydrocarbons generated by thermal cracking of kerogen which was originally in the rock, while the lower peak (348 to 369°C) corresponds to impregnation, most likely by drilling additives (see also Peters, 1986). Thus in these samples the measured S_2 value significantly overestimates the true S_2 value. A graphical approach was applied to remove the effect of contamination and to assess the true S_2. Both measured and corrected S_2 values are included in Appendix D.

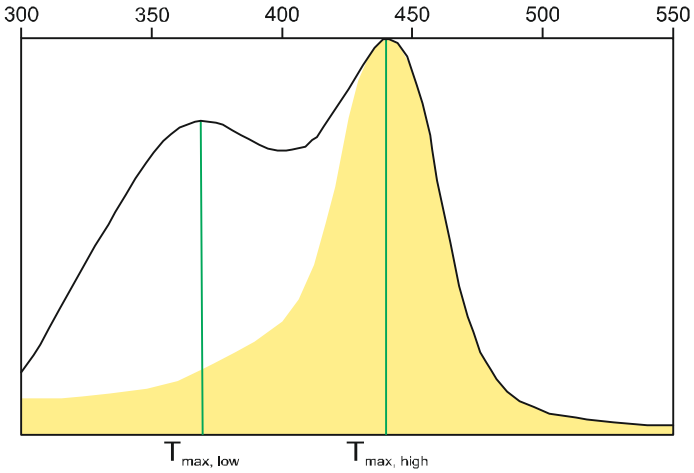

Figure 5.2: An example of a Rock-Eval trace with a double S_2 peak (sample NOR-72-138, depth of 4395 m). The area under the curve corresponds to the measured S_2. The yellow area is the area under the second peak after deconvolution and approximates the true S_2.

The HI log in Fig. 5.1 shows HI values based on both uncorrected S_2 values (open symbols) and corrected S_2 values (red symbols). The corrected HI varies between 75 and 210 mg HC/g TOC (average 128 mg HC/g TOC) and indicates the presence of type III kerogen in Oligocene rocks (see also Fig. 5.3). HI values from Eocene rocks vary between 122 and 402 mg HC/g TOC (average 238 mg HC/g TOC), indicating type III-II kerogen (Fig. 5.3).

Measured vitrinite reflectance values range from 0.41 to 0.56% R_r (see Appendix E) but do not show a clear depth trend (Fig. 5.1). In general, there is a good fit between measured vitrinite reflectance (VR) and vitrinite reflectance calculated from T_{max} using Eq. 4.4 (see Section 4.4). The measured vitrinite reflectance of the NOR-72-184 sample (4748 to 4751 m) is 0.43% R_r, indicating that even the deepest sample is thermally immature. Low maturity is also indicated by vitrinite with orange interior reflections in NOR-72-26 (3825 to 3830 m).

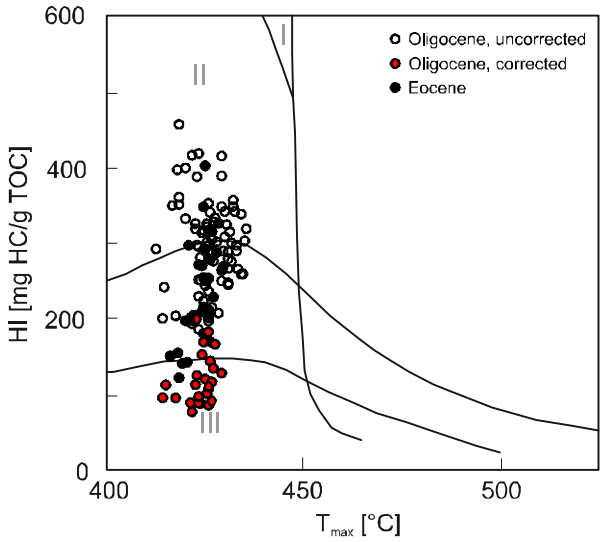

Figure 5.3: Hydrogen Index (HI) based on uncorrected and corrected S_2 values versus T_{max} for Norio-72.

As seen in Table 5.1, PI values in Oligocene (0.26) and Eocene sediments (0.62) differ considerably, which may be an effect of different types of contamination in sample sets delivered separately in October and December 2013. Thus, PI values are of no use for the interpretation of maturity.

5.1.4 Biomarker Proxies

Three Eocene and three Oligocene sample extracts from Norio-72 were analysed for molecular biomarkers, the results of which are included in Appendix F. All Eocene samples show evidence of contamination by OBM. An example chromatogram of these extracts is shown in Fig. 5.4. In these samples, *n*-alkanes, pristane, and phytane could be quantified. However, steranes and hopanes are either absent or occur in amounts below the detection limit. Thus, quantification of aromatic fractions for the Eocene samples was not justified.

C_{29}-sterane isomerization ratios of Oligocene sample extracts from Norio-72 vary significantly (Fig. 5.5) despite similar depths, making it impossible to use this parameter as a maturity indicator. It is likely that this variation is due to contamination, rendering the biomarker data derived from Norio-72 samples unsuitable for further interpretations on depositional setting and source input.

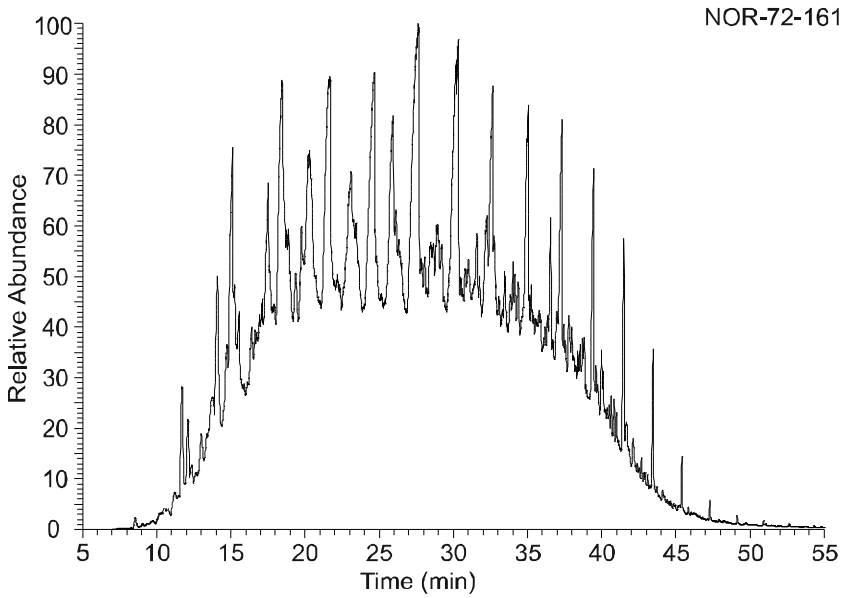

Figure 5.4: A chromatogram of the aliphatic fraction of Eocene sample NOR-72-161. The "hill" could be associated with biodegradation or contamination.

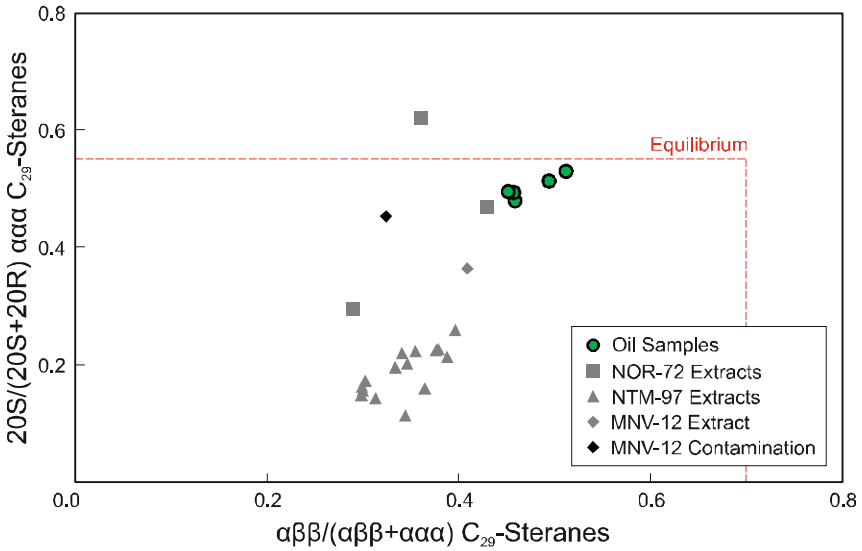

Figure 5.5: Thermal maturity parameters based on apparent isomerization of asymmetric centers in C_{29} steranes for oil samples and rock extracts measured using GC-MS. $\alpha\beta\beta/(\alpha\beta\beta+\alpha\alpha\alpha)$ isomerization is plotted against (20S)/(20S+20R) isomerization.

5.1.5 Maceral Composition

Thirteen organic matter-rich Eocene samples were selected for organic petrological investigations, the results of which are included in Appendix E. Maceral micrographs showing vitrinite, liptinite, and framboidal pyrite in the studied samples can be found in Fig. 5.6,

and a ternary diagram of maceral compositions is shown in Fig. 5.7.

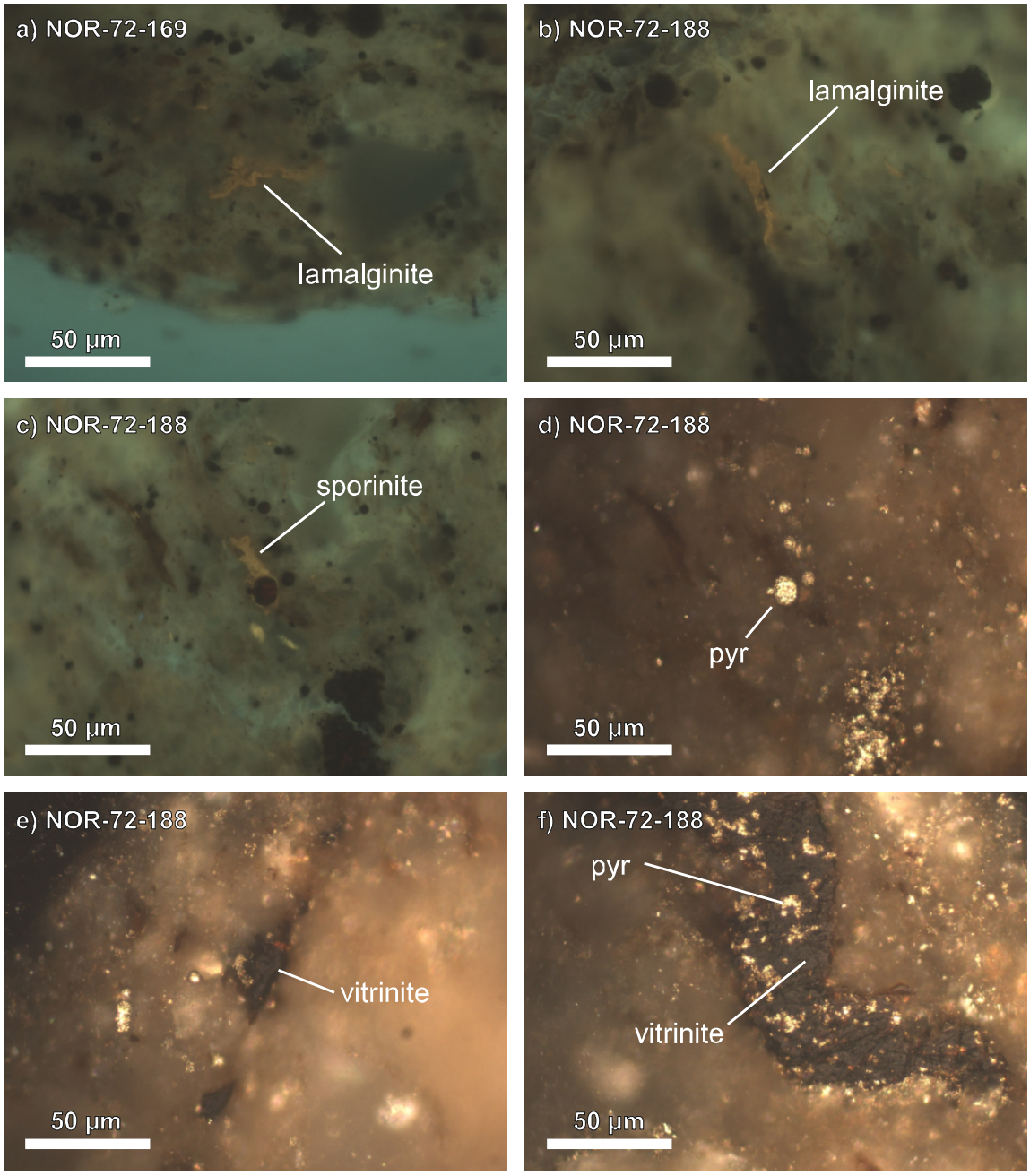

Figure 5.6: Micrographs of macerals in Norio-72 samples under fluorescent light (a-c) and reflected white light (d-f) and oil-immersion objectives (50x magnification); pyr = framboidal pyrite.

In the most of the studied samples, liptinite is the most abundant maceral group (up to 80 vol.%). The only exceptions are NOR-72-181 (4718 to 4721 m), NOR-72-183 (4739 to 4742 m), and NOR-72-195 (4895 to 4862 m), where vitrinite is the most dominant maceral

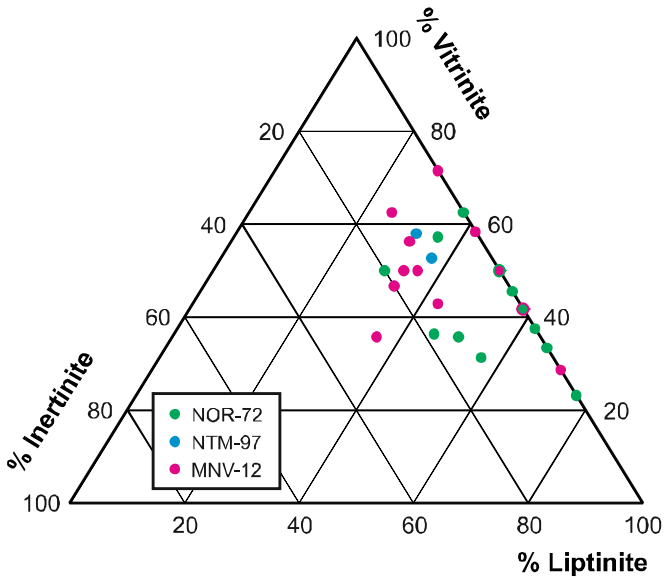

Figure 5.7: Maceral composition of samples from Norio-72, Ninotsminda-97, and Manavi-12.

group. The samples also contain small amounts of inertinite (up to 20 vol.%). There is a general trend that samples with high liptinite/inertinite ratios are characterized by higher HI values than liptinite-poor samples.

The liptinite exhibits orange fluorescence and is present mostly in the form of lamalginite (see Fig. 5.6). However, telalginite and sporinite with visible cell structures as well as liptodetrinite can also be observed. Abundant framboidal pyrite, often occurring within liptinite, suggests that sedimentation may have occurred in a reducing environment. Several large vitrinite grains in NOR-72-184 (4748 to 4751 m) with diameters of up to 50 µm were used for vitrinite reflectance measurements (see previous section).

The hand-picked coal from NOR-72-92 (4155 to 4160 m) occurs as thin layers in mineral matter. Coal in NOR-72-150 (4455 to 4460 m) contains phlobaphenite and funginite.

5.2 Ninotsminda-97

5.2.1 Stratigraphy

Seven samples representing the depth interval between 2335 and 2555 m were analyzed for calcareous nannoplankton, detailed descriptions of which are included in Appendix C. Labels on the sample bags suggest that all of these samples were previously considered to be Upper Eocene. All of the samples, with the exception of NTM-97-12 (2445 to 2450 m), contain *Reticulofenestra umbilica*, a species which existed from NP16 to the upper boundary

of NP22. Because no typical Eocene forms could be observed above 2360 m, these samples are assigned to the Lower Oligocene (Pshekian: NP21/22). Samples between 2375 and 2525 m contain *Cibrocentrum reticulatum*, placing them the Upper Eocene (Priabonian). Thus, the Oligocene/Eocene boundary is located between 2360 and 2375 m (Fig. 5.8).

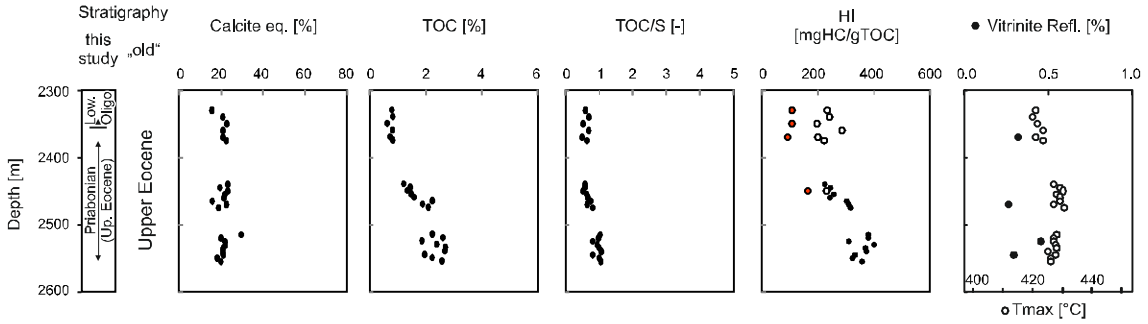

Figure 5.8: Stratigraphy and depth plots of bulk geochemical parameters and vitrinite reflectance in Ninotsminda-97. Corrected HI values are shown by red symbols and uncorrected values by open symbols. See text for further explanation. The relation between vitrinite reflectance and T_{max} is described in Eq. 4.4 in Section 4.4.

5.2.2 Bulk Geochemical Parameters and Vitrinite Reflectance

Depth profiles of bulk geochemical parameters from the Ninotsminda-97 well are illustrated in Fig. 5.8. $Calcite_{eq}$ contents are around 20% and remain constant with depth. TOC (0.6 to 2.7%; average: 1.7%) and S contents (1.18 to 2.97%; average 2.18%) increase with depth. Resulting TOC/S ratios are very low (0.5 to 1.1) and show a downward increasing trend.

Similar to Norio-72 samples, Lower Oligocene samples (2330 to 2365 m) show double-peaked Rock-Eval signals, indicating the presence of contaminating material with T_{max} values around 369°C. Corrected HI values of the shallow interval are around 100 mg/g TOC, indicating the presence of type III kerogen (Fig. 5.9). Average HI values of the organic matter-rich deeper part of the investigated section is 358 mg HC/g TOC, causing a shift from type III to type II kerogen.

T_{max} values vary between 421 and 431°C, resulting in calculated vitrinite reflectance in the order of 0.4 to 0.6% R_o. This maturity range is supported solely by the measured vitrinite reflectance in sample NTM-97-21 (0.55% R_r; 2525 to 2530 m). Other samples yielded lower vitrinite reflectance values which might have been suppressed by bitumen impregnation (e.g., Carr, 2000). Furthermore, low maturity is also confirmed by the presence of orange interior reflections in vitrinite observed in coal particles from NTM-97-9 (2370 to 2375 m;

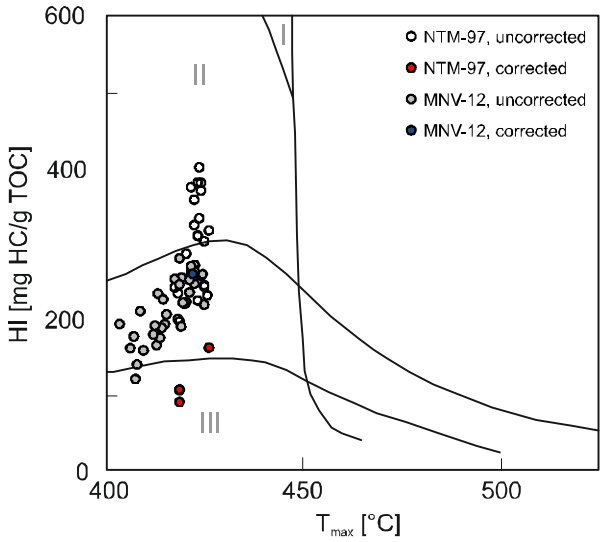

Figure 5.9: Hydrogen Index (HI) based on uncorrected and corrected S_2 values versus T_{max} for Ninotsminda-97 and Manavi-12.

0.32% R_r). Thus, maturity data indicate that the Ninotsminda-97 samples are thermally immature.

PI values decrease with depth (0.29 to 0.14) and therefore could be affected by varying degrees of contamination. For this reason, PI was not considered as a a valid maturity parameter for the Ninotsminda-97 samples.

MPI-1 values for the Ninotsminda-97 extracts range from 0.67 to 0.86, and converting this parameter according to the correlation by Radke and Welte (1983) results in overestimated values for vitrinite reflectance (0.80 to 0.92% R_e). The possibility that the Ninotsminda-97 rocks are more mature than the source rocks from which the analyzed oils were generated can be excluded (see Section 5.4). Therefore, MPI-1 is a maturity parameters which must be used cautiously.

5.2.3 Biomarker Proxies

Because Ninotsminda-97 samples show no evidence of OBM contamination, 16 samples from this well were selected for biomarker analysis. The complete biomarker data for all analyzed samples are included in Appendix F, while facies-related proxies are explained in Section 5.5.

Maturity-related parameters show pronounced depth trends.20S/20R ratios (0.11 to 0.26) and $\beta\beta/\alpha\alpha$ ratios (0.30 to 0.40) of C_{29}-steranes, along with 22S/22R values of C_{31}-

hopanes (0.45 to 0.55), increase downwards. The positions of the samples in the C_{29}-sterane isomerization plot (Fig. 5.5) indicate low maturity, supporting vitrinite reflectance and T_{max} data. Here it is important to remember that that the Ninotsminda-97 samples represent the shallowest depth interval within this study.

5.2.4 Maceral Composition

Three samples from Ninotsminda-97 were selected for semi-quantitative maceral analysis. Maceral micrographs are shown in Fig. 5.10.

Samples from Ninotsminda-97 contain more vitrinite (4 to 6 vol.%) than liptinite (2 to 3 vol.%) and very low amounts of inertinite (up to 1 vol.%, also see Fig. 5.7). Liptinite occurs mostly in the form of lamalginite, although telalginite and liptodetrinite are also present. Sporinite occurs in small amounts. Because of low maturity, the fluorescence color of the liptinite is yellow. Framboidal pyrite is common in all samples.

5.3 Manavi-12

5.3.1 Stratigraphy

Seventeen samples representing the depth interval between 3749 and 4036 m were analyzed for calcareous nannoplankton. Detailed descriptions of the observed taxa are included in Appendix C. According to information provided by CanArgo, the entire studied section represents Oligocene–Lower Miocene "Maykop" sediments (3819 to 4038 m; see Fig. 5.11).

Samples from the upper section (3749 to 3917 m) contain very low amounts of poorly preserved fossils, which hindered age determination. It remains unclear as to whether the samples above 3932 m are from the Upper Eocene or Oligocene. In contrast, samples from the lower section (3932 to 4036 m depth) are rich in calcareous nannoplankton. Based on the co-occurrence of *Cribocentrum reticulatum* and *Isthmolithus recurvus*, these samples are dated as latest Eocene (Priabonian; NP19-21).

5.3.2 Bulk Geochemical Parameters and Vitrinite Reflectance

The depth profiles of bulk geochemical parameters and vitrinite reflectance of the Manavi-12 samples are shown in Fig. 5.11. $Calcite_{eq}$ values are generally low (<10%), but everal layers with high carbonate contents occur in the lower part of the studied section. TOC of the analyzed samples range between 3.3 and 5.4%, while the average TOC is 4.2%. S contents

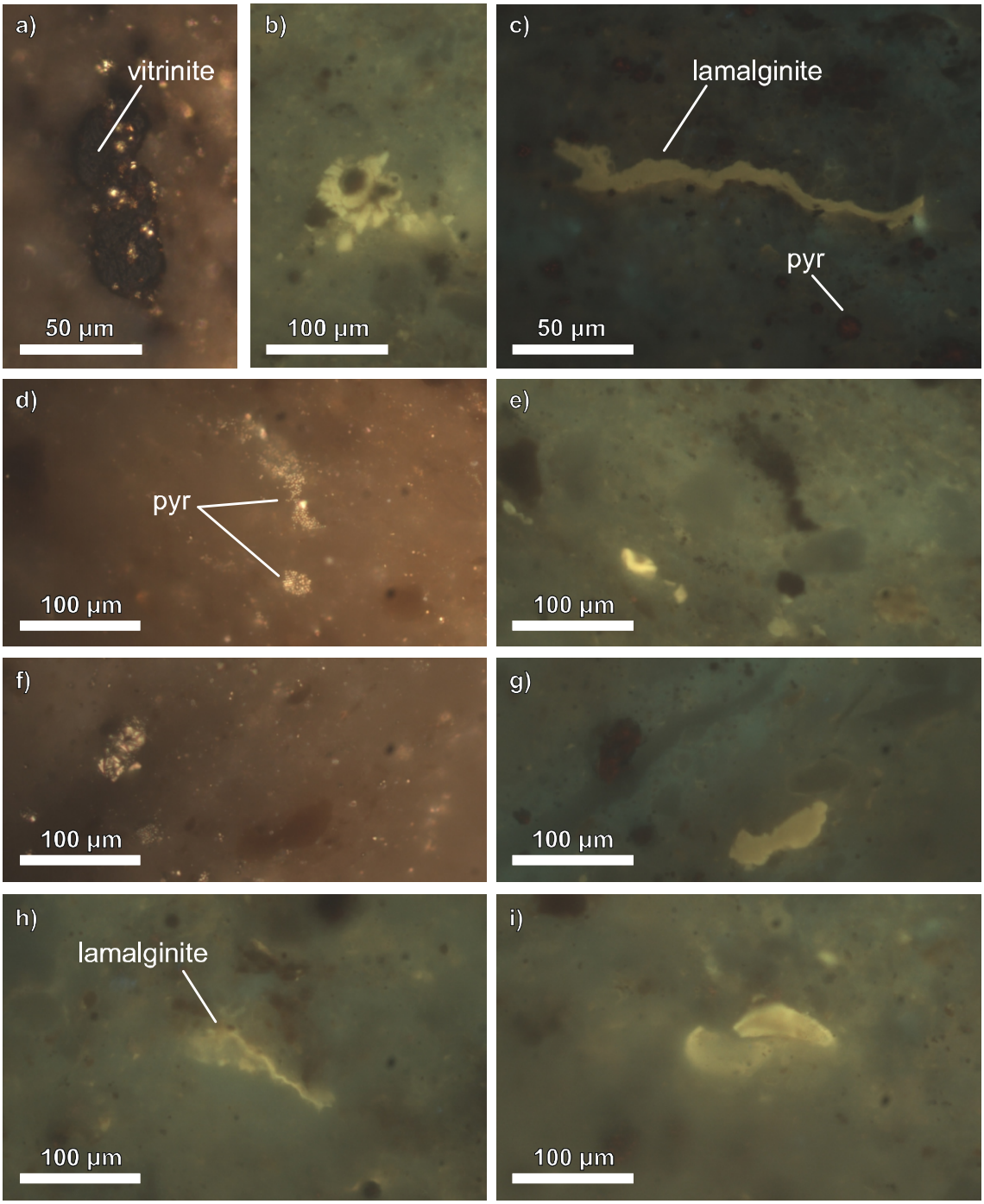

Figure 5.10: Micrographs of macerals in NTM-97-25 (2545 to 2550 m) under reflected white light (a, d, f) and fluorescent light (b, c, e, g, h, i) and oil-immersion objectives (with 50x and 100x magnification); pyr = framboidal pyrite.

vary between 1.6 and 4.1%. TOC/S ratios range from 0.9 to 2.8 and show a downward decreasing trend.

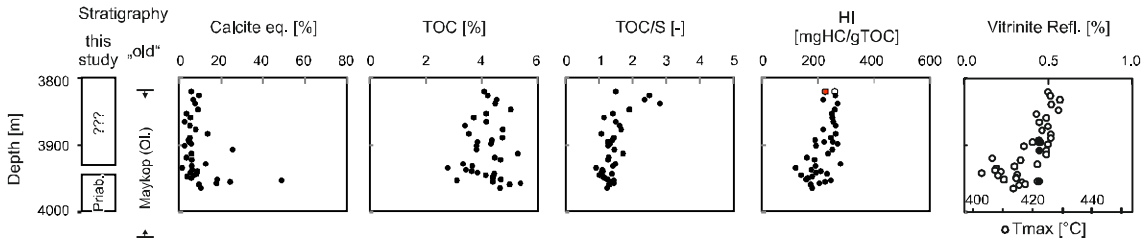

Figure 5.11: Stratigraphy and depth plots of bulk geochemical parameters and vitrinite reflectance in Manavi-12. Corrected HI values are shown by red symbols and uncorrected values by open symbols. See text for further explanation. The relation between vitrinite reflectance and T_{max} is described in Eq. 4.4 in Section 4.4.

HI values vary between 120 and 279 mg HC/g TOC, indicating the presence of type III(-II) kerogen. T_{max} values below 430°C show that the studied interval is thermally immature and has not yet entered the oil window. This is supported by the measured vitrinite reflectance of three samples (0.45% R_r), which deviate only slightly from the estimated vitrinite reflectance (0.44 to 0.49% R_o). Very high PI values (0.52 to 0.73) clearly result from contamination, i.e., adsorption of organic compounds from the OBM to the sample grains.

5.3.3 Biomarker Proxies

The MNV-12-47 sample (3958 to 3960 m) was tested for diesel oil using the GC-MS method. Chloroform was used as a solvent to wash the sample and dissolve organic compounds. Biomarker data of the chloroform-washed sample (MNV-12-47w) and the contamination (MNV-12-47m) is included in Appendix F. The chromatograms and biomarker ratios for both samples are similar. This suggests that the extract of the washed sample still contains a significant amount of contaminant. Therefore, it is assumed that the rest of the samples from Manavi-12 are also contaminated. As is the case with Norio-72, biomarker data from Manavi-12 were plotted in figures but were not used for interpretation (see Fig. 5.5 and other figures in Section 5.5).

5.3.4 Maceral Composition

Thirteen samples from Manavi-12 were selected for semi-quantitative maceral analysis. Maceral micrographs are shown in Fig. 5.12. The amount of vitrinite exceeds the amount of liptinite in most of the samples, although both are present at around 1 to 4 vol.% (Fig. 5.7). Inertinite is present in small amounts (<1 vol.%) and is nearly absent in some samples.

Lamalginite is the most common liptinite maceral occurring in samples from Manavi-12. Liptodetrinite and small amounts of telalginite are also present. Framboidal pyrite is distributed homogeneously throughout the samples. Cutinite was found in sample MNV-12-17 (3872 m). Liptinite macerals in the Manavi-12 samples are characterized by a dark orange fluorescence.

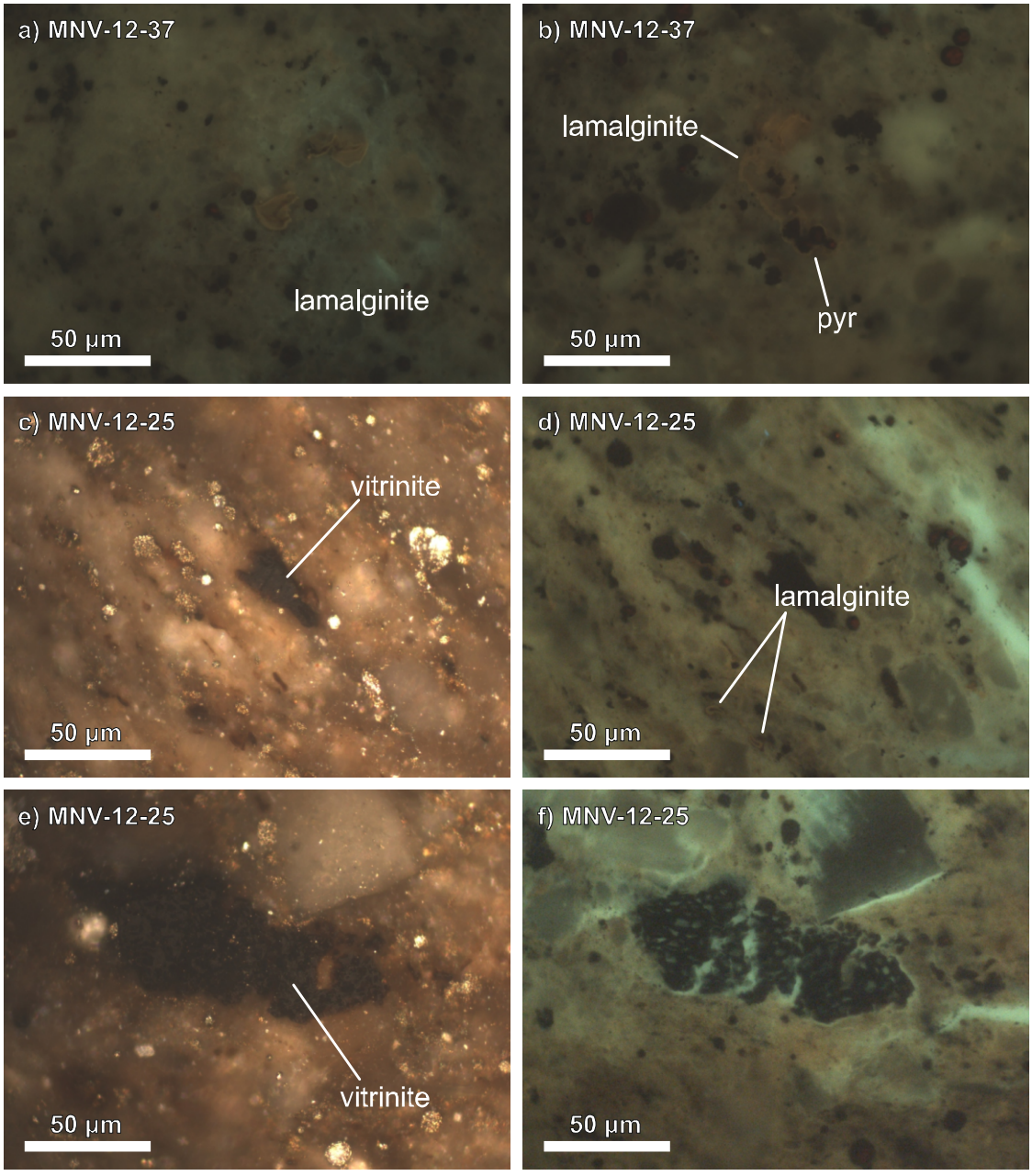

Figure 5.12: Micrographs of macerals in samples MNV-12-37 (a and b; 3938 m) and MNV-12-25 (c through f; 3896 m) under reflected white and fluorescent light and oil-immersion objectives (with 50x magnification); pyr = framboidal pyrite.

5.4 Oil Samples

Biomarker data and chromatograms of aliphatic and aromatic fractions of the five oil samples analyzed using GC-MS are shown in Appendix F. Of the four samples from the Ninotsminda field, three came from an Eocene reservoir and one came from an Oligocene reservoir. A fifth sample originates from a Cretaceous reservoir penetrated by the Manavi-12 well. Example chromatograms of the aliphatic and aromatic fractions of the G-NTM-21 oil sample (Eocene reservoir), in which the quantified peaks are labeled, are presented in Fig. 5.13.

In general, the crude oil samples are characterized by relative proportions of 21 to 43 wt.% saturated compounds and 12 to 16 wt.% aromatic compounds. NSO compounds contribute between 42 and 65 wt.% to the oils. Asphaltene contents are typically very low (1 wt.%).

The oil from the Oligocene reservoir is an exception. The sample contains only 8 wt.% saturated and 4 wt.% aromatic compounds, while 31 wt.% NSO compounds and a relatively high asphaltene content of 57 wt.% are present. The *n*-alkane patterns show that the oil is not biodegraded (see also Fig. 5.16). Therefore, the high asphaltene content is attributed to asphaltene precipitation.

Indicators of source input material and depositional environment (e.g., oleanane index, Fig. 5.14; diasteranes/steranes ratios, Fig. 5.15) are discussed in detail in Section 5.5. These parameters suggest that the oils from the Eocene reservoir in the Ninotsminda field are derived from the same source as the Cretaceous reservoir oil from Manavi-12. In contrast, the Oligocene reservoir oil from the Ninotsminda field is likely to come from a different source.

In the C_{29}-steranes isomerization plot (Fig. 5.5), all of the oil samples form a cluster close to equilibrium, with 20S/20R values between 0.48 and 0.53 and $\beta\beta/\alpha\alpha$ values between 0.45 and 0.51. This indicates that the source rock from which the oils are derived are more mature than the Ninotsminda-97 rock extracts. Similar to 20S/20R C_{29}-steranes isomerization, the 22S/22R C_{31}-hopanes isomerization ratios of the oil samples are also close to equilibrium. Vitrinite reflectance calculated from MPI-1 suggests that the level of thermal maturity of the source rock during hydrocarbon generation approximated 0.8 $\%R_c$.

5.5 Depositional Environment and Source Input

A number of biomarker parameters were plotted in order to determine the depositional environment and source input of (1) the intervals represented by the studied cuttings sam-

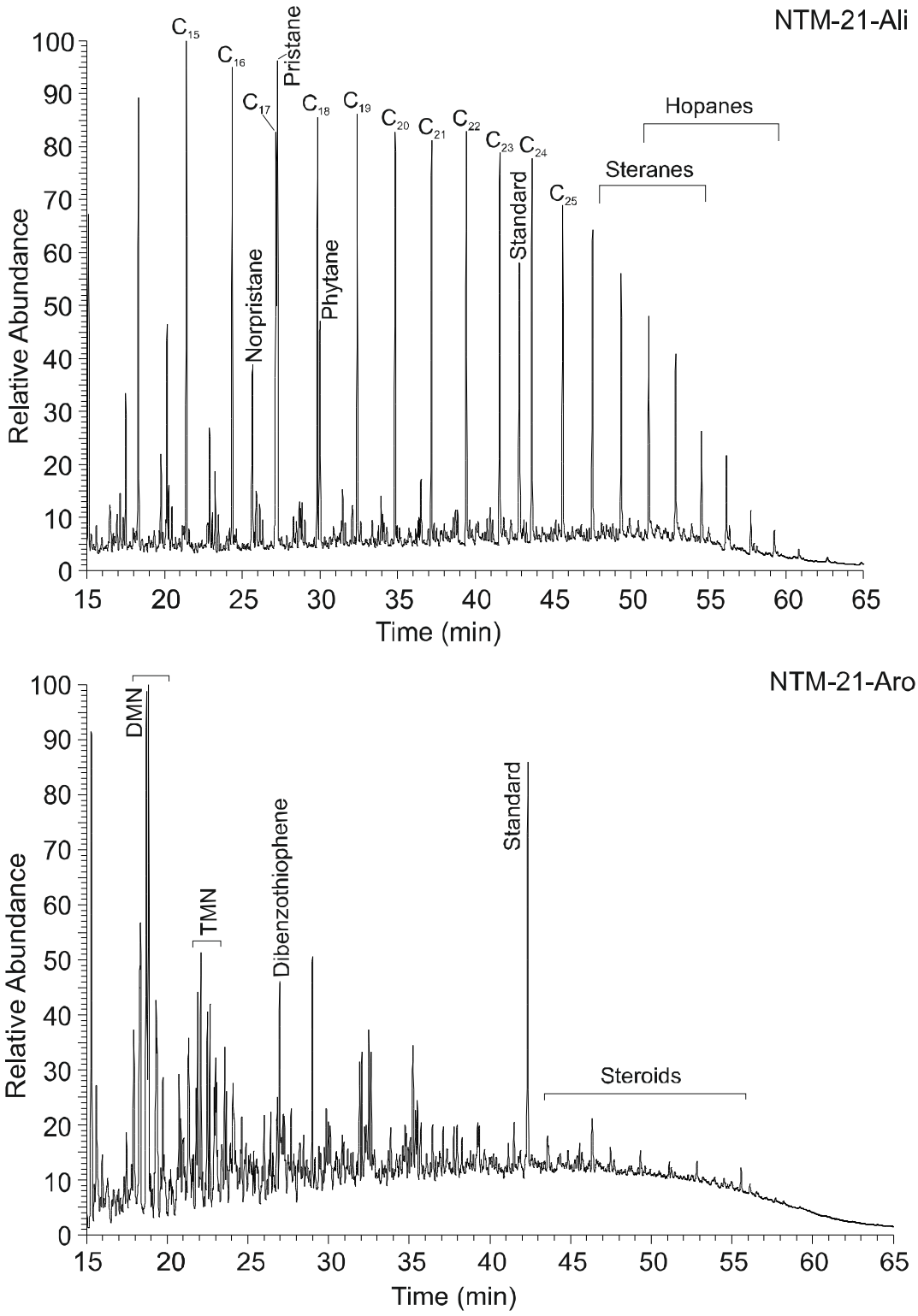

Figure 5.13: Chromatograms of the aliphatic (top) and atomatic (bottom) fractions of the Eocene oil sample G-NTM-21. The labeled peaks were quantified.

ples and (2) the source rocks from which the oil samples were derived (see Section 4.7 for explanation). Because of the impact of contamination on the measured biomarker parameters, GC-MS data of the Norio-72 and Manavi-12 extracts were not used for correlation, as mentioned in the previous sections.

The Pr/Ph ratios of the Ninotsminda-97 extracts (1.3 to 2.3) show that the sediments were deposited under dysaerobic conditions (Fig. 5.14; Didyk et al., 1978). Similarly, Pr/Ph ratios of the oil samples (1.5 to 1.9) also indicate oxygen-depleted conditions during source rock deposition. High S contents (2.10 to 2.97%) in the cuttings samples from which these extracts were derived can be attributed to the abundance of framboidal pyrite, which is also evidence of oxygen-depleted conditions at deposition.

The occurrence of oleanane in all of the extracts and oil samples confirms the presence of terrestrial organic matter in the source rocks. In addition, this age parameter confirms that the rocks are not older than Cretaceous. The oleanane index (Fig. 5.14) increases in the following sample group order: (1) oil from Oligocene reservoir, (2) oil from Eocene and Cretaceous reservoirs, and (3) Ninotsminda-97 extracts.

The C_{28}/C_{29} steranes ratio (Fig. 5.15) also functions as an age parameter for oils derived from marine source rocks. C_{28}/C_{29} steranes ratios for the oil samples (0.82 to 0.95) indicate that the age of the rocks lies between the Late Jurassic and Miocene (Grantham and Wakefield, 1988). In addition, variations in the C_{28}/C_{29} steranes ratios of the Ninotsminda-97 samples (0.9 to 1.2) reflect different amounts of terrestrial input. Ratios below 1.0, similar to those observed in oil samples, are found predominantly in the TOC-rich lower part of the studied section.

In the Pr/n-C_{17} versus Ph/n-C_{17} diagram (Fig. 5.16), the oil samples plot closely to the Ninotsminda-97 extracts, indicating that both are derived from source rocks with mixed marine-terrestrial input. This is supported by the C_{27}-C_{28}-C_{29} steranes ratios ternary plot (Fig. 5.17). Again, a good correlation between Ninotsminda-97 extracts and oil samples can be observed, all of which plot in the center of the diagram. According to Moldowan et al. (1985), this suggests that the source rocks contain mixed planktonic-bacterial-land plant input.

C_{27}-diasteranes/C_{27}-steranes ratios are often useful for distinguishing between clay-rich source rocks deposited under oxic conditions and clay-poor or carbonate source rocks deposited under anoxic conditions. However, high C_{27}-diasteranes/C_{27}-steranes ratios are also associated with high thermal maturity (Seifert and Moldowan, 1978), and therefore these ratios should only be used for source-oil correlation for samples with the same level of

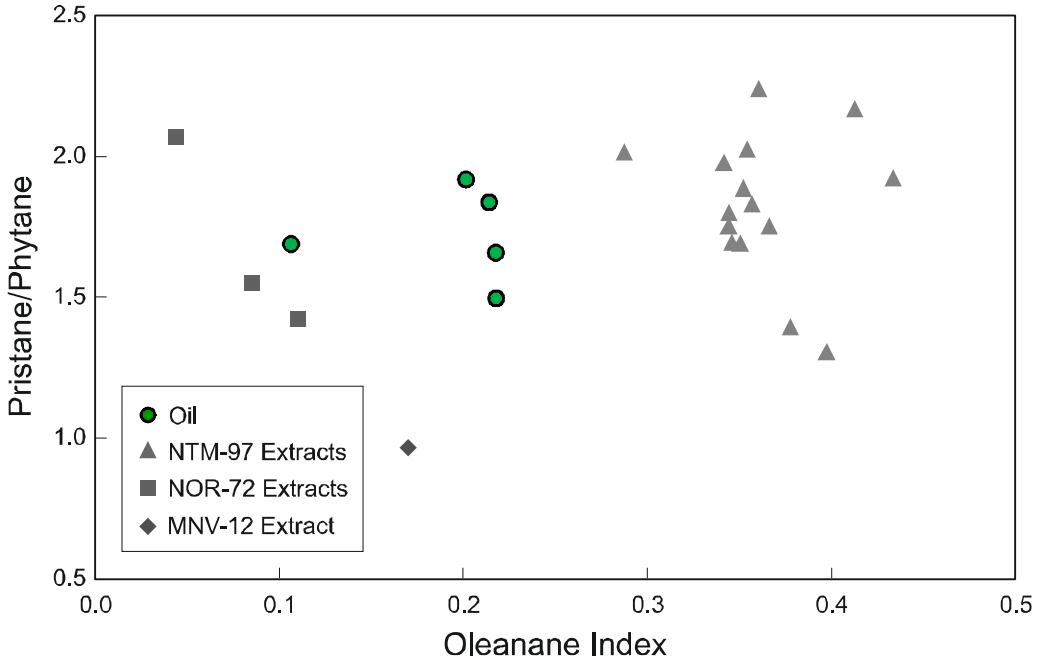

Figure 5.14: Pr/Ph ratios versus oleanane index for oil samples and rock extracts measured using GC-MS.

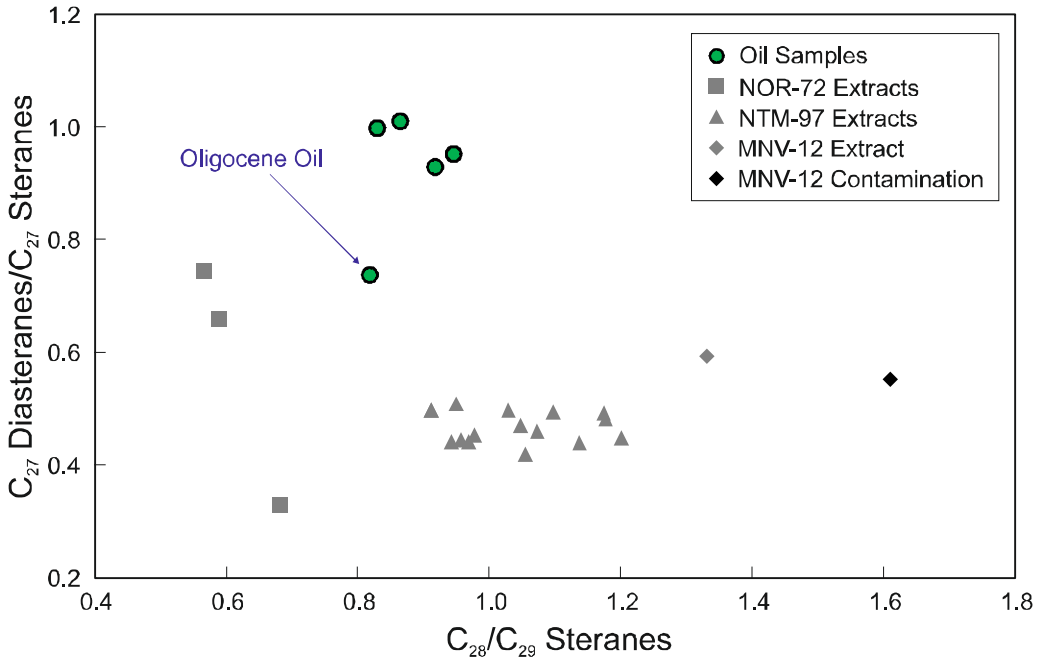

Figure 5.15: C_{27}-diasteranes/C_{27}-steranes plotted against C_{28}/C_{29} steranes ratios for oil samples and rock extracts measured using GC-MS. The Oligocene oil sample G-NTM-78 has a much lower C_{27}-diasteranes/C_{27}-steranes ratio than the other oils.

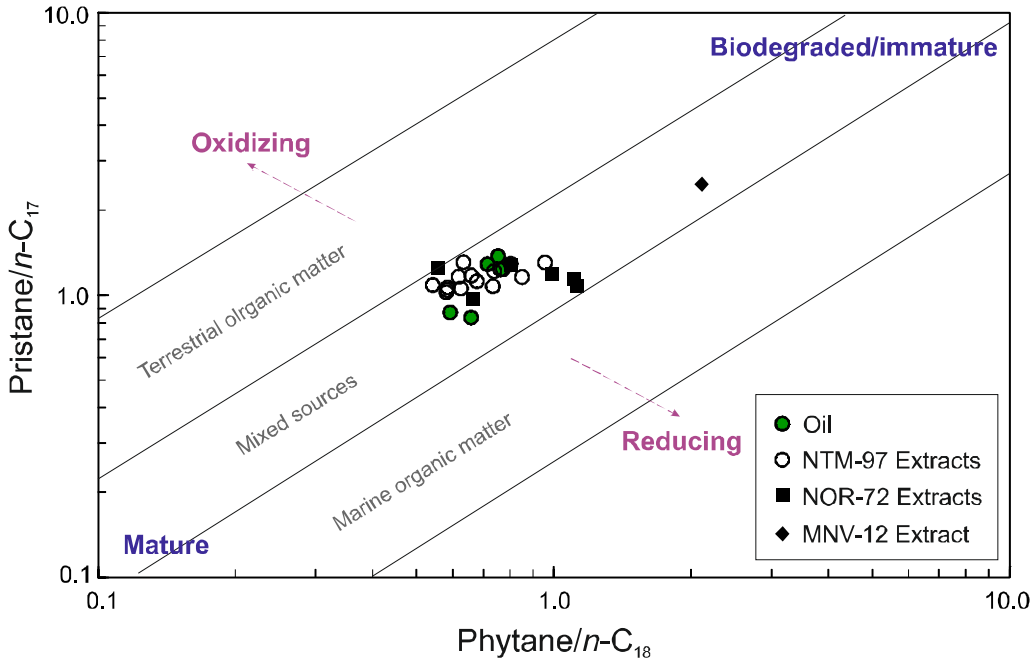

Figure 5.16: Pr/n-C_{17} versus Ph/n-C_{17} ratios for oil samples and rock extracts measured using GC-MS, enabling source-oil correlation and comparison of depositional environment (after Lijmbach, 1975).

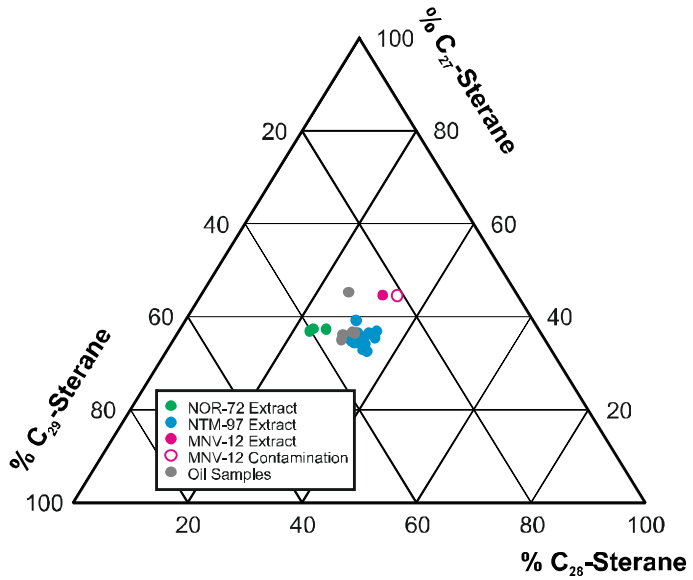

Figure 5.17: A ternary diagram of C_{27}-C_{28}-C_{29} steranes ratios.

maturity. T_{max} and vitrinite reflectance of the the Ninotsminda-97 samples point towards low thermal maturity, while the oil samples were generated from mature source rocks. Because of the difference in maturity levels, the C_{27}-diasteranes/C_{27}-steranes ratios of the oil samples cannot be directly compared with the ratios for the Ninotsminda-97 rock extracts.

The DBT/P ratio distinguishes between source rocks of marine carbonate origin and terrestrial or marine shale origin. Relatively low DBT/P ratios of the analyzed oil samples range from 0.10 to 0.17, which implies that the source rocks are not marine carbonates. DBT/P ratios for Ninotsminda-97 samples are even lower (below 0.10), arguing against free H_2S in the water column. The slight difference in DBT/P ratios between oils and rock samples does not argue against the possibility that the oil samples were generated from the studied Eocene rocks.

Carbonate Isotopy

The complete isotopic data of the O and C in carbonate minerals in selected samples from Norio-72 and Ninotsminda-97 are shown Appendix G.

A plot of the $\delta^{13}C/^{12}C$ versus $\delta^{18}O/^{16}O$ data of the carbonates in selected Norio-72 and Ninotsminda-97 samples (Fig. 5.18) shows great variability in the Norio-72 isotope ratios. These variations could be traced back to changes in diagenetic processes, although it is likely that there is substantial influence from contaminants. Therefore, isotopic data from these samples will not be discussed further.

Ninotsminda-97 samples form two clusters with a noticeable difference in $\delta^{13}C/^{12}C$ ratios. Fluctuations in the $\delta^{18}O/^{16}O$ ratios (-5.6 to -3.5) may be related to changes in water temperature and diagenetic processes. $\delta^{13}C/^{12}C$ ratios show normal marine values (-1.6 to 0) in the upper and lower section. Samples with light C isotopes (-7.8 to -3.8) are restricted to the middle section (2440 to 2475 m). These values might indicate incorporation of bacterially derived, isotopically lighter C into the carbonate minerals.

Implications for Oil-Source Correlation

Biomarker proxies obtained from the oil samples and the Ninotsminda-97 rock extracts have led to several conclusions. Firstly, the oils from the Eocene reservoirs (Ninotsminda field) and Cretaceous reservoir (Manavi-12) form one oil family (Fig. 5.14 and 5.15). These are most likely derived from Eocene organic matter-rich source rocks of marine-terrestrial origin at a maturity between 0.75 and 0.85%R_r.

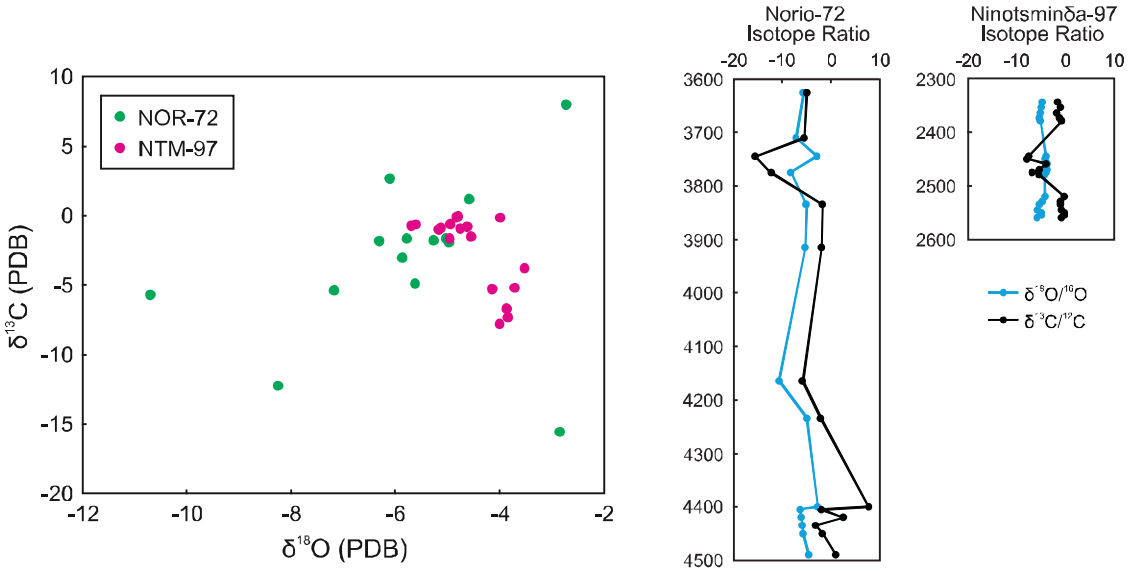

Figure 5.18: $\delta^{13}C/^{12}C$ versus $\delta^{18}O/^{16}O$ of calcite in Oligocene rocks from well Norio-72 and Upper Eocene rocks from Ninotsminda-97 (left); depth plots of isotope ratios (right).

Asphaltene-rich oil from the Oligocene reservoir in the Ninotsminda field (G-NTM-78) forms a separate oil family. It is possible that an additional source rock contributed to the oil accumulation in this reservoir.

5.6 Maturity Modeling

Thermal histories were studied for the Norio-72 and Ninotsminda-97 wells. While modeling the burial history curves, the lithology of the wells and the newly-obtained biostratigraphic data from this study were taken into consideration. The models were calibrated with maturity data (measured vitrinite reflectance, vitrinite reflectance calculated from T_{max}, and sterane and hopane isomerization ratios). Temperature data were not available.

Input data for the models presented in this chapter are listed in Appendix H. The same water depth trends and SWI temperatures were adopted for both wells. The Pliocene and Quaternary were considered as periods of erosion. Pre-defined physical parameters for different lithologies from software were adopted, while the applied time scale follows Gradstein et al. (2004). All of the above information was used to reconstruct de-compacted subsidence histories and the temperature field through time. The models were calibrated by adjusting the heat flow and the thickness of eroded Miocene rocks until a satisfactory fit between measured and calculated vitrinite reflectance and biomarker ratios was obtained.

Vitrinite reflectance was calculated using the kinetic EASY%R_o approach (Sweeney and Burnham, 1990). Biomarker ratios were calculated using kinetic data from Rullkötter and Marzi (1988). Because vitrinite reflectance and biomarker ratios are mainly controlled by maximum temperatures, only the heat flow around times of maximum temperature could be determined precisely. For the sake of simplicity, time-constant heat flow was assumed in the models (see also Patton, 1993). For each of the modeled wells, a "cold" and "hot" scenario was modeled with 40 and 50 mW/m^2 respectively.

"Cold" Heat Flow Scenario (40 mW/m^2)

The burial history curve for the "cold" scenario for Norio-72 is shown in Fig. 5.19. An acceptable fit with biomarker data, measured vitrinite reflectance, and calculated vitrinite data from the Eocene section (Fig. 5.20) was obtained in a model in which the thickness of the eroded sediments was 500 m. The time plots in Fig. 5.21 show that hydrocarbon generation was minor and did not commence until the Late Miocene. Hydrocarbon generation before the Late Miocene was negligible.

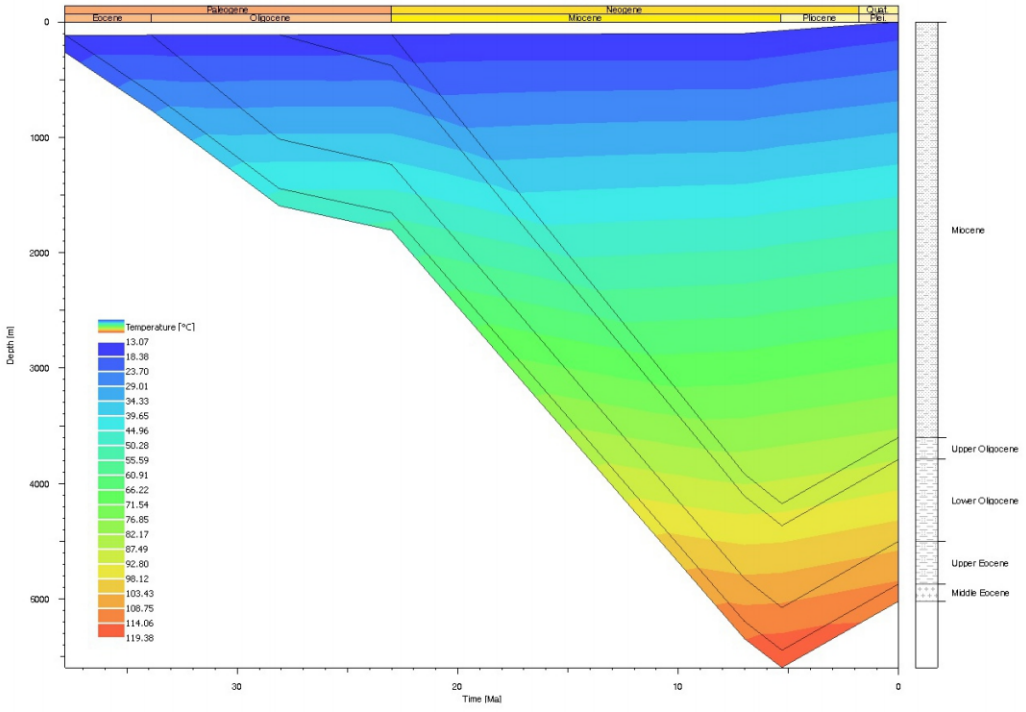

Figure 5.19: Burial history curve for the Norio-72 "cold" scenario.

The burial history curve of the Ninotsminda-97 "cold" scenario is presented in Fig. 5.22. In this well, the "cold" scenario and erosion of 2000 m-thick Miocene sediments result in a good fit with vitrinite reflectance and biomarker data, although hopane isomerization ratios

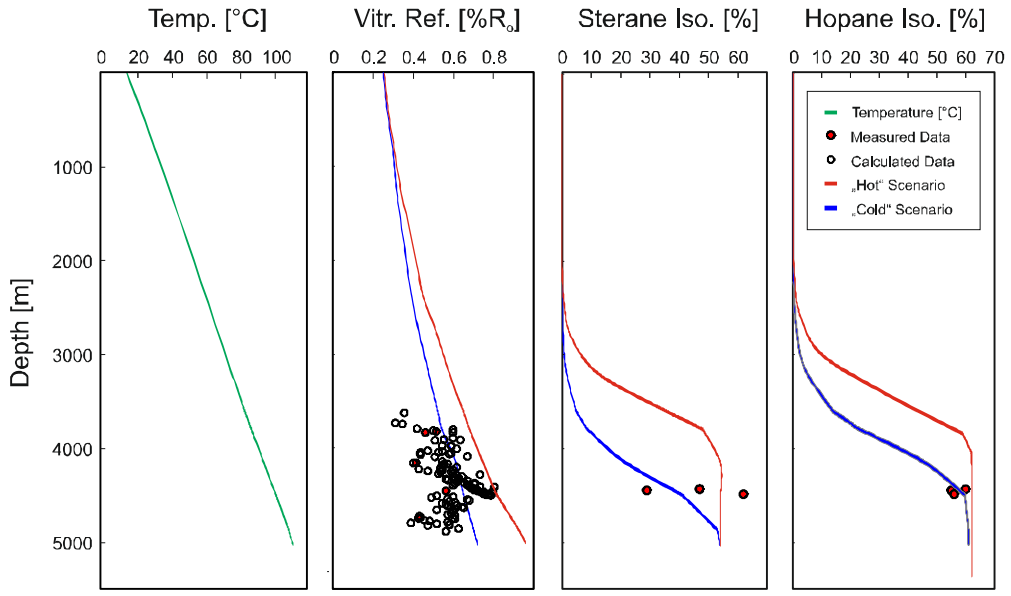

Figure 5.20: Depth plots of temperature, vitrinite reflectance, sterane and hopane isomerization for Norio-72 "cold" and "hot" scenarios. Measured data are shown with red symbols. Calculated vitrinite reflectance data (open symbols) are derived from T_{max} using Eq. 4.4 in Section 4.4.

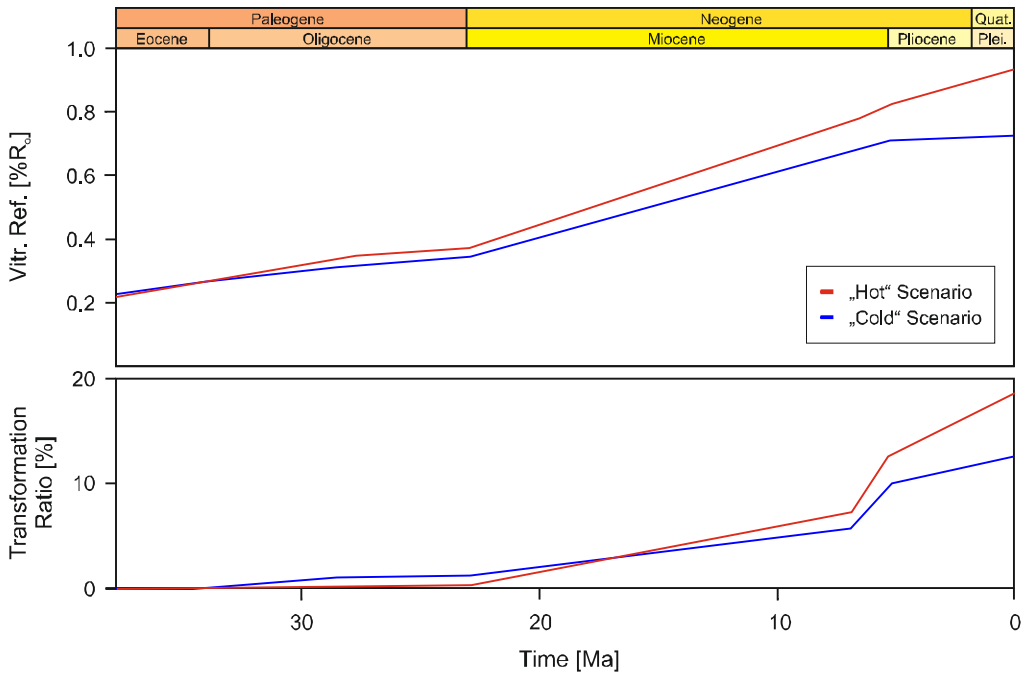

Figure 5.21: Time plots of maturity and transformation ratio for Norio-72 "cold" and "hot" scenarios, calibrated with measured and calculated vitrinite reflectance data.

are slightly underestimated (Fig. 5.23). However, measured vitrinite reflectance data from the lower part of the Oligocene section are overestimated. A time plot of the transformation ratio (Fig. 5.24) shows that no hydrocarbons have been generated from the studied source rock intervals in the Ninotsminda area.

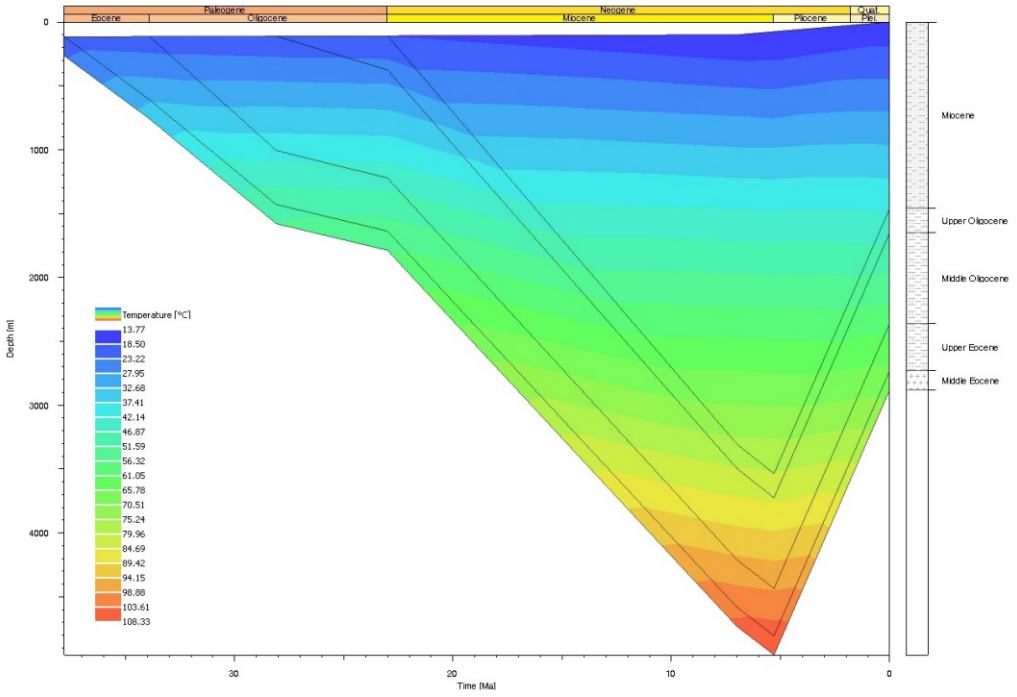

Figure 5.22: Burial history curve for the Ninotsminda-97 "cold" scenario.

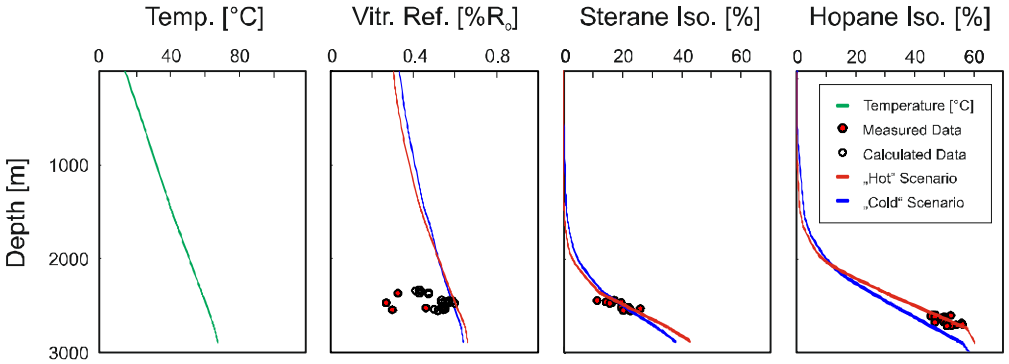

Figure 5.23: Depth plots of temperature, vitrinite reflectance, sterane and hopane isomerization for Ninotsminda-97 "cold" and "hot" scenarios. Measured data are shown with red symbols. Calculated vitrinite reflectance data (open symbols) are derived from T_{max} using Eq. 4.4 in Section 4.4.

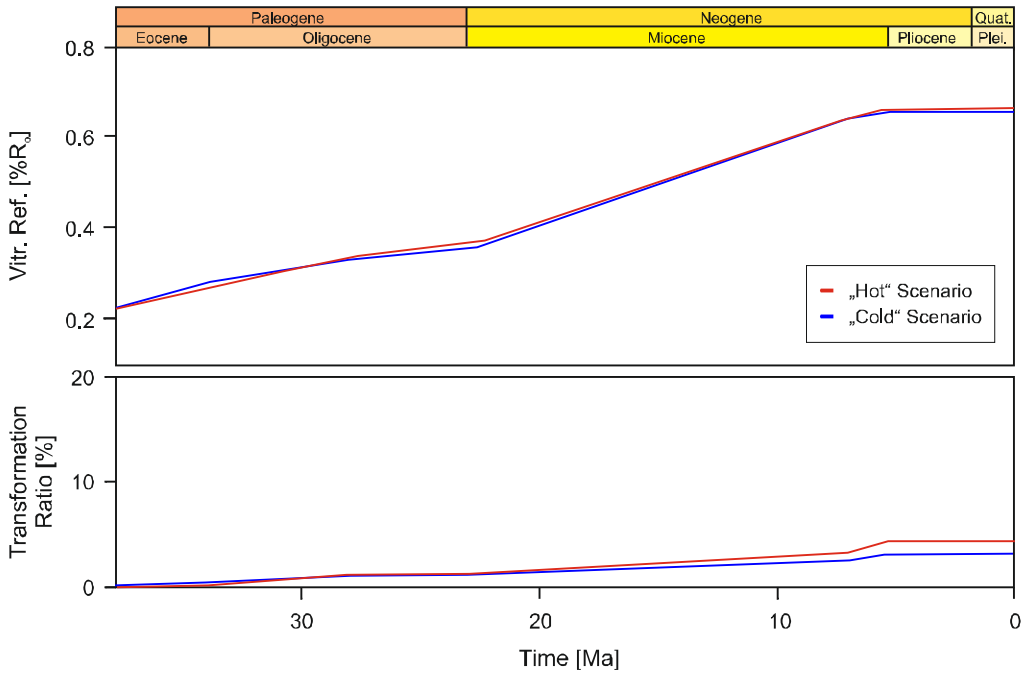

Figure 5.24: Time plots of maturity and transformation ratio for Ninotsminda-97 "cold" and "hot" scenarios, calibrated with measured and calculated vitrinite reflectance data.

"Hot" Heat Flow Scenario (50 mW/m^2)

The burial history curve for the "hot" scenario for Norio-72 and Ninotsminda-97 are shown in Fig. 5.25 and 5.26. In the Norio-72 well, the "hot" heat flow scenario resulted in a fit with vitrinite data near the base of the Oligocene interval. However, the model showed a tendency towards overestimating biomarker ratios, even when no erosion was considered (Fig. 5.20). Only slightly more hydrocarbons were generated in the "hot" scenario than in the "cold" scenario (Fig. 5.21).

In the Ninotsminda-97 well, a heat flow of 50 mW/m^2 resulted in a good fit with calibration data as soon as the eroded thickness was reduced to 800 m (Fig. 5.23). As in the "cold" scenario, no significant hydrocarbon generation occurred in the studied source rocks in this well (Fig. 5.24).

Implications for Heat Flow, Thickness of Eroded Rocks, and HC Generation

Several interpretations could be made based on the four models which have been discussed. Results point to relatively low paleo-heat flow in the order of 40 to 45 mW/m^2. This

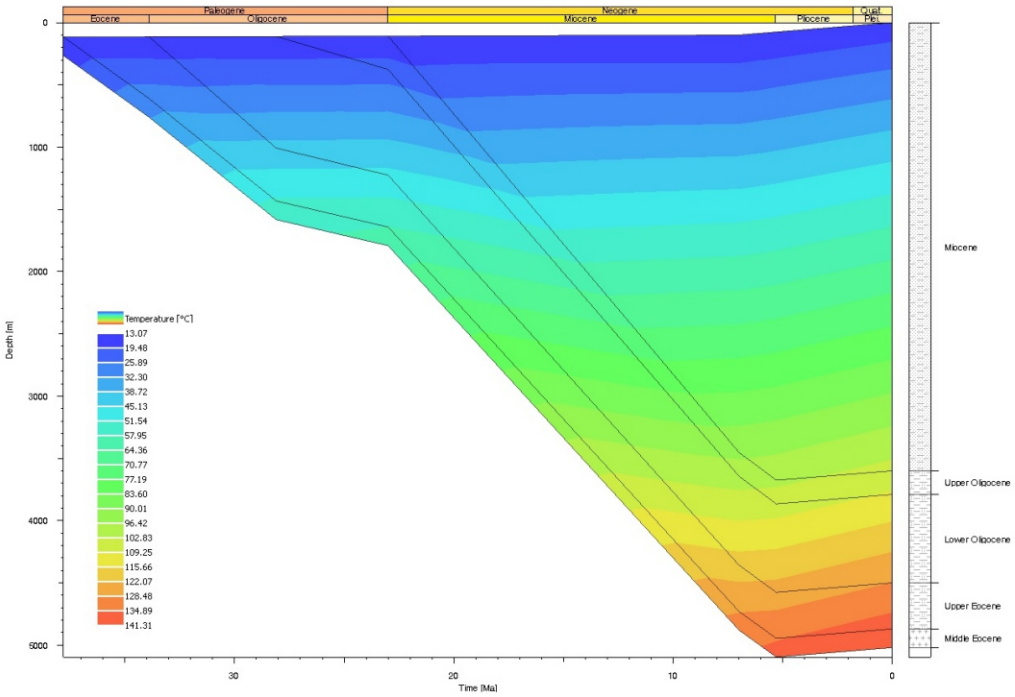

Figure 5.25: Burial history curve for the Norio-72 "hot" scenario.

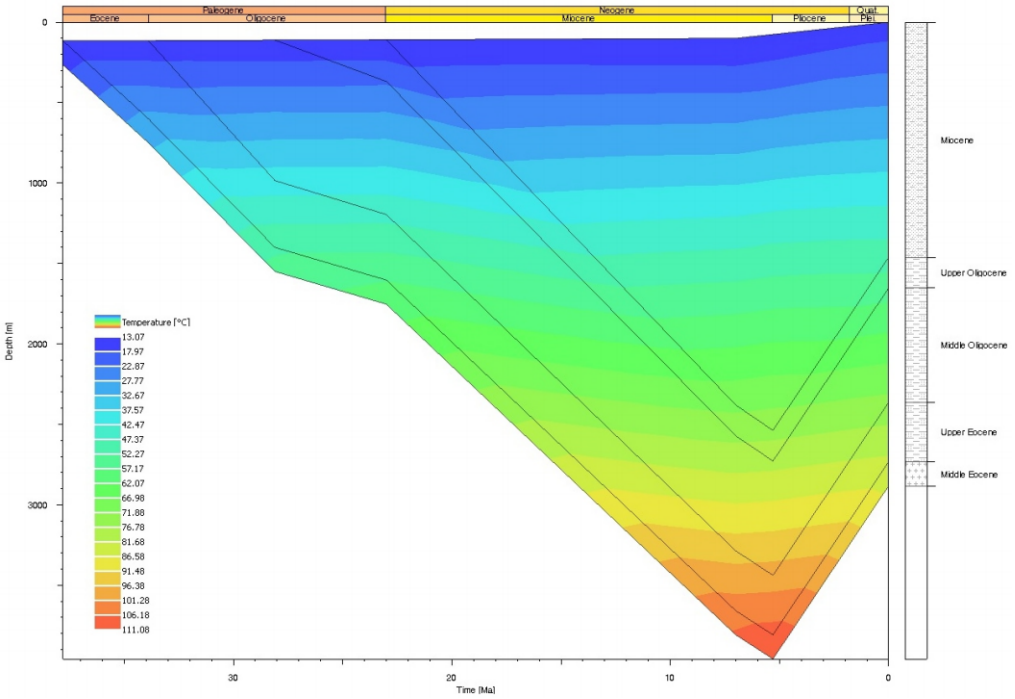

Figure 5.26: Burial history curve for the Ninotsminda-97 "hot" scenario.

estimate agrees with the low geothermal gradients of the area (28°C/km; Patton, 1993). A heat flow higher than 50 mW/m^2 can be excluded.

According to the 1-D models, the thickness of the eroded Miocene rocks in Ninotsminda-97 (800 to 2000 m) was greater than in Norio-72 (0 to 500 m). However, the original thickness of the combined Oligocene and Miocene rocks prior to erosion in Norio-72 (cold scenario: 5000 m: hot scenario: 4500 m) was greater than in Ninotsminda-97 (cold scenario: 4360 m; hot scenario: 3160 m).

Time plots reveal that due to the relatively low heat flow, significant hydrocarbon generation did not occur until a maximum burial depth exceeding 5500 m was reached. This suggests that in the studied area, hydrocarbons could not have been generated by the Oligocene interval, as only the Eocene succession reached the top of the oil window.

6. Conclusions

The study aimed at obtaining a clear stratigraphy of the studied successions represented by the drill cuttings samples and evaluating their hydrocarbon potential. Contamination of the analyzed samples became a key issue throughout the entire study and necessitated modifications in the original analytical program. Because the effects of OBM could not be removed completely (e.g., bimodal peaks in Rock-Eval signals), it is impossible to exclude that the rock data is still affected by residual contamination. Nevertheless, important results on the source rocks and their hydrocarbon potential in the studied area could be obtained.

One of the main findings of this study is the revised biostratigraphy of the studied successions, which were previously assigned to the Upper Eocene (Ninotsminda-97 samples) and the Oligocene–Lower Miocene "Maykop" formations (Norio-72 and Manavi-12 samples). Based on calcareous nannoplankton analysis by S. Ćorić, the following age assignments were established:

Well	**Depth** [m]	**Age**
Norio-72	3625 – 3790	Late Oligocene
	3790 – 4500	Early Oligocene
	4500 – 4891	Eocene
Ninotsminda-97	2330 – 2360/2375	Early Oligocene
	2360/2375 – 2560	Late Eocene
Manavi-12	3749 – 3932	Late Eocene or Late Oligocene
	3932 – 4036	Late Eocene

Table 6.1: Summary of the age assignment of the studied successions.

According to the nomenclature by Peters and Cassa (1994) and based on the quantity of organic matter in the cuttings samples (i.e., TOC), the source potential of the studied successions range from "poor" to "good" in the Oligocene section and from "very good" to "excellent" in the Eocene section of Norio-72. In the case of this well, however, it is possible

that the relatively high TOC contents are associated with migrated foreign hydrocarbons or impregnation by OBM. Throughout the lowermost Oligocene, TOC contents increase with depth. TOC/S ratios below 2.8 indicate sediment deposition in oxygen-deficient environments, which is further supported by biomarker data. Ninotsminda-97 provided the cleanest cuttings samples, with TOC contents within the "fair" to "very good" range. Manavi-12 cuttings, which also show contaminant residue, would normally be categorized as having "very good" to "excellent" potential.

The organic matter input in the studied samples originates from a mixed marine and terrestrial source, resulting in type III-II kerogen (see Fig. 5.3 and 5.9). Type II kerogen prevails in the Eocene succession. Maturity parameters incorporated into this study show that samples from Norio-72 and Manavi-12 are marginal mature, whereas Ninotsminda-97 samples are immature.

Biomarker data enabled oil-source correlation to a limited extent. Oils from the Eocene and Cretaceous reservoirs in the Ninotsminda field and Manavi-12 well may have been generated from Eocene source rocks and form one oil family. On the other hand, the asphaltene-rich oil sample from the Oligocene reservoir in the Ninotsminda field must belong to a separate oil family.

Although the Oligocene and Miocene successions in Norio-72 were thicker than those in Ninotsminda-97, 1-D basin modeling revealed that the magnitude of erosion was greater in the Ninotsminda area. Thermal maturity models created using information about basin history showed that hydrocarbon generation in the studied area could only occur at a maximum burial depth exceeding 5500 m due to a relatively low heat flow of around 45 mW/m^2. Any hydrocarbons generated from source rocks in the studied area could not have originated from the Oligocene succession, as only the Upper Eocene reached the top of the oil window.

To conclude, following the nomenclature of Peters (1986) leads to the determination of a "poor" hydrocarbon potential for the upper part of the Oligocene. The lower part of the Oligocene holds a "fair" gas and oil potential. In contrast, the Eocene succession shows a "very good" generative potential for gas and oil. These results show that although the Oligocene to Lower Miocene ("Maykop") rocks have been widely considered as very important source rocks contributing to hydrocarbon accumulations in the Near-Tbilisi area, the Upper Eocene succession shows greater generation potential. These findings may provide a basis for placing greater attention on the Upper Eocene succession as potential source rocks in the region. Future investigations using core and outcrop samples which have not been affected by contamination may lead to optimized evaluation of the Eocene and Oligocene source potential.

Bibliography

Adamia, S. (1991). The Caucasian Oil and Gas Province. In *Hydrocarbon Prospects in Eastern Europe and USSR. The Paleozoic of the Uralo-Mongolian Fold System*, volume 7(1-11) of *Occasional Publications ESRI New Series*, pages 53–74. Earth Sciences and Resources Institute, University of South Carolina.

Adamia, S., Zakariadze, G., Chkhotua, T., Sadradze, N., Tsereteli, N., Chabukiani, A., and Gventsadze, A. (2011). Geology of the Caucasus: A Review. *Turkish J. Earth Sci.*, 20:189–544.

Berner, R. A. (1984). Sedimentary pyrite formation: An update. *Geochim. Cosmochim. Acta.* 18:605–615.

Berner, R. A. and Raiswell, R. (1983). Burial of organic carbon and pyrite sulphur in sediments over Phanerozoic time: a new theory. *Geochim. Cosmochim. Acta*, 47:855–862.

Brindley, G. W. and Brown, G. (1980). *Crystal Structures of Clay Minerals and Their X-ray Identification.* Mineralogical Society, London.

Carr, A. D. (2000). Suppression and retardation of vitrinite reflectance, part 1: Formation and significance for hydrocarbon generation. *J. Pet. Geol.*, 23:313–343.

Didyk, B. M., Simoneit, B. R. T., Brassell, S. C., and Eglinton, G. (1978). Organic geochemical indicators of paleoenvironmental conditions of sedimentation. *Nature*, 272:216–222.

Eppelbaum, L. and Khesin, B. (2012). Tectonical-Geophysical Setting of the Caucasus. In *Geophysical Studies in the Caucasus*, pages 5–37. Springer Berlin Heidelberg.

Espitalié, J., Laporte, L. J., Madec, M., Marquis, F., Leplat, P., Paulet, J., and Boutefeu, A. (1977). Méthode rapide de characterisation des roches mères de leur potential pétrolier et de leur degree d'evolution. *Rev. Inst. Franc. Pétrole*, 32:23–42.

Gamkrelidze, P. (1964). Geology of the USSR. Georgian SSR. Moscow-Leningrad.

Goossens, H., de Leeuw, J. W., Schenck, P. A., and Brassell, S. C. (1984). Tocopherols as likely precursors of pristane in ancient sediments and crude oils. *Nature*, 312:440–442.

Gradstein, F. M., Ogg, J. G., and Smith, A. G. (2004). *A Geologic Time Scale 2004*. Cambridge University Press, Cambridge.

Grantham, P. J. and Wakefield, L. L. (1988). Variations in the sterane carbon number distributions of marine source rock derived crude oils through geological time. *Org. Geochem.*, 12:61–74.

Graves, W. (1986). Bit-generated rock textures and their effect on evaluation of lithology, porosity, and shows in drill-cutting samples. *AAPG Bull.*, 70:1129–1135.

Guliyev, I. S., Mamedov, P. Z., Feyzullayev, A. A., Huseynov, D. A., Kadirov, F. A., Aliyeva, E. H., and Tagiyev, M. F. (2003). *Hydrocarbon Systems of the South Caspian Basin*. Nafta-Press, Baku.

Hughes, W. B., Holba, A. G., and Dzou, L. I. P. (1995). The ratios of dibenzothiophene to phenanthrene and pristane to phytane as indicators of depositional environment and lithology of petroleum source rocks. *Geochim. Cosmochim. Ac.*, 59:3581–3598.

Khain, V. E. and Koronovsky, N. V. (1997). Caucasus. In Moores, E. M. and Fairbridge, R. W., editors, *Encyclopedia of European and Asian Regional Geology*, volume 19 of *Encyclopedia of Earth Sciences Series*, pages 127–136. Chapman and Hill.

Killops, S. D. and Killops, V. J. (1997). *Einführung in die Organische Geochemie*. Ferdinand Enke Verlag, Stuttgart.

Köster, J., Rospondek, M., Schouten, S., Kotarba, M., Zubrzycki, A., and Damsté, J. S. (1998). Biomarker geochemistry of a foreland basin; the Oligocene Melinite Formation in the Flysch Carpathians of Southeast Poland. *Org. Geochem.*, 29:649–669.

Lijmbach, G. W. M. (1975). On the origin of petroleum. In *Proceedings Ninth World Petroleum Congress*, pages 357–369, London. Applied Sciences Publisher.

Mello, M. R., Gaglianone, P. C., Brassell, S. C., and Maxwell, J. R. (1988). Geochemical and biological marker assessment of depositional environments using Brazilian offshore oils. *Mar. Petrol. Geol.*, 5:205–223.

Mgeladze, Z. V., Nanadze, A. O., and Papova, D. V. (1989). Explanatory Notes for the Map of Oil and Gas Fields, Prospective Structure, Oil Geological Divisions, and Deep Prognosis of Territories with Oil- and Gas-Bearing Prospects in Georgia. Technical report, State Polytechnical Institute, Tbilisi.

Moldowan, J. M., Dahl, J., Huizinga, B. J., Fago, F. J., Hickey, L. J., Peakman, T. M., and Taylor, D. W. (1994). The molecular fossil record of oleanane and its relation to angiosperms. *Science*, 265:768–771.

Moldowan, J. M., Seifert, W. K., and Gallegos, E. J. (1985). Relationship between petroleum composition and depositional environment of petroleum source rocks. *AAPG Bull.*, 69:1255–1268.

Moore, D. M. and Reynolds, R. C. (1997). *X-ray Diffraction and the Identification and Analysis of Clay Minerals*. Oxford University Press, New York.

Mukhopadhyay, P. K. and Dow, W. G. (1994). *Vitrinite Reflectance as a Maturity Parameter: Applications and Limitations*, volume 570 of *ACS symposium series*. American Chemical Society.

Murray, A. P., Sosrowidjojo, I. B., Alexander, R., Kagi, R. I., Norgate, C. M., and Summons, R. E. (1997). Oleananes in oils and sediments: Evidence of marine influence during early diagenesis? *Geochim. Cosmochim. Ac.*, 61:1261–1276.

Patton, D. K. (1993). Samgori Field. Republic of Georgia: Critical Review of Island-Arc Oil and Gas. *J. Petrol. Geol.*, 16:153–167.

Perch-Nielsen, K. (1985). Cenozoic calcareous nannofossils. In Bolli, H. M., Saunders, J. B., and Perch-Nielsen, K., editors, *Plankton Stratigraphy*, volume 1, pages 427–554. Cambridge University Press.

Peters, K. E. (1986). Guidelines for evaluating petroleum source rocks using programmed pyrolysis. *AAPG Bull.*, 70:318–329.

Peters, K. E. and Cassa, M. R. (1994). Applied Source Rock Geochemistry. In Magoon, L. B. and Dow, W. G., editors, *The Petroleum System — From Source to Trap*, volume 60 of *AAPG Memoir*, pages 93–120. American Association of Petroleum Geologists.

Peters, K. E., Clutson, M. J., and Robertson, G. (1999). Mixed marine and lacustrine input to an oil-cemented sandstone breccia from Brora, Scotland. *Org. Geochem.*, 30:237–248.

Peters, K. E. and Moldowan, J. M. (1993). *The Biomarker Guide: Interpreting Molecular Fossils in Petroleum and Ancient Sediments*. Prentice Hall.

Peters, K. E., Walters, C. C., and Moldowan, J. M. (2005a). *The Biomarker Guide: Biomarkers and Isotopes in Petroleum Systems and Earth History*, volume 2 of *The Biomarker Guide*. Cambridge University Press.

Peters, K. E., Walters, C. C., and Moldowan, J. M. (2005b). *The Biomarker Guide: Biomarkers and Isotopes in the Environment and Human History*, volume 1 of *The Biomarker Guide*. Cambridge University Press.

Philip, H., Cisternas, A., Gvishiani, A., and Gorshkov, A. (1989). The Caucasus: An Actual Example of the Initial Stages of Continental Collision. *Tectonophysics*, 161:1–21.

Popov, S. V., Akhmetiev, M. A., Bugrova, E. M., Lopatin, A. V., Andreeva-Grigorovich, A. S., Zherikhin, V. V., Zaporozhets, N. I., Nikolaeva, I. A., Krasheninnikov, V. A., Kuzmicheva, E. I., Sytchevskaya, E. K., and Shcherba, I. G. (2001). Biogeography of the Northern Peri-Tethys from the Late Eocene to the Early Miocene: Part 1. Late Eocene. *Paleontol. J.*, Suppl. 1:S1–S68.

Popov, S. V., Akhmetiev, M. A., Zaporozhets, N. I., Voronina, A. A., and Stolyarov, A. S. (1993). Evolution of Eastern Paratethys in the Late Eocene–Early Miocene. *Stratigr. Geol. Correl.*, 1:572–600.

Popov, S. V., Rögl, F., Rozanov, A. Y., Steininger, F. F., Shcherba, I. G., and Kovac, M., editors (2004). *Lithological-Paleogeographic maps of Paratethys. 10 Maps Late Eocene to Pliocene*, volume 250. Courier Forschungsinstitut Senckenberg.

Preslar, P. L. and McDermaid, J. D. (1984). Polycrystalline diamond compact bit proves effective at South Graham Deese sand unit. *Journal of Petroleum Technology*, 36:2103–2109.

Radke, M. and Welte, D. H. (1983). The Methylphenanthrene Index (MPI): A maturity parameter based on aromatic hydrocarbons. In Bjorøy, M., Albrecht, C., Cornford, C., et al., editors, *Advances in Organic Geochemistry*, pages 504–512. John Wiley and Sons, New York.

Radke, M., Willsch, H., and Welte, D. H. (1980). Preparative hydrocarbon group type determination by automated medium pressure liquid chromatography. *Anal. Chem.*, 52:406–211.

Rubinstein, I., Sieskind, O., and Albrecht, P. (1975). Rearranged steranes in a shale: occurrence of simulated formation. *J. Chem. Soc.*, Perkins Trans I:1833–1836.

Rullkötter, J. and Marzi, R. (1988). Natural and artificial maturation of biological markers in Toarcian shale from northern Germany. *Org. Geochem.*, 13:639–645.

Sachsenhofer, R. F., Stummer, B. Georgiev, G., Dellmour, R., Bechtel, A., Gratzer, R., and Corić (2009). Depositional environment and hydrocarbon source potential of the Oligocene Ruslar Formation (Kamchia Depression; Western Black Sea). *Mar. Petrol. Geol.*, 26:57–84.

Schulz, H.-M., Sachsenhofer, R. F., Bechtel, A., Polesny, H., and Wagner, L. (2002). The origin of hydrocarbon source rocks in the Austrian Molasse Basin (Eocene–Oligocene transition). *Mar. Petrol. Geol.*, 19:683–709.

Seifert, W. K. and Moldowan, J. M. (1978). Application of steranes, terpanes and monoaromatics to the maturation, migration and source of crude oils. *Geochim. Cosmochim. Ac.*, 42:77–95.

Seifert, W. K. and Moldowan, J. M. (1979). The effect of biodegradation on steranes and terpanes in crude oils. *Geochim. Cosmochim. Ac.*, 43:111–126.

Seifert, W. K. and Moldowan, J. M. (1986). Use of biological markers in petroleum exploration. In Johns, R., editor, *Biological Markers in the Sedimentary Record*, pages 261–290. Elsevier, Amsterdam.

Sweeney, J. J. and Burnham, A. K. (1990). Evaluation of a simple model of vitrinite reflectance based on chemical kinetics. *AAPG Bull.*, 74:1559–1570.

Taylor, E. G. H., Teichmüller, M., Davis, A., Diessel, C. F. K., Littke, R., and Robert, P., editors (1998). *Organic Petrology*. Schweizerbart'sche Verlagsbuchhandlung, Stuttgart.

Teixidor, P., Grimait, J. O., Pueyo, J. J., and Rodriguez-Valera, F. (1993). Isopranylglycerol diethers in non-alkaline evaporitic environments. *Geochim. Cosmochim. Ac.*, 57:4479–4489.

ten Haven, H. L., de Leeuw, J. W., Rullkötter, J., and Sinninghe-Damsté, J. (1987). Restricted utility of the pristane/phytane ratio as a palaeoenvironmental indicator. *Nature*, 330:641–643.

Tissot, B. P. and Welte, D. H. (1984). *Petroleum Formation and Occurrence*. Springer-Verlag, Berlin.

Volkman, J. K. and Maxwell, J. R. (1986). Acyclic isoprenoids as biological markers. In Johns, R., editor, *Biological Markers in the Sedimentary Record*, pages 1–42. Elsevier, Amsterdam.

Waples, D. W. (1994). Maturity Modeling: Thermal Indicators, Hydrocarbon Generation, and Oil Cracking. In Magoon, L. B. and Dow, W. G., editors. *The Petroleum System — From Source to Trap*, volume 60 of *AAPG Memoir*, pages 285–322. American Association of Petroleum Geologists.

Yükler, A., Djavadova, A., Siradze, N., and Spiller, R. (2000). The Geology, Geochemistry and Basin Modeling of the Western Kura Basin Depression, Georgia. In *AAPG Search and Discovery*, AAPG Regional International Conference, Istanbul.

List of Figures

1.1 Relief map of Georgia 1
1.2 Paleogeographic map of the Paratethys at the Eocene/Oligocene transition 2

2.1 Stratigraphic correlation of the Paratethys (Upper Eocene–Lower Miocene) and main events in the Eastern Paratethys 5
2.2 Geodynamic evolution of the Transcaucasus intermontane depression 6
2.3 Map of the E-W trending anticlines of the Adjara-Trialeti fold-belt on which the hydrocarbon accumulations of the East-Tbilisi region are located 7
2.4 Structural cross section of the Ninotsminda and Norio fields 8
2.5 Stratigraphic column of the Kura Basin 9
2.6 Map of the sedimentary basins and oil fields in Georgia 12

3.1 Map of the Near-Tbilisi study area, showing the locations of the Norio-72, Ninotsminda-97, and Manavi-12 wells 14
3.2 Photos of representative cuttings samples 16
3.3 Stereomicroscope photograph of cuttings from sample NOR-72-185 (4757 to 4760 m) 17

4.1 Chromatograms of the aliphatic and aromatic fractions of sample NTM-97-16 (2465 to 2470 m) 28

5.1 Stratigraphy and depth plots of bulk geochemical parameters and vitrinite reflectance in Norio-72 34
5.2 An example of a Rock-Eval trace with a double S_2 peak 37
5.3 Hydrogen Index (HI) based on uncorrected and corrected S_2 values versus T_{max} for Norio-72 38
5.4 A chromatogram of the aliphatic fraction of Eocene sample NOR-72-161 . . 39
5.5 Thermal maturity parameters based on apparent isomerization of asymmetric centers in C_{29} steranes 39

5.6 Micrographs of macerals in Norio-72 samples 40
5.7 Maceral composition of samples 41
5.8 Stratigraphy and depth plots of bulk geochemical parameters and vitrinite reflectance in Ninotsminda-97 42
5.9 Hydrogen Index (HI) based on uncorrected and corrected S_2 values versus T_{max} for Ninotsminda-97 and Manavi-12 43
5.10 Micrographs of macerals in NTM-97-25 (2545 to 2550 m) 45
5.11 Stratigraphy and depth plots of bulk geochemical parameters and vitrinite reflectance in Manavi-12 46
5.12 Micrographs of macerals in samples MNV-12-37 (a and b; 3938 m) and MNV-12-25 (e through f; 3896 m) 47
5.13 Chromatograms of the aliphatic and atomatic fractions of the Eocene oil sample G-NTM-21 49
5.14 Pr/Ph ratios versus oleanane index for oil samples and rock extracts 51
5.15 C_{27}-diasteranes/C_{27}-steranes plotted against C_{28}/C_{29} steranes ratios for oil samples and rock extracts 51
5.16 Pr/n-C_{17} versus Ph/n-C_{17} ratios for oil samples and rock extracts 52
5.17 A ternary diagram of C_{27}-C_{28}-C_{29} steranes ratios 52
5.18 $\delta^{13}C/^{12}C$ versus $\delta^{18}O/^{16}O$ of calcite and depth plots isotope ratios 54
5.19 Burial history curve for the Norio-72 "cold" scenario 55
5.20 Depth plots of temperature, vitrinite reflectance, sterane and hopane isomerization for Norio-72 56
5.21 Time plots of maturity and transformation ratio for Norio-72 56
5.22 Burial history curve for the Ninotsminda-97 "cold" scenario 57
5.23 Depth plots of temperature, vitrinite reflectance, sterane and hopane isomerization for Ninotsminda-97 57
5.24 Time plots of maturity and transformation ratio for Ninotsminda-97 58
5.25 Burial history curve for the Norio-72 "hot" scenario 59
5.26 Burial history curve for the Ninotsminda-97 "hot" scenario 59

List of Tables

3.1 Drill cuttings samples provided by CanArgo 15
3.2 Drilling muds used in Norio-72, Ninotsminda-97, and Manavi-12 at various depth intervals 18

4.1 Quantity-based generative potential of immature source rocks 21
4.2 Quality of potential source rocks 23
4.3 Geochemical and optical parameters describing thermal maturation levels . 25
4.4 Reflectivity, fluorescence, and hydrocarbon potential of maceral groups . . . 25

5.1 Summary of bulk geochemical parameters for Norio-72 36

6.1 Summary of the age assignment of the studied successions. 61

List of Appendices

Appendix A Samples and Methods Applied
Appendix B Sample Photographs
Appendix C Calcareous Nannoplankton
Appendix D Bulk Geochemical Parameters
Appendix E Organic Petrology
Appendix F Gas Chromatography-Mass Spectroscopy
Appendix G Carbonate Isotopy
Appendix H 1-D Thermal Maturity Model Input

Appendices

Appendix A: Samples and Methods Applied

Sample	Top	Bottom	RE	LECO	Eltra	CN	VR	MA	GC-MS	CI
NOR-72-1	3625	3630	X	X		X				X
NOR-72-2	3700	3705	X	X						
NOR-72-3	3705	3710								
NOR-72-4	3710	3715	X	X						X
NOR-72-5	3715	3720								
NOR-72-6	3720	3725	X	X						
NOR-72-7	3725	3730								
NOR-72-8	3735	3740	X	X	X					
NOR-72-9	3740	3745				X				
NOR-72-10	3745	3750	X	X						X
NOR-72-11	3750	3755								
NOR-72-12	3755	3760	X	X						
NOR-72-13	3760	3765								
NOR-72-14	3765	3770	X	X						
NOR-72-15	3770	3775								
NOR-72-16	3775	3780	X	X	X					X
NOR-72-17	3780	3785								
NOR-72-18	3785	3790	X	X						
NOR-72-19	3790	3795				X				
NOR-72-20	3795	3800	X	X						X
NOR-72-21	3800	3805								
NOR-72-22	3805	3810	X	X						
NOR-72-23	3810	3815								
NOR-72-24	3815	3820	X	X						
NOR-72-25	3820	3825								
NOR-72-26	3825	3830	X	X	X		X^c			
NOR-72-27	3830	3835				X				
NOR-72-28	3835	3840	X	X	X		X^c			X
NOR-72-29	3840	3845								
NOR-72-30	3845	3850	X	X						
NOR-72-31	3850	3855								
NOR-72-32	3855	3860	X	X						
NOR-72-33	3860	3865								
NOR-72-34	3865	3870	X	X						
NOR-72-35	3870	3875				X				
NOR-72-36	3875	3880	X	X	X					
NOR-72-37	3880	3885								

RE = Rock-Eval; Nanno = Calcareous Nannoplankton; VR = Vitrinite Reflectance; MA = Maceral Analysis; CI = Carbonate Isotopy; X^c = coal sample

Sample	Top	Bottom	RE	LECO	Eltra	CN	VR	MA	GC-MS	CI
NOR-72-38	3885	3890	X	X						
NOR-72-39	3890	3895								
NOR-72-40	3895	3900	X	X						
NOR-72-41	3900	3905								
NOR-72-42	3905	3910	X	X						
NOR-72-43	3910	3915	X		X	X				
NOR-72-44	3915	3920	X	X						X
NOR-72-45	3920	3925	X		X					
NOR-72-46	3925	3930	X	X						
NOR-72-47	3930	3935	X		X					
NOR-72-48	3935	3940	X	X						
NOR-72-49	3940	3945								
NOR-72-50	3945	3950	X	X						
NOR-72-51	3950	3955				X				
NOR-72-52	3955	3960	X	X						
NOR-72-53	3960	3965	X		X					
NOR-72-54	3965	3970	X	X						
NOR-72-55	3970	3975								
NOR-72-56	3975	3980	X	X	X					
NOR-72-57	3980	3985	X		X					
NOR-72-58	3985	3990	X	X						
NOR-72-59	3990	3995	X		X	X				
NOR-72-60	3995	4000	X	X						
NOR-72-61	4000	4005	X		X					
NOR-72-62	4005	4010	X	X						
NOR-72-63	4010	4015	X		X					
NOR-72-64	4015	4020	X	X						
NOR-72-65	4020	4025	X		X					
NOR-72-66	4025	4030	X	X						
NOR-72-67	4030	4035	X		X	X				
NOR-72-68	4035	4040	X	X	X					
NOR-72-69	4040	4045	X		X					
NOR-72-70	4045	4050	X	X						
NOR-72-71	4050	4055	X		X					
NOR-72-72	4055	4060	X	X						
NOR-72-73	4060	4065	X		X					
NOR-72-74	4065	4070	X	X						
NOR-72-75	4070	4075	X		X	X				
NOR-72-76	4075	4080	X	X	X					
NOR-72-77	4080	4085	X		X					
NOR-72-78	4085	4090	X	X						
NOR-72-79	4090	4095	X		X					
NOR-72-80	4095	4100	X	X						
NOR-72-81	4100	4105	X		X					
NOR-72-82	4105	4110	X	X						
NOR-72-83	4110	4115				X				
NOR-72-84	4115	4120	X	X						
NOR-72-85	4120	4125	X		X					
NOR-72-86	4125	4130	X	X	X					
NOR-72-87	4130	4135								
NOR-72-88	4135	4140	X	X						
NOR-72-89	4140	4145	X		X					
NOR-72-90	4145	4150	X	X						

RE = Rock-Eval; Nanno = Calcareous Nannoplankton; VR = Vitrinite Reflectance; MA = Maceral Analysis; CI = Carbonate Isotopy; X^c = coal sample

Sample	Top	Bottom	RE	LECO	Eltra	CN	VR	MA	GC-MS	CI
NOR-72-91	4150	4155				X				
NOR-72-92	4155	4160	X	X			X[c]			
NOR-72-93	4160	4165	X		X					
NOR-72-94	4165	4170	X	X						X
NOR-72-95	4170	4175	X		X					
NOR-72-96	4175	4180	X	X						
NOR-72-97	4180	4185	X		X					
NOR-72-98	4185	4190	X	X						
NOR-72-99	4190	4195				X				
NOR-72-100	4195	4200	X	X	X					
NOR-72-101	4200	4205	X		X					
NOR-72-102	4205	4210	X	X						
NOR-72-103	4210	4215				X				
NOR-72-104	4215	4220	X	X						
NOR-72-105	4225	4230	X		X					
NOR-72-106	4230	4235	X	X						
NOR-72-107	4235	4240	X		X					X
NOR-72-108	4240	4245	X	X						
NOR-72-109	4245	4250	X		X	X				
NOR-72-110	4250	4255	X	X						
NOR-72-111	4255	4260	X		X					
NOR-72-112	4260	4265	X	X	X					
NOR-72-113	4265	4270	X		X					
NOR-72-114	4270	4275	X	X	X					
NOR-72-115	4275	4280	X		X					
NOR-72-116	4280	4285	X	X						
NOR-72-117	4285	4290	X		X	X				
NOR-72-118	4290	4295	X	X	X					
NOR-72-119	4295	4300								
NOR-72-120	4300	4305	X	X	X					
NOR-72-121	4305	4310	X		X					
NOR-72-122	4310	4315	X	X						
NOR-72-123	4315	4320								
NOR-72-124	4320	4325	X	X						
NOR-72-125	4325	4330								
NOR-72-126	4330	4335	X	X						
NOR-72-127	4335	4340								
NOR-72-128	4340	4345	X	X						
NOR-72-129	4345	4350	X		X	X				
NOR-72-130	4350	4355	X	X						
NOR-72-131	4360	4365	X		X					
NOR-72-132	4365	4370	X	X	X					
NOR-72-133	4370	4375								
NOR-72-134	4375	4380	X	X						
NOR-72-135	4380	4385	X		X					
NOR-72-136	4385	4390	X	X	X					
NOR-72-137	4390	4395	X		X					
NOR-72-138	4395	4400	X	X						
NOR-72-139	4400	4405	X		X	X				X
NOR-72-140	4405	4410?	X	X						X
NOR-72-141	4410	4415	X		X					
NOR-72-142	4415	4220?	X	X						
NOR-72-143	4420	4425	X		X					X

RE = Rock-Eval; Nanno = Calcareous Nannoplankton; VR = Vitrinite Reflectance; MA = Maceral Analysis; CI = Carbonate Isotopy; X[c] = coal sample

Sample	Top	Bottom	RE	LECO	Eltra	CN	VR	MA	GC-MS	CI
NOR-72-144	4425	4430	X	X						
NOR-72-145	4430	4435	X		X					
NOR-72-146	4435	4440	X	X	X				X	X
NOR-72-147	4440	4445	X		X					
NOR-72-148	4445	4450	X	X						
NOR-72-149	4450	4455	X		X	X			X	X
NOR-72-150	4455	4460	X	X	X		X[c]			
NOR-72-151	4460	4465	X		X					
NOR-72-152	4465	4470	X	X						
NOR-72-153	4470	4475	X		X					
NOR-72-154	4475	4480	X	X	X					
NOR-72-155	4480	4485								
NOR-72-156	4485	4490	X	X						
NOR-72-157	4490	4495	X		X				X	X
NOR-72-158	4495	4500	X	X	X					
NOR-72-159	4500	4505	X		X	X				
NOR-72-160	4505	4510	X	X						
NOR-72-161	4510	4513	X		X			X		
NOR-72-162	4519	4522	X		X					
NOR-72-163	4528	4531	X		X					
NOR-72-164	4540	4543	X		X					
NOR-72-165	4549	4553	X		X	X		X		
NOR-72-166	4559	4562	X		X			X	X	
NOR-72-167	4568	4571	X		X					
NOR-72-168	4577	4580	X		X			X		
NOR-72-169	4589	4592	X		X			X		
NOR-72-170	4598	4601	X		X	X		X		
NOR-72-171	4607	4610	X		X					
NOR-72-172	4619	4622	X		X					
NOR-72-173	4628	4631	X		X			X		
NOR-72-174	4637	4640	X		X					
NOR-72-175	4649	4652	X		X	X		X		
NOR-72-176	4658	4661	X		X					
NOR-72-177	4667	4670	X		X					
NOR-72-178	4679	4682	X		X					
NOR-72-179	4697	4700	X		X	X				
NOR-72-180	4709	4712	X		X					
NOR-72-181	4718	4721	X		X			X		
NOR-72-182	4727	4730	X		X					
NOR-72-183	4739	4742	X		X			X		
NOR-72-184	4748	4751	X		X	X	X	X		
NOR-72-185	4757	4760	X		X					
NOR-72-186	4769	4772	X		X					
NOR-72-187	4778	4781	X		X					
NOR-72-188	4790	4793	X		X			X		
NOR-72-189	4799	4802	X		X	X				
NOR-72-190	4808	4811	X		X					
NOR-72-191	4817	4820	X		X					
NOR-72-192	4820	4823	X		X					
NOR-72-193	4826	4829	X		X					
NOR-72-194	4847	4850				X				
NOR-72-195	4859	4862	X		X			X		
NOR-72-196	4880	4883								

RE = Rock-Eval; Nanno = Calcareous Nannoplankton; VR = Vitrinite Reflectance; MA = Maceral Analysis; CI = Carbonate Isotopy; X[c] = coal sample

Sample	Top	Bottom	RE	LECO	Eltra	CN	VR	MA	GC-MS	CI
NOR-72-197	4888	4891	X		X	X				
NTM-97-1	2330	2335	X	X						
NTM-97-2	2335	2340				X				
NTM-97-3	2340	2345	X		X					X
NTM-97-4	2345	2350								
NTM-97-5	2350	2355	X	X						X
NTM-97-6	2355	2360				X				
NTM-97-7	2360	2365	X		X					X
NTM-97-8	2365	2370								
NTM-97-9	2370	2375	X	X			X			X
NTM-97-10	2375	2380	X		X	X				X
NTM-97-11	2440	2445	X		X					X
NTM-97-12	2445	2450	X		X	X				X
NTM-97-13	2450	2455	X	X						X
NTM-97-14	2455	2460	X		X					X
NTM-97-15	2460	2465	X		X					X
NTM-97-16	2465	2470	X		X				X	X
NTM-97-17	2470	2475	X	X			X[c]	X		X
NTM-97-18	2475	2480	X		X	X				X
NTM-97-19	2515	2520	X		X					X
NTM-97-20	2520	2525	X		X	X			X	X
NTM-97-21	2525	2530	X	X			X	X		X
NTM-97-22	2530	2535	X		X				X	X
NTM-97-23	2535	2540	X		X					
NTM-97-24	2540	2545	X		X				X	X
NTM-97-25	2545	2550	X	X			X[c]	X		X
NTM-97-26	2550	2555	X		X	X				X
NTM-97-27	2555	2560	X		X					X
MNV-12-1	3821	3824	X	X	X			X		
MNV-12-2	3824	3827				X				
MNV-12-3	3827	3830	X		X					
MNV-12-4	3830	3833								
MNV-12-5	3833	3836	X	X	X			X		
MNV-12-6	3836	3839								
MNV-12-7	3839	3842	X		X					
MNV-12-8	3842	3845				X				
MNV-12-9	3848	3851	X	X	X			X		
MNV-12-10	3851	3854								
MNV-12-11	3854	3857	X		X					
MNV-12-12	3857	3860								
MNV-12-13	3860	3863	X	X	X			X		
MNV-12-13ca	3860	3863				X				
MNV-12-14	3863	3866								
MNV-12-15	3866	3869	X		X					
MNV-12-16	3869	3872								
MNV-12-17	3872	3875	X	X	X			X		
MNV-12-18	3875	3878								
MNV-12-19	3878	3881	X		X	X				
MNV-12-20	3881	3884								
MNV-12-21	3884	3887	X	X	X			X		
MNV-12-22	3887	3890								
MNV-12-23	3890	3893	X		X					
MNV-12-24	3893	3896	X		X					

RE = Rock-Eval; Nanno = Calcareous Nannoplankton; VR = Vitrinite Reflectance; MA = Maceral Analysis; CI = Carbonate Isotopy; X[c] = coal sample

Sample	Top	Bottom	RE	LECO	Eltra	CN	VR	MA	GC-MS	CI
MNV-12-25	3896	3899	X	X	X	X	X	X		
MNV-12-26	3899	3902	X		X					
MNV-12-27	3902	3905	X		X					
MNV-12-28	3905	3908	X		X					
MNV-12-29	3908	3911	X	X	X		X	X		
MNV-12-30	3911	3914								
MNV-12-31	3914	3917	X		X	X				
MNV-12-32	3920	3923	X		X					
MNV-12-33	3923	3926	X	X	X			X		
MNV-12-34	3929	3932	X		X					
MNV-12-35	3932	3935	X		X	X				
MNV-12-36	3935	3938	X		X					
MNV-12-37	3938	3940	X	X	X			X		
MNV-12-38	3940	3942	X		X					
MNV-12-39	3942	3944	X		X					
MNV-12-40	3944	3946	X		X					
MNV-12-41	3946	3948	X	X	X			X		
MNV-12-42	3948	3950	X		X					
MNV-12-43	3950	3952	X		X					
MNV-12-44	3952	3954	X		X	X				
MNV-12-45	3954	3956	X	X	X		X	X		
MNV-12-46	3956	3958	X		X					
MNV-12-47	3958	3960	X		X					
MNV-12-48	3960	3965	X		X					
MNV-12-49	3965	3970	X	X	X			X	X	
MNV-12-50	3970	3975								
MNV-12-51	3975	3980								
MNV-12-52	3749	3752				X				
MNV-12-53	3755	3758								
MNV-12-54	3758	3761				X				
MNV-12-55	3770	3773				X				
MNV-12-56	3773	3776								
MNV-12-57	3779	3782				X				
MNV-12-58	3785	3788								
MNV-12-59	3788	3792								
MNV-12-60	3797	3800								
MNV-12-61	3800	3803								
MNV-12-62	3806	3809				X				
MNV-12-63	3809	3812								
MNV-12-64	3812	3815								
MNV-12-65	3815	3818								
MNV-12-66	3818	3821								
MNV-12-67	3980	3982				X				
MNV-12-68	3984	3986								
MNV-12-69	3990	3992								
MNV-12-70	3994	3996								
MNV-12-71	4000	4002				X				
MNV-12-72	4004	4006								
MNV-12-73	4010	4012								
MNV-12-74	4014	4016								
MNV-12-75	4018	4020								
MNV-12-76	4024	4026				X				
MNV-12-77	4030	4032								

RE = Rock-Eval; Nanno = Calcareous Nannoplankton; VR = Vitrinite Reflectance; MA = Maceral Analysis; CI = Carbonate Isotopy; X^c = coal sample

Sample	Top	Bottom	RE	LECO	Eltra	CN	VR	MA	GC-MS	CI
MNV-12-78	4034	4036				X				
MNV-12-79	4048	4050								

RE = Rock-Eval; Nanno = Calcareous Nannoplankton; VR = Vitrinite Reflectance; MA = Maceral Analysis; CI = Carbonate Isotopy; X^c = coal sample

Appendix B: Sample Photographs

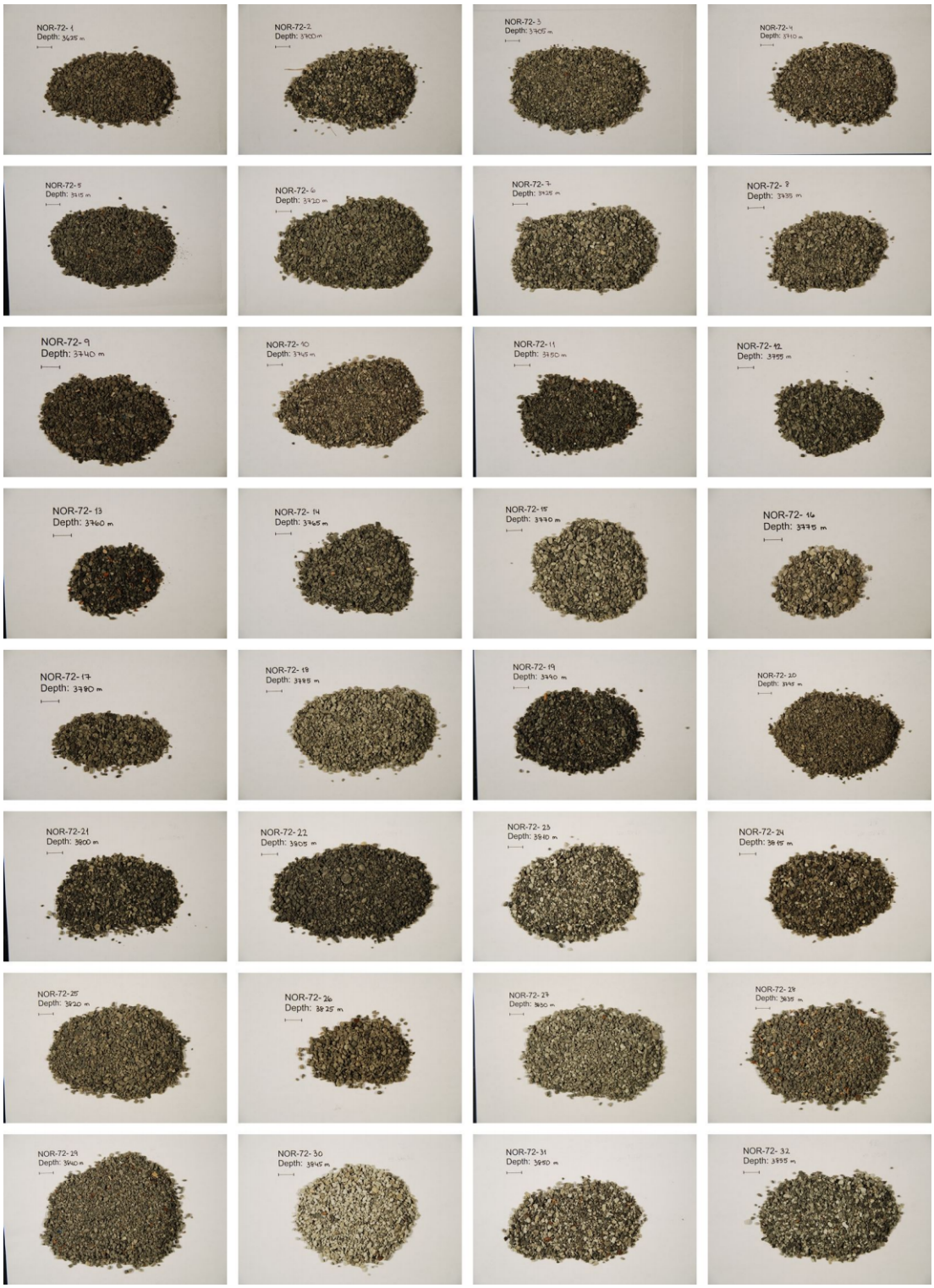

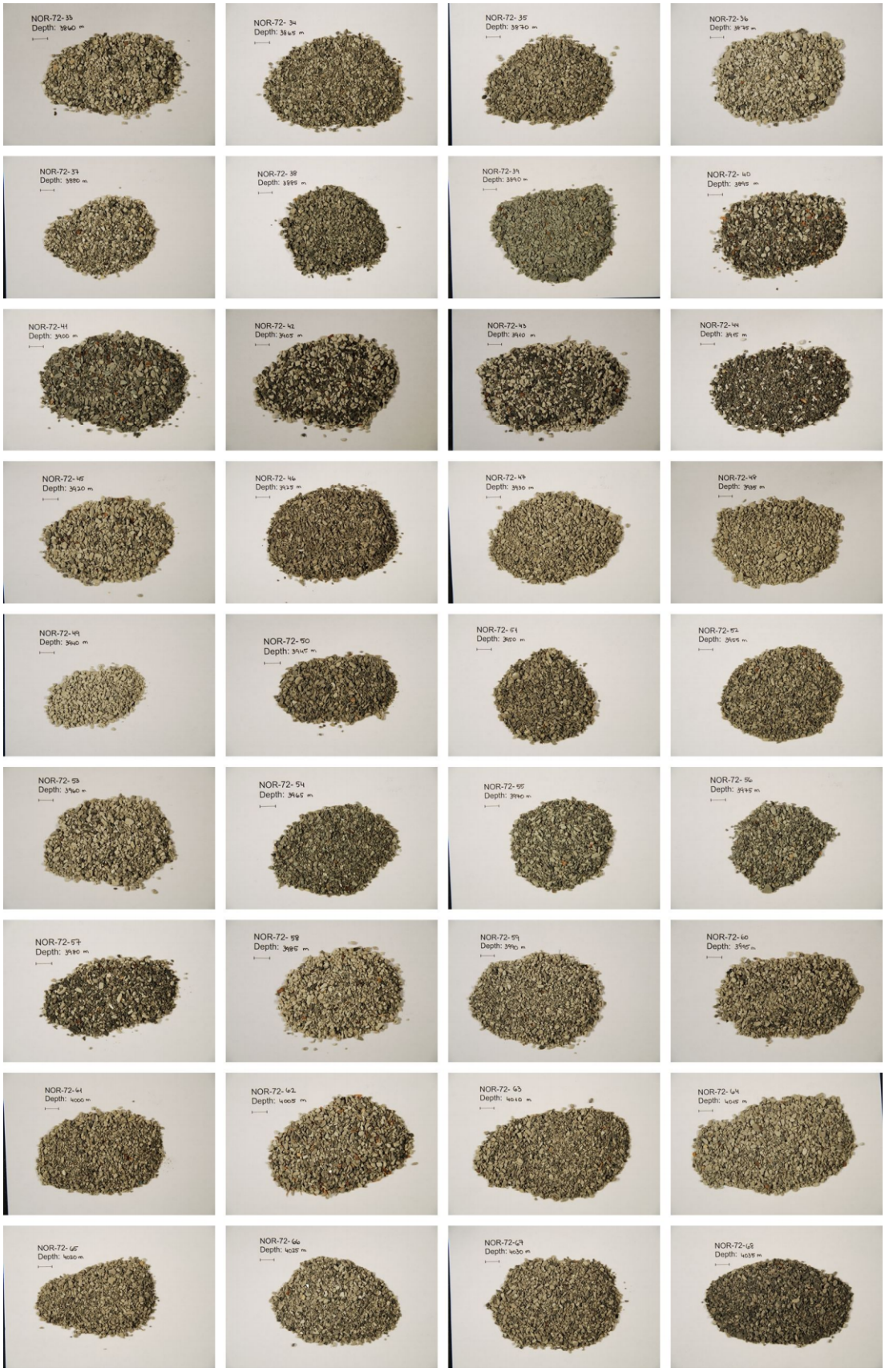
NOR-72-33
NOR-72- 34
NOR-72- 35
NOR-72-36
NOR-72-37
NOR-72- 38
NOR-72- 39
NOR-72- 40
NOR-72-41
NOR-72- 42
NOR-72-43
NOR-72-44
NOR-72- 45
NOR-72- 46
NOR-72- 47
NOR-72- 48
NOR-72- 49
NOR-72- 50
NOR-72- 51
NOR-72- 52
NOR-72- 53
NOR-72- 54
NOR-72- 55
NOR-72- 56
NOR-72- 57
NOR-72- 58
NOR-72- 59
NOR-72- 60
NOR-72- 61
NOR-72- 62
NOR-72- 63
NOR-72- 64
NOR-72- 65
NOR-72- 66
NOR-72- 67
NOR-72- 68

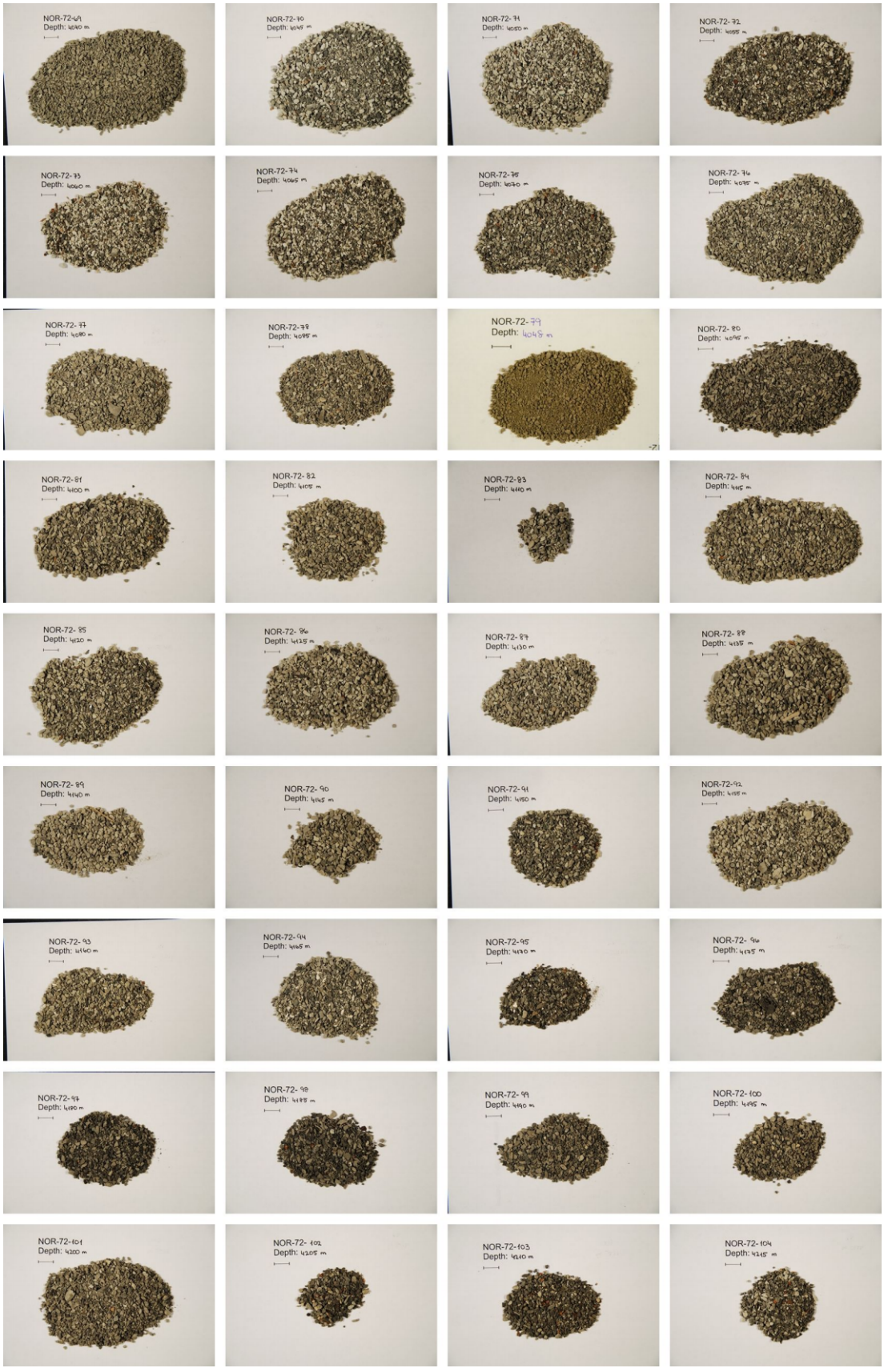
NOR-72-69
NOR-72-70
NOR-72-71
NOR-72-72
NOR-72-73
NOR-72-74
NOR-72-75
NOR-72-76
NOR-72-77
NOR-72-78
NOR-72-79
NOR-72-80
NOR-72-81
NOR-72-82
NOR-72-83
NOR-72-84
NOR-72-85
NOR-72-86
NOR-72-87
NOR-72-88
NOR-72-89
NOR-72-90
NOR-72-91
NOR-72-92
NOR-72-93
NOR-72-94
NOR-72-95
NOR-72-96
NOR-72-97
NOR-72-98
NOR-72-99
NOR-72-100
NOR-72-101
NOR-72-102
NOR-72-103
NOR-72-104

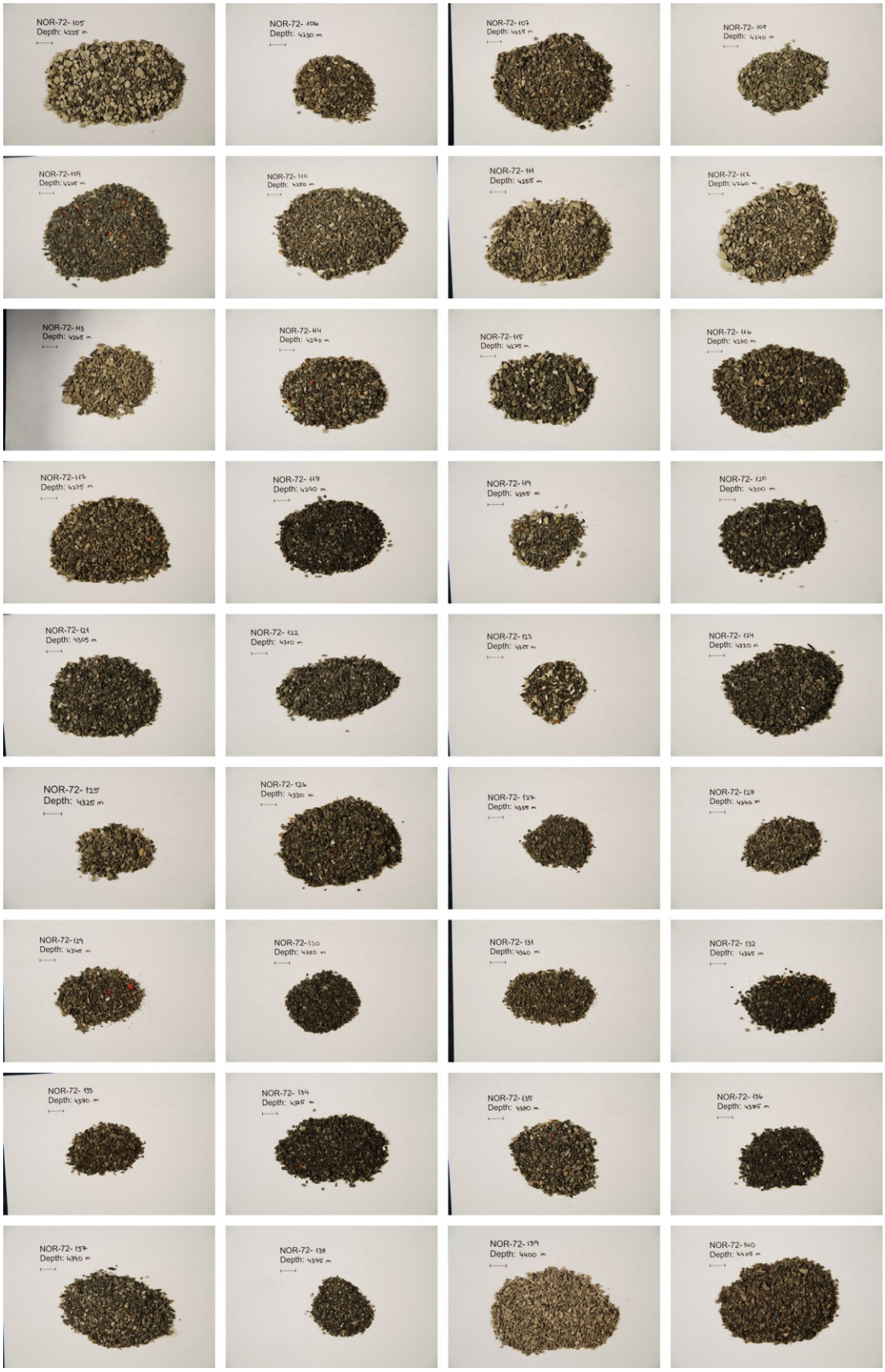
NOR-72- 105
Depth: 4335 m
NOR-72- 106
Depth: 4330 m
NOR-72- 107
Depth: 4335 m
NOR-72- 108
Depth: 4340 m
NOR-72- 109
Depth: 4345 m
NOR-72- 110
Depth: 4350 m
NOR-72- 111
Depth: 4355 m
NOR-72- 112
Depth: 4360 m
NOR-72- 113
Depth: 4368 m
NOR-72- 114
Depth: 4390 m
NOR-72- 115
Depth: 4395 m
NOR-72- 116
Depth: 4390 m
NOR-72- 117
Depth: 4335 m
NOR-72- 118
Depth: 4340 m
NOR-72- 119
Depth: 4345 m
NOR-72- 120
Depth: 4300 m
NOR-72- 121
Depth: 4305 m
NOR-72- 122
Depth: 4340 m
NOR-72- 123
Depth: 4345 m
NOR-72- 124
Depth: 4320 m
NOR-72- 125
Depth: 4325 m
NOR-72- 126
Depth: 4330 m
NOR-72- 127
Depth: 4335 m
NOR-72- 128
Depth: 4340 m
NOR-72- 129
Depth: 4345 m
NOR-72- 130
Depth: 4350 m
NOR-72- 131
Depth: 4340 m
NOR-72- 132
Depth: 4345 m
NOR-72- 133
Depth: 4390 m
NOR-72- 134
Depth: 4395 m
NOR-72- 135
Depth: 4390 m
NOR-72- 136
Depth: 4385 m
NOR-72- 137
Depth: 4390 m
NOR-72- 138
Depth: 4395 m
NOR-72- 139
Depth: 4400 m
NOR-72- 140
Depth: 4405 m

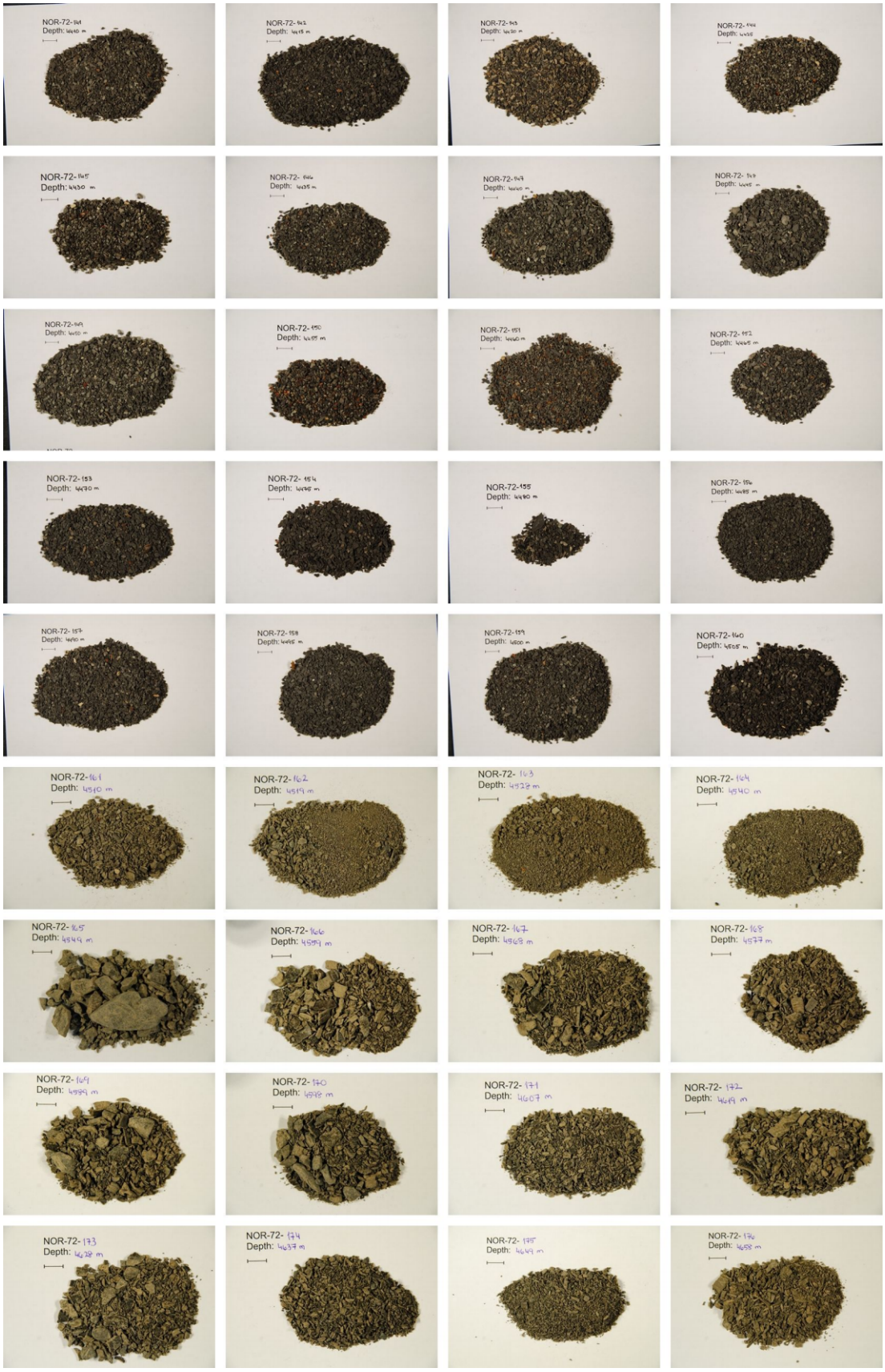


NOR-72-
NTM-97-1
NTM-97-2
NTM-97-3
NTM-97-4
NTM-97-5
NTM-97-6
NTM-97-7
NTM-97-9
NTM-97-10
NTM-97-11
NTM-97-15


NTM-97- 16
NTM-97- 17
NTM-97- 18
NTM-97- 19
NTM-97- 20
NTM-97- 21
NTM-97- 22
NTM-97- 23
NTM-97- 24
NTM-97- 25
NTM-97- 26
NTM-97- 27
MNV-12- 1
MNV-12- 2
MNV-12- 3
MNV-12- 4
MNV-12- 5
MNV-12- 6
MNV-12- 7
MNV-12- 8
MNV-12- 9
MNV-12- 10
MNV-12- 11
MNV-12- 12
MNV-12- 13
MNV-12- 13a
MNV-12- 14
MNV-12- 15
MNV-12- 16
MNV-12- 17
MNV-12- 18
MNV-12- 19
MNV-12- 20
MNV-12- 21
MNV-12- 22
MNV-12- 23


MNV-12- 24
MNV-12- 25
MNV-12- 26
MNV-12- 27
MNV-12- 28
MNV-12- 29
MNV-12- 30
MNV-12- 31
MNV-12- 32
MNV-12- 33
MNV-12- 34
MNV-12- 35
MNV-12- 36
MNV-12- 37
MNV-12- 38
MNV-12- 39
MNV-12- 40
MNV-12- 41
MNV-12- 42
MNV-12- 43
MNV-12- 44
MNV-12- 45
MNV-12- 46
MNV-12- 47
MNV-12- 48
MNV-12- 49
MNV-12- 50
MNV-12- 52
MNV-12- 53
MNV-12- 54
MNV-12- 55
MNV-12- 56
MNV-12- 57
MNV-12- 58
MNV-12- 59
MNV-12- 60

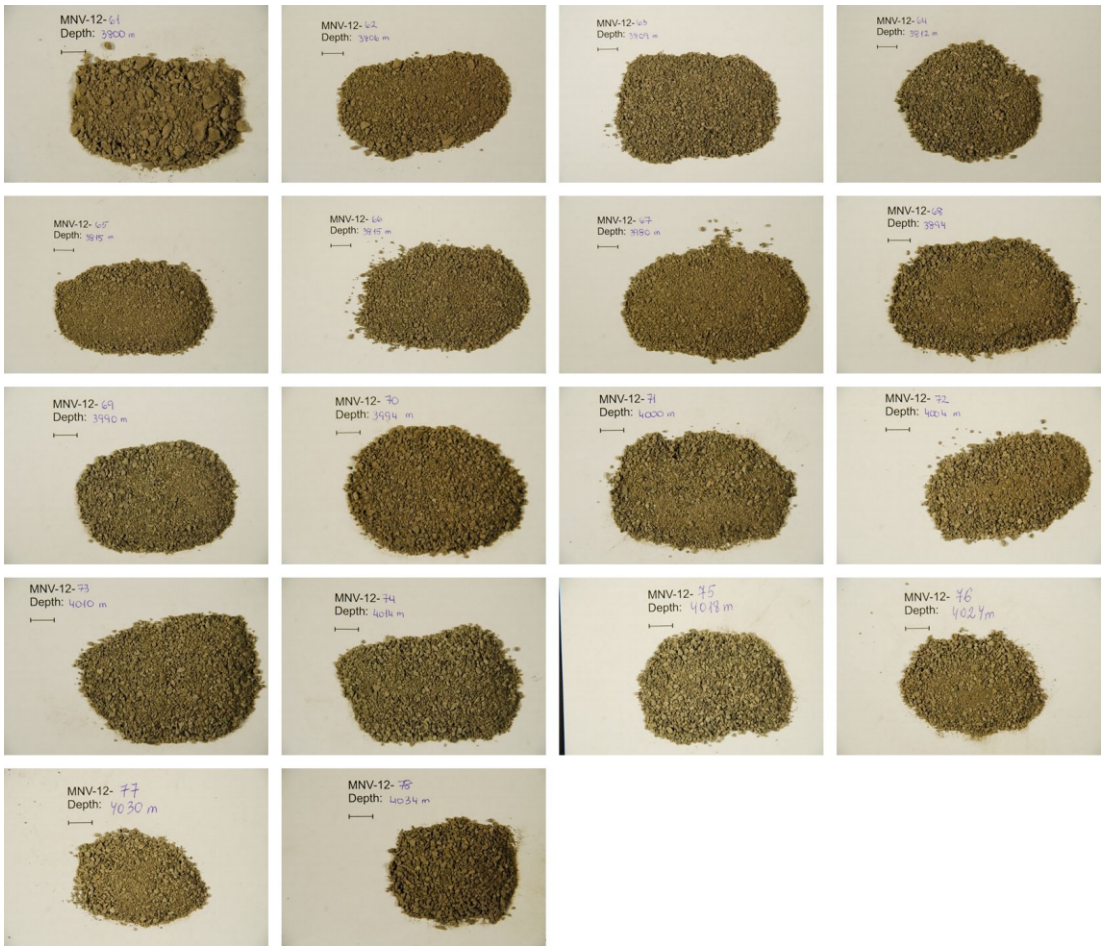
MNV-12-61
Depth: 3800 m
MNV-12-62
Depth: 3806 m
MNV-12-63
Depth: 3909 m
MNV-12-64
Depth: 3912 m
MNV-12-65
Depth: 3915 m
MNV-12-66
Depth: 3915 m
MNV-12-67
Depth: 3980 m
MNV-12-68
Depth: 3994
MNV-12-69
Depth: 3990 m
MNV-12-70
Depth: 3994 m
MNV-12-71
Depth: 4000 m
MNV-12-72
Depth: 4004 m
MNV-12-73
Depth: 4010 m
MNV-12-74
Depth: 4014 m
MNV-12-75
Depth: 4018 m
MNV-12-76
Depth: 4024m
MNV-12-77
Depth: 4030 m
MNV-12-78
Depth: 4034 m

Appendix C: Calcareous Nannoplankton

Analysis by Stjepan Ćorić, Geological Survey of Austria

Sample	Description	NOR-72-1	NOR-72-9	NOR-72-19	NOR-72-27	NOR-72-35	NOR-72-43	NOR-72-51	NOR-72-59	NOR-72-67	NOR-72-75	NOR-72-83	NOR-72-91	NOR-72-99	NOR-72-103	NOR-72-109	NOR-72-117	NOR-72-129	NOR-72-139	NOR-72-149	NOR-72-159	NOR-72-165	NOR-72-170	NOR-72-175	NOR-72-179	NOR-72-184	NOR-72-189	NOR-72-194	NOR-72-197
		r,m	r,m	f,m	r,m	vr,m		vr,m		vr, m	vr, m	vr, m	f, m	vr, m		f/c, g		vr, m	vr, m	vr, m									
Braarudosphaera bigelowii					x											x													
Calcidiscus sp.																x													
Chiasmolithus oamurensis																x													
Chisamolithus sp.													x																
Coccolithus eopelagicus																cf.													
Coccolithus pelagicus		x		x	x			x		x						x				x									
Coccolithus formosus			x	x	x			x			x		x			x				x									
Coccolithus subdistichus													x																
Cyclicargolithus floridanus		x	c	f	c	x		x		x		x	x			x				x									
Cribrocentrum reticulatum			x																										
Discoaster tani nodifer													x																
Discoaster sp.			x																										
Ericsonia robusta				x																									
Ericsonia sp.												x																	
Helicosphaera sp.																			?										
Lanternithus minutus		x	x	x	x			x		x						x													
Micula decussata		x	x	x	x						x	x	x			x				x									
Neococcolithes sp.																x													
Pontosphaera exilis			x													x													
Pontosphaera multipora			x								x																		
Reticulofenestra bisecta		x	x	x	x			x		x	f/c			x		x													
Reticulofenestra dictyda		x				x		x			x		c			c			x										
Reticulofenestra erbae			x																										
Reticulofenestra hillae						r										x													
Reticulofenestra lockeri			x	x									x	x		x													
Reticulofenestra minuta				x	x								x	x		x													
Reticulofenestra cf. *ornata*		x																											
Reticulofenestra stavensis			x					c																					
Reticulofenestra umbilica					x											x													
Reticulofenestra vadae								x								x													
Reticulofenestra sp.								x									x												

Sample	Description	NOR-72-1	NOR-72-9	NOR-72-19	NOR-72-27	NOR-72-35	NOR-72-43	NOR-72-51	NOR-72-59	NOR-72-67	NOR-72-75	NOR-72-83	NOR-72-91	NOR-72-99	NOR-72-103	NOR-72-109	NOR-72-117	NOR-72-129	NOR-72-139	NOR-72-149	NOR-72-159	NOR-72-165	NOR-72-170	NOR-72-175	NOR-72-179	NOR-72-184	NOR-72-189	NOR-72-194	NOR-72-197
Sphenolithus cf. *capricornutus*	r,m		x																										
Sphenolithus dissimilis	r,m	x																											
Sphenolithus sp.	vr,m							x																					
Sphenolithus moriformis	r,m		x								x					x													
Thoracosphaera sp.	f,m			x	x					x						x													
Zygrhablithus bijugatus	r,m		x	x	x			x		x	x	x				x													
reworked Cretaceous																													
Arkhangelskiella cymbiformis			x	x	x						x		x			x													
Biscutum ellipticum													x																
Broinsonia parca parca				x							x					x													
Cribrosphaera ehrenbergii													x																
Cyclagelosphaera reinhardtii		x														x													
Eiffellithus eximius											x																		
Eiffellithus gorkae				x												x													
Micrantholithus decoratus				x												x													
Prediscosphaer cretacea				x	x							x				x													
Retecapsa crenulata																x													
Reinhardtites sp.											x																		
Umiplanarius gothicus												x																	
Watznaueria barnesae			x	x	x			x				x	x	x		f			x										
Watznaueria brittanica				x																									
watznaueria fossacincta				c									x																
Watznaueria manivitae																x													
Zeugrhabdotus diplogramus																x													

Sample	NTM-97-26	NTM-97-20	NTM-97-18	NTM-97-12	NTM-97-10	NTM-97-6	NTM-97-2
Description	r, m	c, g	f, m	r, m	a, m	r, m	r, m
Blackites sp.	×	×	×		×		
Bramletteius serraculoides		×	×		×		
Chiasmolithus oamurensis			?		?		
Coccolithus formosus		×			×	×	
Coccolithus pelagicus		×	×		×	×	×
Coccolithus subdistichus		×					
Cribrocntrum reticulatum		×	×		c		
Cyclicargolithus floridanus	×	×	×		×	×	×
Discoaster barbardiensis					cf.		
Discoaster sp.		×					
Germanicus corranlus					×		
Helicosphaera bramlettei		×					
Helicosphaera compacta		×					
Lanternithus minutus		×	×		f		
Micula decussata		×					
Pemma basquensis		×	×		×		
Pemma papilatim		×					
Pontosphaera exilis		×					
Pontosphaera multipora		×			×		
Pontosphaera sp.							×
Pyrocyclus orangensis			×				
Reticulofenestra bisecta	×	×	×		×	×	×
Reticulofenestra dictyoda		×	×	×	×	×	×
Reticulofenestra erbae					×		
Reticulofenestra cf. *fillewiczae*						cf	cf
Reticulofenestra sp.		×	×	×	×	×	×
Reticulofenestra hillae		×	×		×	×	
Reticulofenestra lockeri		×	×		×	×	×
Reticulofenestra minuta	×	×	×	×	×	×	×
Reticulofenestra scripsae		×	×			×	×
Reticulofenestra stavensis		×	×		×	×	×
Reticulofenestra umbilica	×	×	×		×	×	×
Reticulofenestra wadae		×	×		×	×	×
Sphenolithus editus		×			×		
Sphenolithus moriformis		×	×		×	×	×
Sphenolithus predistentus		×					
Thoracosphaera saxea		×	×		×		
Zygrhablithus bijugatus		×	×		×	×	×
reworked Cretaceous							
Watznaueria barnesae					×		

Sample	MNV-12-78	MNV-12-76	MNV-12-71	MNV-12-67	MNV-12-44	MNV-12-35	MNV-12-31	MNV-12-25	MNV-12-19	MNV-12-13ca	MNV-12-8	MNV-12-2	MNV-12-62	MNV-12-57	MNV-12-55	MNV-12-54	MNV-12-52
Description	c, m	a, m	c, m	c, m		r, m			r, m					vr, m	r, m	vr, m	
Blackites sp.		×															
Bramleteius serraculoides		×	×														
Chiasmolithus grandis			×														
Coccolithus formosus		×	×	×		×											
Coccolithus eopelagicus		×															
Coccolithus pelagicus	×	×	×	×		×								×			
Coccolithus subdistichus	?			×													
Cribrocentrum reticulatum	×	×	×			×											
Cyclicargolithus floridanus	×	×	×	×		×			×								
Helicosphaera compacta				×													
Helicosphaera euphratis				×													
Isthmolithus recurvus		×	×														
Lanternithus minutus	×	×	×	×													
Micula decussata	×			×													
Pontosphaera multipora			×														
Pontosphaera sp.			×														
Reticulofenestra bisecta	×	×	×	×		×									cf.		
Reticulofenestra dictyoda	×	×	×	×		×											
Reticulofenestra lockeri	×	×	×	×													
Reticulofenestra hillae		×	×	×													
Reticulofenestra minuta	×	×	×	×													
Reticulofenestra scripsae	×	×	×	×													
Reticulofenestra stavensis		×	×	×													
Reticulofenestra umbilica	×	×	×			×											
Reticulofenestra wadae	×	×	×	×		×											
Reticulofenestra sp.	×	×	×	×											×		
Scyphosphaera sp.		×															
Sphenolithus moriformis	×	×	×	×													
Sphenolithus predistentus		×															
Sphenolithus pseudoradians			cf.														
Sphenolithus sp.										×							
Thoracosphaera saxea	×		×												×		
Zygrhablithus bijugatus	×	×	×	×													

Sample	Description	MNV-12-78	MNV-12-76	MNV-12-71	MNV-12-67	MNV-12-44	MNV-12-35	MNV-12-31	MNV-12-25	MNV-12-19	MNV-12-13ca	MNV-12-8	MNV-12-2	MNV-12-62	MNV-12-57	MNV-12-55	MNV-12-54	MNV-12-52
		c, m	a, m	c, m	c, m		r, m			r, m					vr, m	r, m	vr, m	
reworked Cretaceous																		
Arkhangelskielly cymbiformis							x									x		
Broinsonia parca parca							x											
Lucianorhabdus cayexii															f			
Microrhabdulus decoratus							x			x					x	c	x	
Prediscosphaera cretacea							x			x								
Retecapsa crenulata																x		
Watznaueria barnesae		x	x				x			c					c	f	x	
Watznaueria fossacincta							x			x								

NOR-72-1

Stratigraphic attribution: *Sphenolithus dissimilis* has short biostratigraphic range: upper NP24 — NN2. Miocene taxa could not be observed. Probably **upper NP24/25; uppermost Oligocene (Chattian)**.

Rare, moderately preserved calcareous nannoplankton; plant remains

Coccolithus pelagicus (Wallich 1877) Schiller 1930, *Cyclicargolithus floridanus* (Roth and Hay in Hay et al., 1967) Bukry, 1971, *Lanternithus minutus* Stradner, 1961, Reticulofenestra bisecta (Hay, Mohler and Wade, 1966) Roth, 1970, *Reticulofenestra dictyoda* (Deflandre in Deflandre & Fert, 1954) Stradner in Stradner & Edwards, 1968, *Sphenolithus dissimilis* Bukry and Percival, 1971.

Reworking from Cretaceous:

Cyclagelosphaera reinhardtii (Perch-Nielsen, 1968) Romein, 1977, *Micula decussata* Vekshina, 1959.

NOR-72-9

Stratigraphic attribution: Sample contains *Sphenolithus* cf. *capricornutus* with stratigraphic range from uppermost NP25-NN1; Miocene nannoflora could not be observed. **Upper NP25; uppermost Oligocene (Chattian)**.

Rare, moderately preserved calcareous nannoplankton; plant remains

Coccolithus formosus (Kamptner, 1963) Wise 1973, *Coccolithus pelagicus* (Wallich 1877) Schiller 1930, *Cyclicargolithus floridanus* (Roth and Hay in Hay et al., 1967) Bukry, 1971, *Lanternithus minutus* Stradner, 1961, *Pontosphaera multipora* (Kamptner, 1948) Roth, 1970, *Reticulofenestra bisecta* (Hay, Mohler and Wade, 1966) Roth, 1970, *Reticulofenestra lockeri* Müller, 1970, *Reticulofenestra stavensis* (Levin & Joerger, 1967) Varol, 1989, *Sphenolithus* cf. *capricornutus* Bukry & Percival 1971, *Sphenolithus moriformis* (Bronnimann and Stradner, 1960) Bramlette and Wilcoxon, 1967, *Zygrhablithus bijugatus* (Deflandre in Deflandre and Fert, 1954) Deflandre, 1959.

Reworking from Cretaceous:

Arkhangelskiella cymbiformis Vekshina, 1959, Micula decussata Vekshina, 1959, Watznaueria barnesae (Black in Black and Barnes, 1959) Perch-Nielsen, 1968.

NOR-72-19

Stratigraphic attribution: Sample contains rare nannoflora with *Coccolithus formosus* whose last occurrence defines NP21/22 boundary. **NP21 (early Oligocene; lower Rupelian).**

Rare, moderately preserved calcareous nannoplankton; plant remains

Coccolithus formosus (Kamptner, 1963) Wise 1973, *Coccolithus pelagicus* (Wallich 1877) Schiller 1930, *Cyclicargolithus floridanus* (Roth and Hay in Hay et al., 1967) Bukry, 1971, *Lanternithus minutus* Stradner, 1961, *Pontosphaera exilis* (Bramlette & Sullivan, 1961) Romein, 1979, *Reticulofenestra bisecta* (Hay, Mohler and Wade, 1966) Roth, 1970, *Reticulofenestra erbae*, *Reticulofenestra lockeri* Müller, 1970, *Reticulofenestra minuta* Roth, 1970, *Thoracosphaera saxea* Stradner, 1961, *Zygrhablithus bijugatus* (Deflandre in Deflandre and Fert, 1954) Deflandre, 1959.

Reworking from Cretaceous:

Arkhangelskiella cymbiformis Vekshina, 1959, *Broinsonia parca* (Stradner 1963) Bukry 1969, *Micula decussata* Vekshina, 1959, *Eiffellithus gorkae* Reinhardt, 1965, *Microrhabdulus decoratus* Deflandre 1959, *Micula decussata* Vekshina, 1959, *Prediscosphaera cretacea* (Arkhangelsky, 1912) Gartner, 1968, *Watznaueria barnesae* (Black in Black and Barnes, 1959) Perch-Nielsen, 1968, *Watznaueria britannica* (Stradner, 1963) Reinhardt, 1964, *Watznaueria fossacincta* (Black, 1971) Bown in Bown & Cooper, 1989.

NOR-72-27

Stratigraphic attribution: Sample contains *Coccolithus formosus* and *Reticulofenestra umbilicus*. No typical Eocene taxa could be observed; **NP21; early Oligocene; lower Rupelian.**

Rare, moderately preserved calcareous nannoplankton; plant remains

Braarudosphaera bigelowii (Gran & Braarud 1935) Deflandre 1947, *Coccolithus formosus* (Kamptner, 1963) Wise 1973, *Coccolithus pelagicus* (Wallich 1877) Schiller 1930, *Cribrocentrum reticulatum* (Gartner & Smith, 1967) Perch-Nielsen, 1971, *Cyclicargolithus floridanus* (Roth and Hay in Hay et al., 1967) Bukry, 1971, *Discoaster* sp., *Lanternithus minutus* Stradner, 1961, *Reticulofenestra bisecta* (Hay, Mohler and Wade, 1966) Roth, 1970, *Reticulofenestra minuta* Roth, 1970, *Reticulofenestra umbilicus* (Levin, 1965) Martini & Ritzkowski, 1968, *Thoracosphaera saxea* Stradner, 1961, *Zygrhablithus bijugatus* (Deflandre in Deflandre and Fert, 1954) Deflandre, 1959.

Reworking from Cretaceous:

Arkhangelskiella cymbiformis Vekshina, 1959, *Micula decussata* Vekshina, 1959, *Prediscosphaera cretacea* (Arkhangelsky, 1912) Gartner, 1968, *Watznaueria barnesae* (Black in Black and Barnes, 1959) Perch-Nielsen, 1968.

NOR-72-35

Stratigraphic attribution: Based on the ocurrence of *Reticulofenestra hillae* **upper Eocene or lower Oligocene (NP17-NP22).**

Very rare, moderately preserved calcareous nannoplankton; plant remains

Cyclicargolithus floridanus (Roth and Hay in Hay et al., 1967) Bukry, 1971, *Reticulofenestra dictyoda* (Deflandre in Deflandre & Fert, 1954) Stradner in Stradner & Edwards, 1968, *Reticulofenestra hillae* Bukry & Percival, 1971.

NOR-72-43

Barren by calcareous nannofossils

NOR-72-51

Stratigraphic attribution: Based on the presence of *Coccolithus formosus*, *Lanternithus minutus* and the absence of typical Eocene discoasterids: **NP21; lower Oligocene; Rupelian**.

Very rare, moderately preserved calcareous nannoplankton; plant remains

Coccolithus formosus (Kamptner, 1963) Wise 1973, *Coccolithus pelagicus* (Wallich 1877) Schiller 1930, *Cyclicargolithus floridanus* (Roth and Hay in Hay et al., 1967) Bukry, 1971, *Lanternithus minutus* Stradner, 1961, *Reticulofenestra bisecta* (Hay, Mohler and Wade, 1966) Roth, 1970, *Reticulofenestra dictyoda* (Deflandre in Deflandre & Fert, 1954) Stradner in Stradner & Edwards, 1968, *Reticulofenestra stavensis* (Levin & Joerger, 1967) Varol, 1989, *Reticulofenestra vadae*, *Reticulofenesta* sp., *Sphenolithus* sp., *Zygrhablithus bijugatus* (Deflandre in Deflandre and Fert, 1954) Deflandre, 1959.

Reworking from Cretaceous:

Watznaueria barnesae (Black in Black and Barnes, 1959) Perch-Nielsen, 1968.

NOR-72-59

Barren by calcareous nannofossils; plant remains

NOR-72-67

Stratigraphic attribution: Very rare calcareous nannoplankton with *Lanternithus minutus*, which has the last occurrence in **NP21; Lowest Oligocene**?

Very rare, moderately preserved calcareous nannoplankton

Coccolithus pelagicus (Wallich 1877) Schiller 1930, *Cyclicargolithus floridanus* (Roth and Hay in Hay et al., 1967) Bukry, 1971, *Lanternithus minutus* Stradner, 1961, *Reticulofenestra bisecta* (Hay, Mohler and Wade, 1966) Roth, 1970, *Thoracosphaera saxea* Stradner, 1961, *Zygrhablithus bijugatus* (Deflandre in Deflandre and Fert, 1954) Deflandre, 1959.

NOR-72-75

Stratigraphic attribution: assemblage with *Coccolithus formosus* **NP21; lower Oligocene**?

Very rare, moderately preserved calcareous nannoplankton

Coccolithus formosus (Kamptner, 1963) Wise 1973, *Pontosphaera multipora* (Kamptner, 1948) Roth, 1970, *Reticulofenestra bisecta* (Hay, Mohler and Wade, 1966) Roth, 1970, *Reticulofenestra dictyoda* (Deflandre in Deflandre & Fert, 1954) Stradner in Stradner & Edwards, 1968, *Sphenolithus moriformis* (Bronnimann and Stradner, 1960) Bramlette and Wilcoxon, 1967, *Zygrhablithus bijugatus* (Deflandre in Deflandre and Fert, 1954) Deflandre, 1959.

Reworking from Cretaceous:

Arkhangelskiella cymbiformis Vekshina, 1959, *Broinsonia parca* (Stradner 1963) Bukry 1969, *Eiffellithus eximius* (Stover, 1966) Perch-Nielsen, 1968, *Micula decussata* Vekshina, 1959

NOR-72-83

Stratigraphic attribution: nannoplankton assemblage with *Reticulofenestra lockeri* and *Zygrhablithus bijugatus*; **Eocene/Oligocene**.

Very rare, moderately preserved calcareous nannoplankton; plant remains

Cyclicargolithus floridanus (Roth and Hay in Hay et al., 1967) Bukry, 1971, *Ericsonia* sp., *Reticulofenestra lockeri* Müller, 1970, *Zygrhablithus bijugatus* (Deflandre in Deflandre and Fert, 1954) Deflandre, 1959.

Reworking from Cretaceous:

Prediscosphaera cretacea (Arkhangelsky, 1912) Gartner, 1968, *Micula decussata* Vekshina, 1959, *Uniplanarius gothicus* (Deflandre, 1959) Hattner & Wise, 1980, *Watznaueria barnesae* (Black in Black and Barnes, 1959) Perch-Nielsen, 1968.

NOR-72-91

Stratigraphic attribution: The co-occurrence of *Clausicoccus subdistichus*, *Coccolithus formosus* and *Discoaster tani nodifer*: **NP21; early Oligocene, Rupelian**.

Few, moderately preserved calcareous nannoplankton *Chiasmolithus* sp., *Clausicoccus subdistichus* (Roth & Hay in Hay et al., 1967) Prins, 1979, *Coccolithus formosus* (Kamptner, 1963) Wise 1973, *Cyclicargolithus floridanus* (Roth and Hay in Hay et al., 1967) Bukry, 1971, *Discoaster tani nodifer* Bramlette & Riedel, 1954, *Reticulofenestra bisecta* (Hay, Mohler and Wade, 1966) Roth, 1970, *Reticulofenestra dictyoda* (Deflandre in Deflandre & Fert, 1954)

Stradner in Stradner & Edwards, 1968, *Reticulofenestra lockeri* Müller, 1970, *Reticulofenestra minuta* Roth, 1970.

Reworking from Cretaceous:

Arkhangelskiella cymbiformis Vekshina, 1959, *Biscutum ellipticum* (Górka, 1957) Grün in Grün and Allemann, 1975, *Cribrocentrum reticulatum* (Gartner & Smith, 1967) Perch-Nielsen, 1971, *Micula decussata* Vekshina, 1959, *Watznaueria barnesae* (Black in Black and Barnes, 1959) Perch-Nielsen, 1968, *Watznaueria fossacincta* (Black, 1971) Bown in Bown & Cooper, 1989.

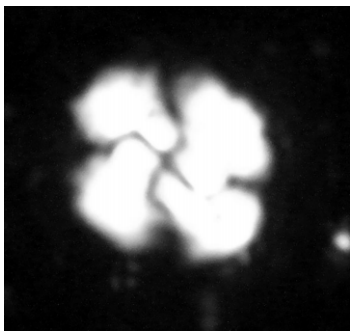

Reticulofenestra bisecta

NOR-72-99

Stratigraphic attribution: Very rare nannoplankton with *Reticulofenestra bisecta* and *Reticulofenestra lockeri*; **middle Eocene/Oligocene**.

Very rare, moderately preserved calcareous nannoplankton

Reticulofenestra bisecta (Hay, Mohler and Wade, 1966) Roth, 1970, *Reticulofenestra lockeri* Müller, 1970, *Reticulofenestra minuta* Roth, 1970.

Reworking from Cretaceous:

Micula decussata Vekshina, 1959, *Watznaueria barnesae* (Black in Black and Barnes, 1959) Perch-Nielsen, 1968.

NOR-72-103

Barren by calcareous nannofossils

NOR-72-109

Stratigraphic attribution: Nannoplankton assemblage with *Chiasmolithus oamaurensis*, *Coccolithus formosus* and *Reticulofenestra umbilicus*; **NP21 early Oligocene; Rupelian.**

Few, well preserved calcareous nannoplankton

Braarudosphaera bigelowii (Gran & Braarud 1935) Deflandre 1947, *Calcidiscus* sp., *Chiasmolithus oamaurensis* (Deflandre 1954) Hay, Mohler & Wade 1966, *Coccolithus formosus* (Kamptner, 1963) Wise 1973, *Coccolithus pelagicus* (Wallich 1877) Schiller 1930, *Cyclicargolithus floridanus* (Roth and Hay in Hay et al., 1967) Bukry, 1971, *Lanternithus minutus* Stradner, 1961, *Neococcolithes* sp., *Pontosphaera exilis* (Bramlette & Sullivan, 1961) Romein, 1979, *Reticulofenestra bisecta* (Hay, Mohler and Wade, 1966) Roth, 1970, *Reticulofenestra dictyoda* (Deflandre in Deflandre & Fert, 1954) Stradner in Stradner & Edwards, 1968, *Reticulofenestra hillae* Bukry & Percival, 1971, *Reticulofenestra lockeri* Müller, 1970, *Reticulofenestra minuta* Roth, 1970, *Reticulofenestra umbilicus* (Levin, 1965) Martini & Ritzkowski, 1968, *Reticulofenestra vadae*, *Sphenolithus moriformis* (Bronnimann and Stradner, 1960) Bramlette and Wilcoxon, 1967, *Thoracosphaera saxea* Stradner, 1961, *Zygrhablithus bijugatus* (Deflandre in Deflandre and Fert, 1954) Deflandre, 1959.

Reworking from Cretaceous:

Arkhangelskiella cymbiformis Vekshina, 1959, *Broinsonia parca* (Stradner 1963) Bukry 1969, *Cyclagelosphaera reinhardtii* (Perch-Nielsen, 1968) Romein, 1977, *Eiffellithus gorkae* Reinhardt, 1965, *Microrhabdulus decoratus* Deflandre 1959, *Micula decussata* Vekshina, 1959, *Prediscosphaera cretacea* (Arkhangelsky, 1912) Gartner, 1968, *Retecapsa crenulata* (Bramlette & Martini, 1964) Grün in Grün and Allemann, 1975, *Watznaueria barnesae* (Black in Black and Barnes, 1959) Perch-Nielsen, 1968, *Watznaueria manivitae* Bukry, 1973, *Zeugrhabdotus diplogrammus* (Deflandre, 1954) Burnett, 1996.

NOR-72-117

Barren by calcareous nannofossils

NOR-72-129

Stratigraphic attribution: Genus *Reticulofenstra* has a long stratigraphic range: lower Eocene–recent.

Very rare, moderately preserved calcareous nannoplankton

Reticulofenestra sp.

NOR-72-149

Stratigraphic attribution: Nannoplankton assemblage does not allow precise stratigraphic attribution: **Eocene/Oligocene**.

Very rare, moderately preserved calcareous nannoplankton *Coccolithus pelagicus* (Wallich 1877) Schiller 1930, *Cyclicargolithus floridanus* (Roth and Hay in Hay et al., 1967) Bukry, 1971, *Reticulofenestra dictyoda* (Deflandre in Deflandre & Fert, 1954) Stradner in Stradner & Edwards, 1968.

Reworking from Cretaceous:

Watznaueria barnesae (Black in Black and Barnes, 1959) Perch-Nielsen, 1968

NOR-72-159

Stratigraphic attribution: *Coccolithus formosus* has its last occurrence in early Oligocene; up to NP21/22 boundary.

Very rare, moderately preserved calcareous nannoplankton; plant remains

Coccolithus formosus (Kamptner, 1963) Wise 1973

Reworking from Cretaceous:

Micula decussata Vekshina, 1959

NOR-72-165

Barren by calcareous nannofossils

NOR-72-170

Barren by calcareous nannofossils

NOR-72-175

Barren by calcareous nannofossils

NOR-72-179

Barren by calcareous nannofossils

NOR-72-184

Barren by calcareous nannofossils

NOR-72-189

Barren by calcareous nannofossils

NOR-72-194

Barren by calcareous nannofossils

NOR-72-197

Barren by calcareous nannofossils

NTM-97-2

Stratigraphic attribution: *Reticulofenestra umbilica* has stratigraphic range NP16-NP22. Its last occurrence defines NP22/23 boundary. This sample doesn't contain any Miocene taxa and no typical Eocene forms could be observed; **NP22; early Oligocene; Rupelian.**

Rare, moderately preserved calcareous nannoplankton

Coccolithus pelagicus (Wallich 1877) Schiller 1930, *Cyclicargolithus floridanus* (Roth and Hay in Hay et al., 1967) Bukry, 1971, *Pontosphaera* sp., *Reticulofenestra bisecta* (Hay, Mohler and Wade, 1966) Roth, 1970, *Reticulofenestra dictyoda* (Deflandre in Deflandre & Fert, 1951) Stradner in Stradner & Edwards, 1968, *Reticulofenestra lockeri* Müller, 1970, *Reticulofenestra minuta* Roth, 1970, *Reticulofenestra scripsae*, *Reticulofenestra stavensis* (Levin & Joerger, 1967) Varol, 1989, *Reticulofenestra umbilica* (Levin, 1965) Martini & Ritzkowski, 1968, *Reticulofenestra wadae*, *Reticulofenestra* sp., *Sphenolithus moriformis* (Bronnimann and Stradner, 1960) Bramlette and Wilcoxon, 1967, *Zygrhablithus bijugatus* (Deflandre in Deflandre and Fert, 1954) Deflandre, 1959.

NTM-97-6

Stratigraphic attribution: Occurrences of *Coccolithus formosus* and *Reticulofenestra umbilica* allow the attribution to **NP21; early Oligocene; Rupelian**.

Rare, moderately preserved calcareous nannoplankton

Coccolithus formosus (Kamptner, 1963) Wise 1973, *Coccolithus pelagicus* (Wallich 1877) Schiller 1930. *Cyclicargolithus floridanus* (Roth and Hay in Hay et al., 1967) Bukry, 1971. *Reticulofenestra bisecta* (Hay, Mohler and Wade, 1966) Roth, 1970, *Reticulofenestra dictyoda* (Deflandre in Deflandre & Fert, 1954) Stradner in Stradner & Edwards, 1968, *Reticulofenestra hillae* Bukry & Percival, 1971, *Reticulofenestra lockeri* Müller, 1970, *Reticulofenestra minuta* Roth, 1970, *Reticulofenestra scripsae*, *Reticulofenestra stavensis* (Levin & Joerger, 1967) Varol, 1989, *Reticulofenestra umbilica* (Levin, 1965) Martini & Ritzkowski, 1968, *Reticulofenestra wadae*, *Reticulofenestra* sp., *Sphenolithus moriformis* (Bronnimann and Stradner, 1960) Bramlette and Wilcoxon, 1967, *Zygrhablithus bijugatus* (Deflandre in Deflandre and Fert, 1954) Deflandre, 1959.

NTM-97-10

Stratigraphic attribution: The assemblage with *Cribrocentrum reticulatum* and *Discoaster* cf. *barbardiensis*: **Eocene; NP15-NP21**.

Abundant, moderately preserved calcareous nannoplankton

Blackites sp., *Bramletteius serraculoides* Gartner, 1969, *Chiasmolithus* cf. *oamaurensis* (Deflandre 1954) Hay, Mohler & Wade 1966, *Coccolithus formosus* (Kamptner, 1963) Wise 1973. *Coccolithus pelagicus* (Wallich 1877) Schiller 1930. *Coranulus germanicus* Stradner, 1962, *Cribrocentrum reticulatum* (Gartner & Smith, 1967) Perch-Nielsen, 1971, *Cyclicargolithus floridanus* (Roth and Hay in Hay et al., 1967) Bukry, 1971, *Discoaster* cf. *barbardiensis* Tan, 1927, *Lanternithus minutus* Stradner, 1961, *Pemma basquensis* (Martini, 1959) Báldi-Beke, 1971, *Pontosphaera multipora* (Kamptner, 1948) Roth, 1970, *Reticulofenestra bisecta* (Hay, Mohler and Wade, 1966) Roth, 1970, *Reticulofenestra dictyoda* (Deflandre in Deflandre & Fert, 1954) Stradner in Stradner & Edwards, 1968, *Reticulofenestra erbae*, *Reticulofenestra hillae* Bukry & Percival, 1971, *Reticulofenestra lockeri* Müller, 1970, *Reticulofenestra minuta* Roth, 1970, *Reticulofenestra stavensis* (Levin & Joerger, 1967) Varol, 1989, *Reticulofenestra umbilica* (Levin, 1965) Martini & Ritzkowski, 1968, *Reticulofenestra wadae*, *Reticulofenestra* sp., *Sphenolithus editus* Perch-Nielsen in Perch-Nielsen et al. 1978, *Sphenolithus moriformis* (Bronnimann and Stradner, 1960) Bramlette and Wilcoxon, 1967,

Thoracosphaera saxea Stradner, 1961, *Zygrhablithus bijugatus* (Deflandre in Deflandre and Fert, 1954) Deflandre, 1959.

Reworking from Cretaceous:

Watznaueria barnesae (Black in Black and Barnes, 1959) Perch-Nielsen, 1968.

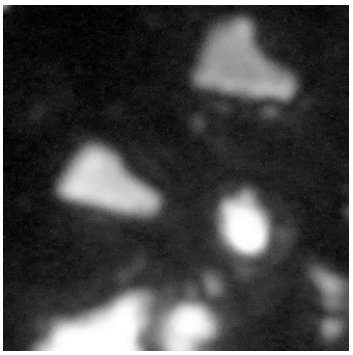

Bramletteius serraculoides

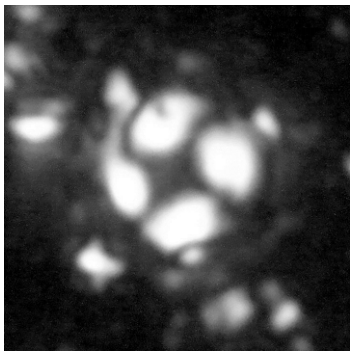

Coccolithus formosus

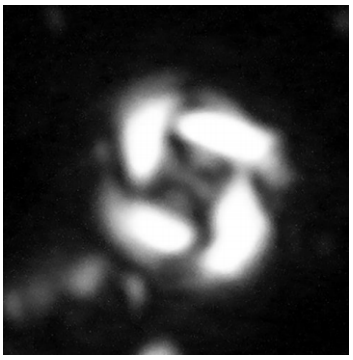

Cribrocentrum reticulatum

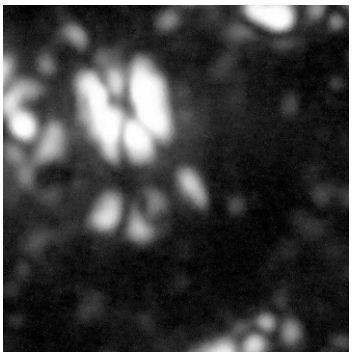

Lanternithus minutus

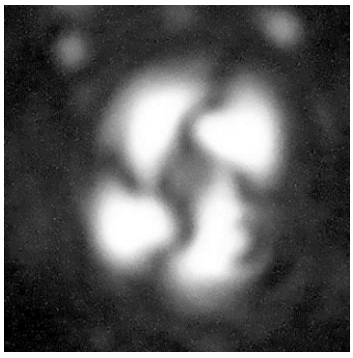

Reticulofenestra dictyoda

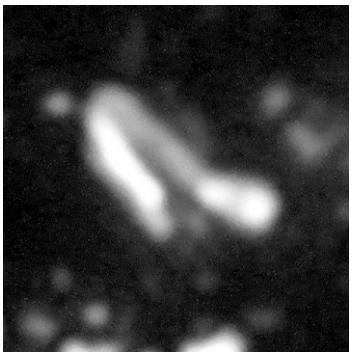

Zygrhablithus bijugatus

NTM-97-12

Stratigraphic attribution: *Reticulofenestra dictyoda* has FO in NP13 whereas its LO is not well documented.

Rare, moderately preserved calcareous nannoplankton

Reticulofenestra dictyoda (Deflandre in Deflandre & Fert, 1954) Stradner in Stradner & Edwards, 1968, *Reticulofenestra minuta* Roth, 1970, *Reticulofenestra* sp.

NTM-97-18

Stratigraphic attribution: Sample contains *Cribrocentrum reticulatum* and *Chiasmolithus* cf. *oamaurensis*: **NP18-NP21; uppermost Bartonian/Priabonian.**

Few, moderately preserved calcareous nannoplankton; common plant remains

Blackites sp., *Bramletteius serraculoides* Gartner, 1969, *Chiasmolithus* cf. *oamaurensis* (Deflandre 1954) Hay, Mohler & Wade 1966. *Coccolithus pelagicus* (Wallich 1877) Schiller 1930, *Cribrocentrum reticulatum* (Gartner & Smith, 1967) Perch-Nielsen, 1971, *Cyclicargolithus floridanus* (Roth and Hay in Hay et al., 1967) Bukry, 1971, *Lanternithus minutus* Stradner, 1961. *Pemma basquensis* (Martini, 1959) Báldi-Beke, 1971, *Pyrocyclus orangensis* (Bukry 1971), *Reticulofenestra bisecta* (Hay, Mohler and Wade, 1966) Roth, 1970, *Reticulofenestra dictyoda* (Deflandre in Deflandre & Fert, 1954) Stradner in Stradner & Edwards, 1968, *Reticulofenestra hillae* Bukry & Percival, 1971, *Reticulofenestra lockeri* Müller, 1970, *Reticulofenestra minuta* Roth, 1970, *Reticulofenestra scripsae*, *Reticulofenestra stavensis* (Levin & Joerger, 1967) Varol, 1989, *Reticulofenestra umbilica* (Levin, 1965) Martini & Ritzkowski, 1968, *Reticulofenestra wadae*, *Reticulofenestra* sp., *Sphenolithus moriformis* (Bronnimann and Stradner, 1960) Bramlette and Wilcoxon, 1967, *Thoracosphaera saxea* Stradner, 1961, *Zygrhablithus bijugatus* (Deflandre in Deflandre and Fert, 1954) Deflandre, 1959.

NTM-97-20

Stratigraphic attribution: *Cribrocentrum reticulatum*, *Clausicoccus subdistichus*, *Sphenolithus predistentus*: **NP17-NP21; uppermost Bartonian/Priabonian.**

Common, moderately preserved calcareous nannoplankton; common plant remains

Blackites sp., *Bramletteius serraculoides* Gartner, 1969, *Clausicoccus subdistichus* (Roth & Hay in Hay et al., 1967) Prins, 1979, *Coccolithus formosus* (Kamptner, 1963) Wise 1973, *Coccolithus pelagicus* (Wallich 1877) Schiller 1930, *Cribrocentrum reticulatum* (Gartner & Smith, 1967) Perch-Nielsen, 1971, *Cyclicargolithus floridanus* (Roth and Hay in Hay et al., 1967) Bukry, 1971, *Discoaster* sp., *Helicosphaera compacta* Bramlette & Wilcoxon, 1967, *Helicosphaera bramlettei* (Müller, 1970) Jafar & Martini, 1975, *Lanternithus minutus* Stradner, 1961, *Pemma basquensis* (Martini, 1959) Báldi-Beke, 1971, *Pemma papillatum* Martini, 1959, *Pontosphaera exilis* (Bramlette & Sullivan, 1961) Romein, 1979, *Pontosphaera multipora* (Kamptner, 1948) Roth, 1970, *Reticulofenestra bisecta* (Hay, Mohler and Wade, 1966) Roth, 1970, *Reticulofenestra dictyoda* (Deflandre in Deflandre & Fert, 1954) Stradner in

Stradner & Edwards, 1968, *Reticulofenestra hillae* Bukry & Percival, 1971, *Reticulofenestra lockeri* Müller, 1970, *Reticulofenestra minuta* Roth, 1970, *Reticulofenestra scripsae*, *Reticulofenestra stavensis* (Levin & Joerger, 1967) Varol, 1989, *Reticulofenestra umbilica* (Levin, 1965) Martini & Ritzkowski, 1968, *Reticulofenestra wadae*, *Reticulofenestra* sp., *Sphenolithus editus* Perch-Nielsen in Perch-Nielsen et al. 1978, *Sphenolithus predistentus* Bramlette & Wilcoxon 1967, *Sphenolithus moriformis* (Bronnimann and Stradner, 1960) Bramlette and Wilcoxon, 1967, *Thoracosphaera saxea* Stradner, 1961, *Zygrhablithus bijugatus* (Deflandre in Deflandre and Fert, 1954) Deflandre, 1959.

Reworking from Cretaceous:

Micula decussata Vekshina, 1959.

NTM-97-26

Stratigraphic attribution: *Reticulofenestra umbilica*: **NP16-NP22; middle Eocene–early Oligocene**.

Rare, moderately preserved calcareous nannoplankton

Blackites sp., *Cyclicargolithus floridanus* (Roth and Hay in Hay et al., 1967) Bukry, 1971, *Reticulofenestra bisecta* (Hay, Mohler and Wade, 1966) Roth, 1970, *Reticulofenestra minuta* Roth, 1970, *Reticulofenestra umbilica* (Levin, 1965) Martini & Ritzkowski, 1968.

MNV-12-52

Barren by calcareous nannofossils

MNV-12-54

Stratigraphic attribution: Sample contains only Mesozoic taxa.

Very rare, moderately preserved calcareous nannoplankton

Micula decussata Vekshina, 1959, *Watznaueria barnesae* (Black in Black and Barnes, 1959) Perch-Nielsen, 1968.

MNV-12-55

Stratigraphic attribution: Rare nannoplankton with *Reticulofenestra bisecta* suggest **Early Eocene–Early Miocene** age.

Rare, moderately preserved calcareous nannoplankton

Reticulofenestra bisecta (Hay, Mohler and Wade, 1966) Roth, 1970, *Thoracosphaera saxea* Stradner, 1961

Reworking from Cretaceous:

Arkhangelskiella cymbiformis Vekshina, 1959, *Micula decussata* Vekshina, 1959, *Retecapsa crenulata* (Bramlette & Martini, 1964) Grün in Grün and Allemann, 1975, *Watznaueria barnesae* (Black in Black and Barnes, 1959) Perch-Nielsen, 1968.

MNV-12-57

Stratigraphic attribution: *Coccolithus pelagicus* has long stratigraphic range: **Paleocene–recent**.

Very rare, moderately preserved calcareous nannoplankton

Coccolithus pelagicus (Wallich 1877) Schiller 1930

Reworking from Cretaceous:

Lucianorhabdus cayexii Deflandre, 1959, *Micula decussata* Vekshina, 1959, *Watznaueria barnesae* (Black in Black and Barnes, 1959) Perch-Nielsen, 1968.

MNV-12-62

Barren by calcareous nannofossils

MNV-12-2

Barren by calcareous nannofossils

MNV-12-8

Barren by calcareous nannofossils

MNV-12-13ca

Barren by calcareous nannofossils

MNV-12-19

Stratigraphic attribution: The last occurrence of *Cyclicargolithus floridanus* is placed in the middle Miocene (NN6).

Rare, moderately preserved calcareous nannoplankton

Cyclicargolithus floridanus (Roth and Hay in Hay et al., 1967) Bukry, 1971

Reworking from Cretaceous:

Micula decussata Vekshina, 1959, *Prediscosphaera cretacea* (Arkhangelsky, 1912) Gartner, 1968, *Watznaueria barnesae* (Black in Black and Barnes, 1959) Perch-Nielsen, 1968, *Watznaueria fossacincta* (Black, 1971) Bown in Bown & Cooper, 1989.

MNV-12-25

Barren by calcareous nannofossils: plant remains

MNV-12-31

Barren by calcareous nannofossils: plant remains

MNV-12-35

Stratigraphic attribution: Sample contains *Cribrocentrum reticulatum*, which has its last occurrence in the **uppermost Eocene, NP21; Priabonian**. Stratigraphic range of *Cribrocentrum reticulatum*: NP15-NP21.

Rare, moderately preserved calcareous nannoplankton

Coccolithus formosus (Kamptner, 1963) Wise 1973, *Coccolithus pelagicus* (Wallich 1877) Schiller 1930, *Cribrocentrum reticulatum* (Gartner & Smith, 1967) Perch-Nielsen, 1971, *Cyclicargolithus floridanus* (Roth and Hay in Hay et al., 1967) Bukry, 1971, *Reticulofenestra bisecta* (Hay, Mohler and Wade, 1966) Roth, 1970, *Reticulofenestra dictyoda* (Deflandre in Deflandre & Fert, 1954) Stradner in Stradner & Edwards, 1968, *Reticulofenestra umbilicus* (Levin, 1965) Martini & Ritzkowski, 1968, *Reticulofenestra vadae*.

Reworking from Cretaceous:

Arkhangelskiella cymbiformis Vekshina, 1959, *Broinsonia parca* (Stradner 1963) Bukry 1969, *Micula decussata* Vekshina, 1959, *Prediscosphaera cretacea* (Arkhangelsky, 1912)

Gartner, 1968, *Watznaueria barnesae* (Black in Black and Barnes, 1959) Perch-Nielsen, 1968, *Watznaueria fossacincta* (Black, 1971) Bown in Bown & Cooper, 1989.

MNV-12-44

Barren by calcareous nannofossils; plant remains

MNV-12-67

Stratigraphic attribution: Rich nannoplankton with *Cribrocentrum reticulatum* and *Clausicoccus subdistichus*: **upper Eocene.**

Common, moderately preserved calcareous nannoplankton

Clausicoccus subdistichus (Roth & Hay in Hay et al., 1967) Prins, 1979, *Coccolithus formosus* (Kamptner, 1963) Wise 1973, *Coccolithus pelagicus* (Wallich 1877) Schiller 1930, *Cribrocentrum reticulatum* (Gartner & Smith, 1967) Perch-Nielsen, 1971, *Cyclicargolithus floridanus* (Roth and Hay in Hay et al., 1967) Bukry, 1971, *Helicosphaera compacta* Bramlette & Wilcoxon, 1967, *Helicosphaera euphratis* Haq, 1966, *Isthmolithus recurvus* Deflandre in Deflandre and Fert, 1954, *Lanternithus minutus* Stradner, 1961, *Reticulofenestra bisecta* (Hay, Mohler and Wade, 1966) Roth, 1970, *Reticulofenestra dictyoda* (Deflandre in Deflandre & Fert, 1954) Stradner in Stradner & Edwards, 1968, *Reticulofenestra hillae* Bukry & Percival, 1971, *Reticulofenestra lockeri* Müller, 1970, *Reticulofenestra minuta* Roth, 1970, *Reticulofenestra scripsae*, *Reticulofenestra stavensis* (Levin & Joerger, 1967) Varol, 1989, *Reticulofenestra vadae*, *Reticulofenestra* sp., *Sphenolithus predistentus* Bramlette & Wilcoxon 1967, *Sphenolithus moriformis* (Bronnimann and Stradner, 1960) Bramlette and Wilcoxon, 1967, *Zygrhablithus bijugatus* (Deflandre in Deflandre and Fert, 1954) Deflandre, 1959.

Reworking from Cretaceous:

Micula decussata Vekshina, 1959

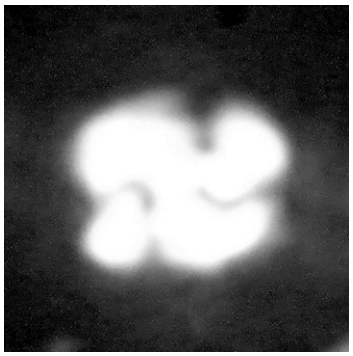

Reticulofenestra bisecta

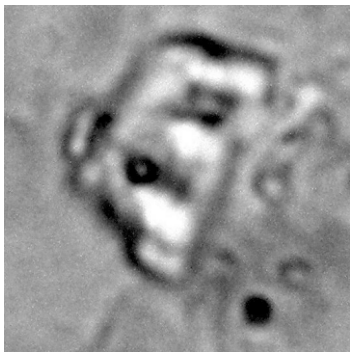

Isthmolithus recurvus

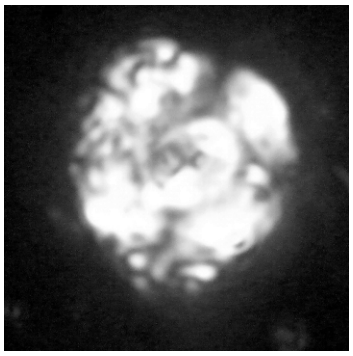

Reticulofenestra stavensis

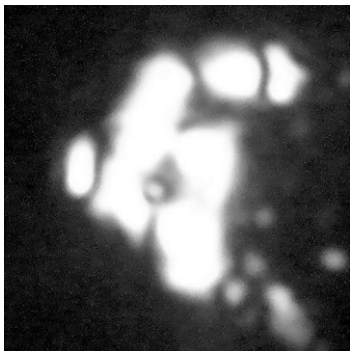

Isthmolithus recurvus

MNV-12-71

Stratigraphic attribution: Based on the co-occurrence of *Isthmolithus recurvus* and *Cribrocentrum reticulatum* this sample can be attributed into **NP19-21; uppermost Eocene; Priabonian**.

Common, moderately preserved calcareous nannoplankton

Bramletteius serraculoides Gartner, 1969, *Chiasmolithus grandis* (Bramlette & Riedel, 1954) Radomski, 1968, *Coccolithus formosus* (Kamptner, 1963) Wise 1973, *Coccolithus pelagicus* (Wallich 1877) Schiller 1930, *Cribrocentrum reticulatum* (Gartner & Smith, 1967) Perch-Nielsen, 1971, *Cyclicargolithus floridanus* (Roth and Hay in Hay et al., 1967) Bukry, 1971, *Isthmolithus recurvus* Deflandre in Deflandre and Fert, 1954, *Lanternithus minutus* Stradner, 1961, *Pontosphaera multipora* (Kamptner, 1948) Roth, 1970, *Pontosphaera* sp., *Reticulofenestra bisecta* (Hay, Mohler and Wade, 1966) Roth, 1970, *Reticulofenestra dictyoda* (Deflandre in Deflandre & Fert, 1954) Stradner in Stradner & Edwards, 1968, *Reticulofenestra hillae* Bukry & Percival, 1971, *Reticulofenestra lockeri* Müller, 1970, *Reticulofenestra minuta* Roth, 1970, *Reticulofenestra scripsae*, *Reticulofenestra stavensis* (Levin & Joerger,

1967) Varol, 1989, *Reticulofenestra umbilicus* (Levin, 1965) Martini & Ritzkowski, 1968, *Reticulofenestra vadae*, *Reticulofenestra* sp., *Sphenolithus* cf. *pseudoradians* Bramlette & Wilcoxon 1967, *Sphenolithus moriformis* (Bronnimann and Stradner, 1960) Bramlette and Wilcoxon, 1967, *Thoracosphaera saxea* Stradner, 1961, *Zygrhablithus bijugatus* (Deflandre in Deflandre and Fert, 1954) Deflandre, 1959.

MNV-12-76

Stratigraphic attribution: **NP19-21; uppermost Eocene; Priabonian**, based on the co-occurrence of *Isthmolithus recurvus* and *Cribrocentrum reticulatum*.

Abundant, moderately preserved calcareous nannoplankton

Blackites sp., *Bramletteius serraculoides* Gartner, 1969, *Coccolithus eopelagicus* (Bramlette & Riedel, 1954) Bramlette & Sullivan, 1961, *Coccolithus formosus* (Kamptner, 1963) Wise 1973, *Coccolithus pelagicus* (Wallich 1877) Schiller 1930, *Cribrocentrum reticulatum* (Gartner & Smith, 1967) Perch-Nielsen, 1971, *Cyclicargolithus floridanus* (Roth and Hay in Hay et al., 1967) Bukry, 1971, *Isthmolithus recurvus* Deflandre in Deflandre and Fert, 1954, *Lanternithus minutus* Stradner, 1961, *Reticulofenestra bisecta* (Hay, Mohler and Wade, 1966) Roth, 1970, *Reticulofenestra dictyoda* (Deflandre in Deflandre & Fert, 1954) Stradner in Stradner & Edwards, 1968, *Reticulofenestra hillae* Bukry & Percival, 1971, *Reticulofenestra lockeri* Müller, 1970, *Reticulofenestra minuta* Roth, 1970, *Reticulofenestra scripsae*, *Reticulofenestra slavensis* (Levin & Joerger, 1967) Varol, 1989, *Reticulofenestra umbilicus* (Levin, 1965) Martini & Ritzkowski, 1968, *Reticulofenestra vadae*, *Reticulofenestra* sp., *Scyphosphaera* sp., *Sphenolithus predistentus* Bramlette & Wilcoxon 1967, *Sphenolithus moriformis* (Bronnimann and Stradner, 1960) Bramlette and Wilcoxon, 1967, *Zygrhablithus bijugatus* (Deflandre in Deflandre and Fert, 1954) Deflandre, 1959.

Reworking from Cretaceous:

Watznaueria barnesae (Black in Black and Barnes, 1959) Perch-Nielsen, 1968.

MNV-12-78

Stratigraphic attribution: *Cribrocentrum reticulatum* and *Isthmolithus recurvus*: **NP19-21; uppermost Eocene; Priabonian**.

Common, moderately preserved calcareous nannoplankton

Coccolithus pelagicus (Wallich 1877) Schiller 1930, *Cribrocentrum reticulatum* (Gartner & Smith, 1967) Perch-Nielsen, 1971, *Cyclicargolithus floridanus* (Roth and Hay in Hay et al., 1967) Bukry, 1971, *Isthmolithus recurvus* Deflandre in Deflandre and Fert, 1954, *Reticulofenestra bisecta* (Hay, Mohler and Wade, 1966) Roth, 1970, *Reticulofenestra dictyoda* (Deflandre in Deflandre & Fert, 1954) Stradner in Stradner & Edwards, 1968, *Reticulofenestra lockeri* Müller, 1970, *Reticulofenestra minuta* Roth, 1970, *Reticulofenestra scripsae*, *Reticulofenestra umbilica* (Levin, 1965) Martini & Ritzkowski, 1968, *Reticulofenestra vadae*, *Reticulofenestra* sp., *Sphenolithus moriformis* (Bronnimann and Stradner, 1960) Bramlette and Wilcoxon, 1967, *Thoracosphaera saxea* Stradner, 1961, *Zygrhablithus bijugatus* (Deflandre in Deflandre and Fert, 1954) Deflandre, 1959.

Reworking from Cretaceous:

Watznaueria barnesae (Black in Black and Barnes, 1959) Perch-Nielsen, 1968.

Appendix D: Bulk Geochemical Parameters

An explanation for $S_{2,corr}$, T_{max1}, T_{max2}, and HI_{corr} can be found in Section 5.1.

Sample	S_1	S_2	$S_{2,corr}$	T_{max1}	T_{max2}	TIC	TOC	S	TOC/S	PI	HI	HI_{corr}
	[mg HC/g]			[C]			[%]		[-]		[mg HC/g TOC]	
NOR-72-1	0.58	1.68	0.79	364	418	2.08	0.70	1.35	0.51	0.26	242	182
NOR-72-2	0.50	1.36		365		1.49	0.44	0.58	0.76	0.27	309	
NOR-72-4	0.40	1.27		366		3.66	0.48	0.88	0.55	0.24	262	
NOR-72-6	0.54	1.31		360		1.82	0.49	1.06	0.46	0.29	268	
NOR-72-8	0.47	1.53		361	415	1.79	0.52	0.89	0.59	0.23	292	
NOR-72-10	0.36	1.08	0.52	362	417	5.59	0.54	1.55	0.35	0.25	200	181
NOR-72-12	0.40	1.38		355		1.74	0.52	0.95	0.54	0.22	265	
NOR-72-14	0.54	1.82		360		1.71	0.62	0.88	0.70	0.23	294	
NOR-72-16	0.44	1.11		356		3.23	0.50	0.39	1.28	0.28	228	
NOR-72-18	0.65	1.79		355		1.08	0.43	0.76	0.57	0.27	416	
NOR-72-20	0.54	1.54	0.72	350	421	2.09	0.76	0.85	0.89	0.26	204	175
NOR-72-22	0.25	1.11	0.48	356	431	2.02	0.56	0.68	0.83	0.18	198	178
NOR-72-24	0.50	1.32	0.58	351	426	1.81	0.65	1.05	0.62	0.27	202	175
NOR-72-26	0.61	2.00		354		1.48	0.81	1.16	0.70	0.23	246	
NOR-72-28	0.69	2.94	1.55	369	431	2.21	0.99	1.59	0.62	0.19	296	185
NOR-72-30	0.38	0.83				0.91	0.30	0.30	0.98	0.31	278	
NOR-72-32	0.35	1.04		353		1.39	0.43	0.61	0.72	0.25	240	
NOR-72-34	0.43	0.92		356		1.42	0.37	0.43	0.86	0.32	249	
NOR-72-36	0.78	1.44		356		0.52	0.42	0.28	1.49	0.35	342	
NOR-72-38	0.67	1.89		358		1.05	0.64	0.78	0.82	0.26	294	
NOR-72-40	0.49	1.16	0.61	349	431	1.42	0.57	0.67	0.86	0.30	201	175
NOR-72-42	0.60	1.84		362		1.11	0.44	0.57	0.77	0.25	417	
NOR-72-43	1.09	3.28		362	429			0.50		0.25		
NOR-72-44	0.65	2.32	1.16	359	433	2.07	0.70	1.17	0.60	0.22	333	180
NOR-72-45	0.72	2.20		363	426	1.40	0.53	0.53	0.99	0.25	416	
NOR-72-46	0.75	2.50		363		1.88	0.73	0.97	0.75	0.23	343	
NOR-72-47	0.98	2.84		359		0.97	0.68	0.53	1.29	0.26	419	
NOR-72-48	0.79	1.84		359		1.10	0.41	0.53	0.78	0.30	448	
NOR-72-50	0.66	2.16		357		1.32	0.59	0.51	1.16	0.23	364	
NOR-72-52	0.60	1.75		356		0.92	0.55	0.48	1.15	0.25	319	
NOR-72-53	0.67	1.74		353		1.39	0.45	0.41	1.10	0.28	386	
NOR-72-54	0.58	1.78		356		0.98	0.41	0.25	1.67	0.24	429	
NOR-72-56	0.52	1.16		350	428	0.83	0.39	0.36	1.09	0.29	295	
NOR-72-57	0.76	1.58		351	431	1.25	0.52	0.57	0.92	0.32	301	
NOR-72-58	0.67	1.72		358		1.46	0.35	0.44	0.79	0.28	488	
NOR-72-59	0.82	1.96		356		0.76	0.57	0.40	1.41	0.29	344	
NOR-72-60	0.65	1.78		360		0.93	0.44	0.59	0.74	0.27	408	
NOR-72-61	0.93	2.29		357		1.03	0.66	0.51	1.28	0.29	349	
NOR-72-62	0.57	1.42		352		0.90	0.58	0.43	1.35	0.29	244	
NOR-72-63	0.75	1.67		356	432	1.02	0.58	0.48	1.20	0.31	287	
NOR-72-64	0.62	1.81		360		1.16	0.51	0.48	1.06	0.26	358	
NOR-72-65	0.77	2.02		356		1.12	0.59	0.44	1.35	0.28	341	
NOR-72-66	0.51	1.53		361		1.24	0.45	0.38	1.20	0.25	338	
NOR-72-67	0.76	2.37		355	424	1.35	0.59	0.41	1.46	0.24	399	
NOR-72-68	0.47	1.73	0.72	358	428	1.79	0.93	1.04	0.89	0.21	186	179
NOR-72-69	0.84	1.93		356		0.95	0.66	0.43	1.54	0.30	292	
NOR-72-70	0.56	1.76	0.61	363	427	1.27	0.54	0.74	0.73	0.24	326	181
NOR-72-71	0.88	2.53		359	422	1.24	0.55	0.40	1.39	0.26	456	
NOR-72-72	0.61	2.10	0.77	366	431	1.86	0.65	0.95	0.69	0.22	321	183
NOR-72-73	0.79	2.24		362	422	2.03	0.62	0.50	1.25	0.26	360	
NOR-72-74	0.42	1.21	0.60	349	430	1.82	0.50	0.74	0.67	0.26	244	175
NOR-72-75	0.82	2.12		353	422	1.06	0.61	0.51	1.19	0.28	351	
NOR-72-76	0.69	2.82		364		1.42	0.72	0.74	0.96	0.20	393	
NOR-72-77	1.07	2.47		363		1.29	0.84	0.52	1.62	0.30	293	
NOR-72-78	0.58	1.90		360		1.45	0.61	0.62	0.98	0.23	313	
NOR-72-79	1.00	3.16		363	435	1.27	0.76	0.49	1.55	0.21	415	
NOR-72-80	0.46	1.13	0.44	349	426	1.03	0.58	0.64	0.91	0.29	193	174
NOR-72-81	0.80	1.48		357		0.87	0.50	0.41	1.22	0.35	293	
NOR-72-82	0.80	2.56		363		0.95	0.59	0.50	1.17	0.24	437	
NOR-72-84	0.67	1.98		360		1.04	0.52	0.44	1.17	0.25	384	
NOR-72-85	1.12	2.31		361		1.06	0.64	0.46	1.40	0.32	368	
NOR-72-86	0.71	1.56		359		1.69	0.43	0.33	1.33	0.31	360	
NOR-72-88	0.84	2.07		358		1.08	0.46	0.47	0.97	0.29	450	
NOR-72-89	1.06	2.13		357		1.04	0.60	0.31	1.92	0.33	353	

Sample	S_1	S_2	$S_{2,corr}$	T_{max1}	T_{max2}	TIC	TOC	S	TOC/S	PI	HI	HI_{corr}
	[mg HC/g]			[C]			[%]		[-]		[mg HC/g TOC]	
NOR-72-90	1.09	1.88		353	428	1.14	0.45	0.39	1.14	0.34	418	
NOR-72-92	0.96	1.92		361	418	1.32	0.46	0.45	1.01	0.30	421	
NOR-72-93	1.08	2.26		354	420	1.40	0.65	0.47	1.39	0.32	349	
NOR-72-94	0.68	1.61		360		2.55	0.48	0.52	0.91	0.30	337	
NOR-72-95	1.08	2.34		358	430	1.63	1.05	0.77	1.36	0.31	223	
NOR-72-96	0.80	1.78	0.62	355	429	1.04	0.71	0.62	1.14	0.31	251	178
NOR-72-97	0.95	2.27		358	429	1.53	0.81	0.74	1.08	0.29	281	
NOR-72-98	0.85	1.81	0.64	354	428	1.14	0.72	0.76	0.95	0.32	251	177
NOR-72-100	0.98	2.14		359		1.04	0.86	0.66	1.29	0.31	249	
NOR-72-101	0.89	2.36		360		1.24	0.74	0.68	1.09	0.27	319	
NOR-72-102	0.76	2.50	0.95	365	432	1.58	0.82	1.01	0.81	0.23	305	182
NOR-72-104	0.58	1.90	0.80	364	428	1.68	0.64	0.87	0.73	0.23	297	182
NOR-72-105	0.87	2.61		363	422	1.53	0.66	0.76	0.87	0.25	397	
NOR-72-106	0.85	2.23	0.82	361		1.67	0.88	1.01	0.87	0.28	254	181
NOR-72-107	1.13	3.41		366	431	2.10	0.97	1.76	0.55	0.25	352	
NOR-72-108	0.65	1.51	0.64	351	428	1.45	0.66	0.84	0.78	0.30	229	177
NOR-72-109	0.98	2.71		366	424	1.75	0.82	0.93	0.88	0.26	332	
NOR-72-110	0.82	3.45	1.77	367	428	1.81	0.89	1.00	0.89	0.19	387	184
NOR-72-111	0.89	2.81		358	431	1.64	0.86	0.94	0.91	0.21	326	
NOR-72-112	0.78	2.37	0.88	368		1.93	0.84	1.01	0.83	0.25	283	184
NOR-72-113	1.25	3.29		365		1.47	1.01	1.56	0.65	0.28	326	
NOR-72-114	0.63	1.93	0.81	365	431	1.52	0.82	0.99	0.83	0.25	236	182
NOR-72-115	0.77	2.35		362	427	1.19	0.74	0.91	0.81	0.25	318	
NOR-72-116	0.69	2.17	0.79	362		1.39	0.86	1.17	0.73	0.24	252	181
NOR-72-117	0.92	3.02		362	439	1.48	0.85	1.06	0.80	0.23	356	
NOR-72-118	0.56	1.67	0.64	350	432	1.38	0.78	0.85	0.91	0.25	215	175
NOR-72-120	0.51	1.87	0.69	363		1.22	0.81	0.99	0.82	0.21	230	182
NOR-72-121	1.07	2.63		358	434	1.68	0.87	0.88	0.99	0.29	301	
NOR-72-122	0.60	2.14	1.07	358	432	1.78	0.75	1.10	0.68	0.22	287	179
NOR-72-124	0.77	2.42	1.18	356	433	1.80	0.88	1.15	0.76	0.24	276	178
NOR-72-126	0.63	2.68	1.30	365	429	1.91	0.85	1.23	0.70	0.19	313	182
NOR-72-128	0.76	2.74	1.46	362	430	1.70	0.86	1.27	0.68	0.22	317	181
NOR-72-129	0.99	3.21		364	433	1.74	0.98	1.05	0.93	0.24	328	
NOR-72-130	0.96	2.49	1.26	352	435	1.12	1.00	0.72	1.38	0.28	250	176
NOR-72-131	1.15	2.96		350	432	1.80	1.02	1.38	0.74	0.28	289	
NOR-72-132	0.81	2.18	1.19	349	434	1.32	1.05	1.52	0.69	0.27	207	175
NOR-72-134	0.94	3.15	1.49	358	437	1.41	1.13	1.46	0.77	0.23	279	179
NOR-72-135	1.18	3.77		359	432	1.49	1.11	1.28	0.86	0.24	340	
NOR-72-136	0.92	2.84	1.19	357	437	1.40	1.16	1.66	0.70	0.21	245	178
NOR-72-137	1.33	4.29			432	1.48	1.10	1.30	0.85	0.22	389	
NOR-72-138	1.53	4.69	2.53	367	435	1.80	1.35	1.59	0.85	0.25	348	183
NOR-72-139	1.09	3.41			430	8.58	1.09	0.41	2.63	0.24	314	
NOR-72-140	1.04	3.15	1.77	359	436	2.42	1.09	1.28	0.85	0.25	289	179
NOR-72-141	1.37	4.65		357	439	1.09	1.33	1.70	0.79	0.23	348	
NOR-72-142	0.98	4.33	2.83	353	443	0.83	1.36	1.33	1.02	0.18	319	177
NOR-72-143	1.19	4.31		356	436	3.49	1.26	1.49	0.85	0.22	342	
NOR-72-144	0.78	3.15	1.71	362	436	1.64	1.02	1.84	0.56	0.20	308	181
NOR-72-145	1.12	3.72		361	437	1.59	1.15	1.47	0.78	0.23	324	
NOR-72-146	1.09	3.67	1.96	359	437	0.83	1.48	1.95	0.76	0.23	247	179
NOR-72-147	1.27	3.36		355	437	1.10	1.26	1.75	0.72	0.25	266	
NOR-72-148	1.25	4.03	1.94	360	438	0.81	1.28	2.73	0.47	0.21	315	180
NOR-72-149	1.88	4.10		352	432	1.27	1.42	2.63	0.54	0.23	288	
NOR-72-150	1.14	3.58	1.73	358	438	0.99	1.30	1.42	0.92	0.24	275	179
NOR-72-151	1.55	4.06		354	438	0.95	1.35	1.03	1.31	0.28	300	
NOR-72-152	1.25	3.34	1.43	363	434	0.81	1.10	0.70	1.58	0.21	303	182
NOR-72-153	1.22	3.36		352	440	0.75	1.16	0.53	2.19	0.27	289	
NOR-72-154	1.10	4.17	2.54	349	439	0.52	1.22	0.65	1.88	0.21	342	174
NOR-72-156	0.95	3.34	1.92	348	441	0.56	1.29	0.90	1.44	0.22	259	174
NOR-72-157	1.43	4.58		352	440	0.47	1.54	0.94	1.64	0.21	297	
NOR-72-158	0.92	3.68	2.41	350	440	0.67	1.39	1.32	1.05	0.20	265	175
NOR-72-159	1.28	4.88		351	441	0.71	1.44	1.28	1.13	0.21	338	
NOR-72-160	0.95	1.17	2.45	359	442	0.39	1.61	1.31	1.22	0.18	259	180
NOR-72-161	12.80	7.13			427	0.47	3.57	0.79	4.50	0.64	200	
NOR-72-162	8.53	7.38			431	0.43	2.91	0.81	3.61	0.54	253	
NOR-72-163	7.85	8.03			425	0.34	2.70	1.55	1.74	0.49	297	
NOR-72-164	6.59	10.37			430	0.42	2.98	1.83	1.63	0.39	347	
NOR-72-165	5.47	5.76			435	0.17	2.19	1.63	1.34	0.49	263	
NOR-72-166	13.99	11.34			436	0.79	4.22	2.17	1.95	0.55	269	
NOR-72-167	11.35	9.12			430	0.94	3.12	2.16	1.45	0.55	292	
NOR-72-168	12.85	10.07			432	1.04	3.62	2.18	1.67	0.56	278	
NOR-72-169	11.37	8.94			428	1.13	3.30	2.54	1.30	0.56	271	

Sample	S_1	S_2	$S_{2,corr}$	T_{max1}	T_{max2}	TIC	TOC	S	TOC/S	PI	HI	HI_{corr}
	[mg HC/g]			[C]			[%]		[-]		[mg HC/g TOC]	
NOR-72-170	11.71	8.83			429	0.84	3.27	2.38	1.37	0.57	270	
NOR-72-171	12.75	10.52			432	0.85	3.34	2.38	1.40	0.55	315	
NOR-72-172	15.42	8.82			430	0.90	3.47	2.38	1.46	0.61	254	
NOR-72-173	12.88	10.25			431	0.61	3.57	2.11	1.69	0.56	287	
NOR-72-174	11.09	11.18			434	0.49	3.43	2.25	1.52	0.50	326	
NOR-72-175	8.64	10.15			432	0.55	3.19	2.58	1.24	0.46	318	
NOR-72-176	13.18	6.71			427	0.78	3.41	2.68	1.27	0.66	197	
NOR-72-177	15.37	8.94			431	1.07	3.54	2.67	1.32	0.63	252	
NOR-72-178	13.60	7.13			431	0.85	3.36	2.46	1.37	0.66	212	
NOR-72-179	14.83	7.46			431	0.63	3.63	2.91	1.25	0.67	206	
NOR-72-180	15.67	7.79			430	0.74	3.62	2.78	1.30	0.67	215	
NOR-72-181	14.09	7.19			432	0.79	3.47	2.72	1.28	0.66	207	
NOR-72-182	11.80	4.60			422	0.63	2.98	2.67	1.11	0.72	155	
NOR-72-183	14.19	3.75			422	1.01	3.08	2.47	1.25	0.79	122	
NOR-72-184	16.91	6.90			431	1.06	3.38	3.10	1.09	0.71	204	
NOR-72-185	16.97	7.02			432	0.50	4.14	2.90	1.43	0.71	169	
NOR-72-186	10.80	4.09			423	0.63	2.91	2.52	1.15	0.73	141	
NOR-72-187	12.35	4.23			425	0.57	2.97	2.16	1.37	0.74	143	
NOR-72-188	17.01	6.79			430	0.64	3.76	2.95	1.28	0.71	180	
NOR-72-189	16.85	4.78			419	1.04	3.18	2.85	1.12	0.78	150	
NOR-72-190	7.40	4.93			427	0.32	2.41	2.69	0.89	0.60	205	
NOR-72-191	9.03	11.42			430	0.48	2.84	2.22	1.28	0.44	402	
NOR-72-192	17.46	7.68			430	0.96	3.07	1.88	1.64	0.69	250	
NOR-72-193	21.02	8.42			424	0.71	4.27	2.53	1.69	0.71	197	
NOR-72-195	22.21	7.25			433	1.01	3.17	0.97	3.29	0.75	228	
NOR-72-197	23.52	9.55			429	0.80	4.56	3.03	1.50	0.71	209	
NTM-97-1	0.64	1.83	0.83	361	422	1.86	0.79	1.33	0.59	0.26	233	181
NTM-97-3	0.73	1.97		362	421	2.49	0.82	1.18	0.69	0.27	241	
NTM-97-5	0.35	1.23	0.66	358	422	2.73	0.63	1.20	0.52	0.22	196	179
NTM-97-7	0.83	2.32		361	424	2.50	0.81	1.18	0.69	0.26	286	
NTM-97-9	0.60	1.47	0.66		422	2.52	0.73	1.51	0.49	0.29	199	89
NTM-97-10	0.58	1.82			424	2.69	0.82	1.29	0.63	0.24	221	
NTM-97-11	0.79	2.73			428	2.77	1.22	2.10	0.58	0.22	224	
NTM-97-12	1.07	3.54			430	2.32	1.45	2.49	0.58	0.23	244	
NTM-97-13	0.59	3.12	2.18		431	2.79	1.35	2.63	0.51	0.16	230	161
NTM-97-14	0.90	3.82			429	2.61	1.49	2.38	0.63	0.19	257	
NTM-97-15	0.87	3.85			430	2.57	1.59	2.37	0.67	0.18	242	
NTM-97-16	1.56	6.76			430	1.88	2.24	2.97	0.75	0.19	302	
NTM-97-17	1.35	5.81			428	2.70	1.88	2.91	0.65	0.19	309	
NTM-97-18	1.52	6.61			431	2.26	2.09	2.59	0.81	0.19	316	
NTM-97-19	1.86	8.52			429	3.54	2.25	2.18	1.03	0.18	379	
NTM-97-20	2.11	9.96			428	2.40	2.62	2.67	0.98	0.17	380	
NTM-97-21	0.97	5.81			428	2.60	1.87	2.31	0.81	0.11	310	
NTM-97-22	1.89	9.58			428	2.63	2.40	2.54	0.94	0.16	400	
NTM-97-23	2.05	9.98			429	2.52	2.71	2.72	1.00	0.17	369	
NTM-97-24	1.59	10.01			426	2.48	2.68	2.51	1.07	0.14	373	
NTM-97-25	1.31	6.52			428	2.53	1.96	2.44	0.80	0.17	332	
NTM-97-26	2.29	7.20			427	2.17	2.23	2.24	1.00	0.24	323	
NTM-97-27	2.14	9.25			427	2.38	2.59	2.47	1.05	0.19	357	
MNV-12-1	14.43	10.57	9.25		426	0.68	4.08	2.74	1.49	0.58	259	259
MNV-12-3	21.49	11.03		340	426	1.14	4.21	1.69	2.50	0.66	262	
MNV-12-5	25.97	9.90			430	0.79	4.54	1.94	2.34	0.72	218	
MNV-12-7	19.34	12.14			427	0.92	4.49	1.60	2.80	0.61	271	
MNV-12-9	26.12	13.04			429	1.07	5.04	2.65	1.90	0.67	258	
MNV-12-11	12.42	10.39			422	0.42	4.17	2.97	1.41	0.51	249	
MNV-12-13	12.44	9.35			425	0.66	3.73	3.27	1.14	0.57	251	
MNV-12-15	14.78	10.59			423	0.30	4.17	2.80	1.49	0.58	254	
MNV-12-17	10.66	8.98			426	0.62	3.41	2.13	1.60	0.54	263	
MNV-12-19	21.07	10.42			424	0.94	4.75	2.87	1.65	0.67	219	
MNV-12-21	19.51	9.31			427	1.62	3.54	3.31	1.07	0.68	263	
MNV-12-23	18.34	11.65			427	0.61	4.74	3.31	1.43	0.61	246	
MNV-12-24	16.96	8.28			423	0.53	4.37	3.15	1.39	0.67	189	
MNV-12-25	15.17	9.62			423	0.59	4.35	3.38	1.29	0.61	221	
MNV-12-26	11.05	9.74			421	0.59	3.86	3.08	1.25	0.53	252	
MNV-12-27	12.98	11.68			426	0.69	4.34	3.28	1.32	0.53	269	
MNV-12-28	10.99	7.33			418	0.31	3.81	3.02	1.26	0.60	192	
MNV-12-29	17.50	9.56			425	3.05	3.81	2.62	1.45	0.65	251	
MNV-12-31	21.80	12.40			425	0.71	5.29	3.10	1.71	0.64	234	
MNV-12-32	13.64	7.19			407	0.42	4.48	3.50	1.28	0.65	161	
MNV-12-33	20.97	8.77			417	0.72	4.67	3.70	1.26	0.71	188	
MNV-12-34	12.81	9.32			422	1.52	3.34	2.25	1.48	0.58	279	

Sample	S_1	S_2	$S_{2,corr}$	T_{max1}	T_{max2}	TIC	TOC	S	TOC/S	PI	HI	HI_{corr}
	[mg HC/g]			[C]			[%]		[-]		[mg HC/g TOC]	
MNV-12-35	10.02	6.99			415	0.72	3.67	2.60	1.41	0.59	190	
MNV-12-36	3.93	3.36			409	0.17	2.80	3.09	0.91	0.54	120	
MNV-12-37	10.64	6.04			408	0.74	3.43	3.13	1.10	0.61	176	
MNV-12-38	9.79	7.61			410	1.04	3.64	3.28	1.11	0.56	209	
MNV-12-39	7.96	7.40			404	0.63	3.85	3.61	1.07	0.52	193	
MNV-12-40	12.82	10.36			415	1.00	4.45	3.23	1.38	0.55	233	
MNV-12-41	10.21	5.77			409	0.86	4.15	4.10	1.01	0.61	139	
MNV-12-42	14.82	7.92			415	0.45	4.41	3.98	1.11	0.65	180	
MNV-12-43	15.36	7.22			415	0.68	4.39	3.77	1.16	0.68	164	
MNV-12-44	16.88	7.40			411	2.18	4.69	3.73	1.26	0.70	158	
MNV-12-45	17.44	7.63			422	5.86	3.12	2.17	1.43	0.70	245	
MNV-12-46	17.90	9.89			417	2.91	4.39	3.27	1.34	0.61	225	
MNV-12-47	17.30	11.05			418	2.14	5.38	3.73	1.44	0.61	205	
MNV-12-48	18.74	8.72			416	1.14	5.00	3.84	1.30	0.68	174	
MNV-12-49	22.51	8.33			414	1.26	4.66	3.78	1.23	0.73	179	

Appendix E: Organic Petrology

Sample	Top	Bottom	TOC	Maceral Content			Vitrinite Reflectance			
				Vitrinite	Liptinite	Inertinite	Mean	Std. Dev.	No. of Points	Estimated*
	[m]		[%]	%]			[% R_o]		[-]	[% R_o]
NOR-72-26[c]	3825	3830	0.81				0.51	0.02	50	
NOR-72-28[c]	3835	3840	0.99				0.46	0.03	50	0.60
NOR-72-92[c]	4155	4160	0.46				0.41	0.01	30	
NOR-72-150[c]	4455	4460	1.3				0.56	0.01	52	0.72
NOR-72-161	4510	4513	3.57	2–3	3–4	<1				0.53
NOR-72-165	4549	4553	2.19	2–3	2–3					0.67
NOR-72-166	4559	4562	4.22	2–3	4–6	1				0.69
NOR-72-168	4577	4580	3.62	1–2	1–2					0.62
NOR-72-169	4589	4592	3.3	2–3	3					0.54
NOR-72-170	4598	4601	3.27	1–2	5					0.56
NOR-72-173	4628	4631	3.57	1–2	2–3					0.64
NOR-72-175	4649	4652	3.19	2–3	3–4					0.63
NOR-72-181	4718	4721	3.47	1	2–3	0.5				0.61
NOR-72-183	4739	4742	3.08	2–3	1–2					0.41
NOR-72-184	4748	4751	3.38	2–3	5		0.43	0.02	3	0.58
NOR-72-188	4799	4793	3.76	2	2–3	<1				0.54
NOR-72-195	4859	4862	3.17	2–3	1–2	1				0.60
NTM-97-9[c]	2370	2375	0.73				0.32	0.01	30	0.44
NTM-97-17	2470	2475	1.88	5	3–4	<1	0.37	0.01	26	0.54
NTM-97-21	2525	2530	1.87	5–6	3	1	0.55	0.02	24	0.54
NTM-97-21[c]	2525	2530	1.87				0.46	0.01	50	0.54
NTM-97-25	2545	2550	1.96	4–5	2–3	<1	0.30	0.02	41	0.54
MNV-12-1	3821	3824	4.08	2–3	3–4					0.51
MNV-12-5	3833	3836	4.54	>1	2–3					0.58
MNV-12-9	3848	3851	5.04	1–2	>1	0.5				0.56
MNV-12-13	3860	3863	3.73	2–3	2–3					0.49
MNV-12-17	3872	3875	3.41	2–3	<1					0.51
MNV-12-21	3884	3887	3.54	3–4	2–3					0.53
MNV-12-25	3896	3899	4.35	3–4	2–3	<1	0.45	0.02	39	0.45
MNV-12-29	3908	3911	3.81	3–4	2–3	1–2	0.45	0.02	22	0.49
MNV-12-33	3923	3926	4.67	1–2	1–2					0.35
MNV-12-37	3938	3940	3.43	2–3	2–3	2				0.18
MNV-12-41	3946	3948	4.15	1–2	1–2	0.5				0.26
MNV-12-45	3954	3956	3.12	3–4	3–4		0.45	0.02	10	0.44
MNV-12-49	3965	3970	4.66	2–3	1	0.5				0.29

[c]coal sample; *estimated from T_{max}

Appendix F: Gas Chromatography-Mass Spectroscopy

Oil	Reservoir	Sat. HC	Arom. HC	NSO	Asph.	Resins	*n*-Alkanes	Isoprenoids	*n*-C_{15-19} / *n*-Alkanes	*n*-C_{21-25} / *n*-Alkanes	*n*-C_{27-31} / *n*-Alkanes	CPI
		[wt.%]	[wt.%]	[wt.%]	[wt.%]	[wt.%]	[µg/g Oil]	[µg/g Oil]				
G-NTM-21	Eocene	24	16	59	1	60	33352	8027	0.37	0.33	0.17	1.03
G-NTM-59	Eocene	21	14	65	1	65	27073	6588	0.36	0.33	0.18	1.02
G-NTM-78	Oligocene	8	4	31	57	89	10066	2183	0.35	0.35	0.18	1.04
G-NTM-98	Eocene	43	15	42	1	42	57752	11848	0.39	0.33	0.16	1.04
G-MNV-12	Cretaceous	35	12	52	1	53	10256	2178	0.42	0.32	0.13	1.02

Extract	Top	Bottom	Sat. HC	Arom. HC	NSO	Asph.	Resins	*n*-Alkanes	Isoprenoids	*n*-C_{15-19} / *n*-Alkanes	*n*-C_{21-25} / *n*-Alkanes	*n*-C_{27-31} / *n*-Alkanes	CPI
	[m]	[m]	[wt.%]	[wt.%]	[wt.%]	[wt.%]	[wt.%]	[µg/g TOC]	[µg/g TOC]				
NOR-72-146	4435	4440	22	13	62	3		5188	927	0.34	0.38	0.15	1.14
NOR-72-149	4450	4455	38	11	40	11		1911	388	0.33	0.35	0.19	1.23
NOR-72-157	4490	4495	43	8	43	6		8900	1552	0.33	0.36	0.18	1.16
NOR-72-166	4559	4562	30	16	53	1		1569	766	0.69	0.20	0.00	1.73
NOR-72-193	4826	4829	13	11	76	1		4801	2196	0.68	0.20	0.00	
NOR-72-197	4888	4891	17	15	68	1		5109	2414	0.68	0.20	0.00	1.59
NTM-97-11	2440	2445	17	9	48	26		1140	442	0.63	0.17	0.09	1.55
NTM-97-12	2445	2450	29	13	55	4		3339	1505	0.73	0.14	0.06	1.29
NTM-97-13	2450	2455	26	13	58	4		2592	835	0.64	0.18	0.08	1.21
NTM-97-14	2455	2460	24	13	55	8		1719	546	0.61	0.20	0.09	1.24
NTM-97-15	2460	2465	21	11	60	8		1514	441	0.58	0.22	0.10	1.26
NTM-97-16	2465	2470	63	15	10	12		7085	3452	0.68	0.17	0.03	1.22
NTM-97-17	2470	2475	28	13	53	5		3543	1394	0.70	0.16	0.05	1.18
NTM-97-18	2475	2480	22	13	62	3		1259	446	0.60	0.22	0.09	1.20
NTM-97-19	2515	2520	21	11	62	6		4264	1085	0.46	0.30	0.13	1.09
NTM-97-20	2520	2525	38	15	28	19				0.65	0.16	0.08	1.01
NTM-97-21	2525	2530	20	11	65	5		3857	813	0.42	0.32	0.14	1.11
NTM-97-22	2530	2535	33	11	48	8		4992	1153	0.39	0.35	0.13	1.14
NTM-97-24	2540	2545	27	11	59	3		5598	1346	0.41	0.33	0.13	1.06
NTM-97-25	2545	2550	18	10	68	4		3624	928	0.49	0.28	0.11	1.09
NTM-97-26	2550	2555	34	15	47	4		8473	3485	0.66	0.19	0.07	1.06
NTM-97-27	2555	2560	27	11	58	4		8220	2196	0.47	0.30	0.11	1.06
MNV-12-47w	3965	3970	27	5	61	7		3982	2693	0.51	0.34	0.01	1.70
MNV-12-47m	3965	3970	41	17	42	0				0.63	0.24	0.01	1.28

Oil	Reservoir	Pr / *n*-C_{17}	Ph / *n*-C_{18}	Pr / Ph	C_{25} HBI Alkane	C_{25} HBI / *n*-C21	Steranes	C_{27} Diasteranes / C_{27} Steranes	C_{27} Steranes / Steranes	C_{28} Steranes / Steranes	C_{29} Steranes / Steranes
					[µg/g Oil]		[µg/g Oil]				
G-NTM-21	Eocene	1.29	0.72	1.92	141	0.06	304	0.93	0.36	0.30	0.33
G-NTM-59	Eocene	1.37	0.75	1.84	106	0.06	255	1.00	0.36	0.29	0.35
G-NTM-78	Oligocene	1.24	0.77	1.69	48	0.06	125	0.74	0.35	0.29	0.36
G-NTM-98	Eocene	0.87	0.59	1.66	141	0.04	318	1.01	0.45	0.26	0.30
G-MNV-12	Cretaceous	0.83	0.65	1.50	50	0.07	54	0.95	0.36	0.31	0.33

Extract	Top	Bottom	Pr / *n*-C_{17}	Ph / *n*-C_{18}	Pr / Ph	C_{25} HBI Alkane	C_{25} HBI / *n*-C21	Steranes	C_{27} Diasteranes / C_{27} Steranes	C_{27} Steranes / Steranes	C_{28} Steranes / Steranes	C_{29} Steranes / Steranes
	[m]	[m]				[µg/g TOC]		[µg/g TOC]				
NOR-72-146	4435	4440	0.97	0.66	1.55	10	0.02	41	0.75	0.37	0.23	0.41
NOR-72-149	4450	4455	1.28	0.81	1.42	8		29	0.33	0.37	0.26	0.37
NOR-72-157	4490	4495	1.25	0.56	2.07	11	0.02	34	0.66	0.37	0.23	0.40
NOR-72-166	4559	4562	1.14	1.11	1.10	0	0.00	0				
NOR-72-193	4826	4829	1.18	0.99	1.17	53	0.11	0				
NOR-72-197	4888	4891	1.07	1.12	1.10	61	0.13	0				
NTM-97-11	2440	2445	1.23	0.76	1.70	4	0.06	28	0.42	0.34	0.34	0.32
NTM-97-12	2445	2450	1.29	0.80	2.25	4	0.03	52	0.46	0.32	0.35	0.33
NTM-97-13	2450	2455	1.09	0.54	2.03	4	0.03	56	0.44	0.34	0.32	0.34
NTM-97-14	2455	2460	1.04	0.58	1.89	4	0.04	42	0.44	0.36	0.34	0.30
NTM-97-15	2460	2465	1.02	0.58	1.80	3	0.03	34	0.50	0.32	0.34	0.33
NTM-97-16	2465	2470	1.30	0.96	1.31	79	0.15	68	0.50	0.34	0.31	0.34
NTM-97-17	2470	2475	1.22	0.74	1.93	8	0.04	54	0.45	0.36	0.35	0.29
NTM-97-18	2475	2480	1.31	0.63	2.18	3	0.05	34	0.48	0.36	0.35	0.29
NTM-97-19	2515	2520	1.16	0.62	2.02	7	0.02	80	0.49	0.35	0.35	0.30
NTM-97-20	2520	2525					0.15		0.50	0.34	0.31	0.34
NTM-97-21	2525	2530	1.06	0.58	1.84	9	0.03	68	0.49	0.36	0.33	0.30
NTM-97-22	2530	2535	1.08	0.73	1.40	22	0.05	102	0.51	0.39	0.30	0.31
NTM-97-24	2540	2545	1.17	0.66	1.76	24	0.05	119	0.45	0.34	0.33	0.33
NTM-97-25	2545	2550	1.06	0.63	1.76	17	0.06	67	0.44	0.36	0.31	0.32
NTM-97-26	2550	2555	1.16	0.85	1.98	43	0.10	98	0.45	0.39	0.30	0.31
NTM-97-27	2555	2560	1.12	0.68	1.69	29	0.05	146	0.47	0.35	0.33	0.32
MNV-12-47w	3965	3970	2.46	2.11	0.96	110	0.25	25	0.59	0.44	0.32	0.24
MNV-12-47m	3965	3970					0.18		0.55	0.44	0.34	0.21

Oil	Reservoir	20S / (20S+20R) αααC$_{29}$-Steranes	αββ/(αββ + ααα) C$_{29}$-Steranes	C$_{28}$ / C$_{29}$ Steranes	Hopanes	Ts / (Ts+Tm)	Hopane / Moretane	Oleanane Index	C$_{35}$ / (C$_{31}$-C$_{35}$) Hopanes	22S / (22S+22R) C$_{31}$-Hopanes
					[µg/g Oil]					
G-NTM-21	Eocene	0.48	0.46	0.92	639	0.51	7.16	0.20	0.06	0.58
G-NTM-59	Eocene	0.49	0.46	0.83	565	0.55	7.10	0.22	0.06	0.58
G-NTM-78	Oligocene	0.50	0.45	0.82	437	0.50	7.30	0.11	0.07	0.59
G-NTM-98	Eocene	0.51	0.49	0.86	629	0.59	7.77	0.22	0.06	0.59
G-MNV-12	Cretaceous	0.53	0.51	0.95	130	0.62	8.34	0.22	0.00	0.61

Extract	Top	Bottom	20S / (20S+20R) αααC$_{29}$-Steranes	αββ/(αββ + ααα) C$_{29}$-Steranes	C$_{28}$ / C$_{29}$ Steranes	Hopanes	Ts / (Ts+Tm)	Hopane / Moretane	Oleanane Index	C$_{35}$ / (C$_{31}$-C$_{35}$) Hopanes	22S / (22S+22R) C$_{31}$-Hopanes
	[m]	[m]				[µg/g TOC]					
NOR-72-146	4435	4440	0.47	0.43	0.56	204	0.67	8.18	0.09	0.00	0.60
NOR-72-149	4450	4455	0.29	0.29	0.68	86	0.62	7.21	0.11	0.00	0.55
NOR-72-157	4490	4495	0.62	0.36	0.59	468	0.73	10.00	0.05	0.00	0.56
NOR-72-166	4559	4562				0					
NOR-72-193	4826	4829				0					
NOR-72-197	4888	4891				0					
NTM-97-11	2440	2445	0.17	0.30	1.06	30	0.41	5.49	0.35	0.00	0.46
NTM-97-12	2445	2450	0.11	0.34	1.07	52	0.44	5.36	0.36	0.00	0.45
NTM-97-13	2450	2455	0.16	0.36	0.94	54	0.48	5.69	0.36	0.00	0.51
NTM-97-14	2455	2460	0.15	0.30	1.14	39	0.51	6.19	0.35	0.00	0.45
NTM-97-15	2460	2465	0.14	0.31	1.03	35	0.48	5.28	0.35	0.00	0.49
NTM-97-16	2465	2470	0.19	0.33	0.91	65	0.43	4.38	0.40	0.00	0.46
NTM-97-17	2470	2475	0.16	0.30	1.20	49	0.39	6.20	0.43	0.00	0.49
NTM-97-18	2475	2480	0.16	0.30	1.18	33	0.48	5.40	0.41	0.00	0.48
NTM-97-19	2515	2520	0.22	0.34	1.18	85	0.52	6.89	0.29	0.00	0.49
NTM-97-20	2520	2525	0.19	0.33	0.91		0.43	4.38		0.00	0.46
NTM-97-21	2525	2530	0.21	0.39	1.10	77	0.52	6.53	0.36	0.00	0.55
NTM-97-22	2530	2535	0.26	0.40	0.95	106	0.55	5.43	0.38	0.00	0.50
NTM-97-24	2540	2545	0.22	0.38	0.98	116	0.53	6.40	0.35	0.00	0.55
NTM-97-25	2545	2550	0.22	0.35	0.97	66	0.45	6.42	0.37	0.00	0.53
NTM-97-26	2550	2555	0.20	0.35	0.96	100	0.45	5.07	0.34	0.00	0.51
NTM-97-27	2555	2560	0.23	0.38	1.05	148	0.48	7.44	0.35	0.00	0.50
MNV-12-47w	3965	3970	0.36	0.41	1.33	26	0.44	5.62	0.17	0.00	0.49
MNV-12-47m	3965	3970	0.45	0.32	1.61		0.54	6.41		0.00	0.52

Oil	Reservoir	100 x (Tricycl. / (Tri- + Pentacycl.))	24:4 / 23:3 Terpanes	MN	DMN	TMN	MP	MPI-1	R$_c$	MDR	R$_c$ Type-I/II	DBT / P	TA	Steranes / Hopanes	Moretane Index
				[µg/g Oil]	[µg/g Oil]	[µg/g Oil]	[µg/g Oil]		[%]		[%]		[µg/g Oil]		
G-NTM-21	Eocene	15.19	1.57	4305	7915	4258	1455	0.61	0.77	4.13	0.81	0.11	136	0.75	0.14
G-NTM-59	Eocene	12.77	2.01	1543	4546	1712	721	0.62	0.77	3.99	0.80	0.10	70	0.69	0.14
G-NTM-78	Oligocene	8.31	1.61	423	855	569	190	0.60	0.76	3.51	0.77	0.13	51	0.45	0.14
G-NTM-98	Eocene	19.23	1.63	1757	3872	2250	939	0.72	0.83	4.53	0.85	0.11	48	0.78	0.13
G-MNV-12	Cretaceous	23.38	1.46	369	1419	1299	628	0.74	0.84	4.56	0.86	0.17	28	0.66	0.12

Extract	Top	Bottom	100 x (Tricycl. / (Tri- + Pentacycl.))	24:4 / 23:3 Terpanes	MN	DMN	TMN	MP	MPI-1	R$_c$	MDR	R$_c$ Type-I/II	DBT / P	TA	Steranes / Hopanes	Moretane Index
	[m]	[m]			[µg/g TOC]	[µg/g TOC]	[µg/g TOC]	[µg/g TOC]		[%]		[%]		[µg/g TOC]		
NOR-72-146	4435	4440	0.00		0	101	165	252	0.70	0.82	4.75	0.88	0.06	19	0.30	0.12
NOR-72-149	4450	4455	0.00		0	101	165	252	0.70	0.82	4.75	0.88	0.06	19	0.51	0.14
NOR-72-157	4490	4495	0.00		0	26	52	53	0.68	0.81	4.14	0.81	0.07	1	0.11	0.10
NOR-72-166	4559	4562							0.68	0.81	4.76	0.88	15.05			
NOR-72-193	4826	4829			0	872	1570	1129	0.75	0.85	3.47	0.77	0.08	2		
NOR-72-197	4888	4891			0	1362	2217	1404	0.63	0.78	3.57	0.77	0.09	3		
NTM-97-11	2440	2445	0.00		0	37	95	80	0.70	0.82	3.23	0.76	0.03	3	1.40	0.18
NTM-97-12	2445	2450	0.00		0	292	286	99	0.69	0.81	4.18	0.81	0.04	4	1.52	0.19
NTM-97-13	2450	2455	0.00		0	224	213	94	0.72	0.83	3.03	0.75	0.03	5	1.58	0.18
NTM-97-14	2455	2460	0.00		0	81	119	64	0.72	0.83	3.50	0.77	0.04	3	1.63	0.16
NTM-97-15	2460	2465	0.00		0	69	115	67	0.67	0.80	3.42	0.77	0.04	4	1.48	0.19
NTM-97-16	2465	2470	54.23	1.57	0	27	125	277	0.86	0.92	2.67	0.74	0.07	11	1.59	0.23
NTM-97-17	2470	2475	0.00		0	313	361	170	0.70	0.82	3.31	0.76	0.06	5	1.66	0.16
NTM-97-18	2475	2480	0.00		0	128	149	86	0.74	0.85	3.00	0.75	0.05	4	1.57	0.19
NTM-97-19	2515	2520	0.00		0	197	195	164	0.67	0.80	3.19	0.76	0.07	8	1.42	0.15
NTM-97-20	2520	2525		1.57	0	128	424	632	0.71	0.83	2.71	0.74	0.08	23	1.59	0.23
NTM-97-21	2525	2530	0.00		0	180	155	140	0.67	0.80	2.71	0.74	0.05	7	1.33	0.15
NTM-97-22	2530	2535	0.00		0	18	44	181	0.80	0.88	2.50	0.73	0.06	12	1.45	0.18
NTM-97-24	2540	2545	0.00		0	22	172	144	0.80	0.88	2.58	0.74	0.07	16	1.56	0.16
NTM-97-25	2545	2550	0		0	219	212	170	0.70	0.82	3.22	0.76	0.07	6	1.54	0.16
NTM-97-26	2550	2555	0.00		0	521	708	336	0.70	0.82	3.30	0.76	0.06	10	1.48	0.20
NTM-97-27	2555	2560	0.00		0	72	300	398	0.73	0.84	2.55	0.74	0.07	20	1.49	0.13
MNV-12-47w	3965	3970	0.00		0	51	209	297	0.81	0.89	4.39	0.84	0.04	2	1.43	0.18
MNV-12-47m	3965	3970							0.82	0.89	4.95	0.92	0.04		1.37	0.16

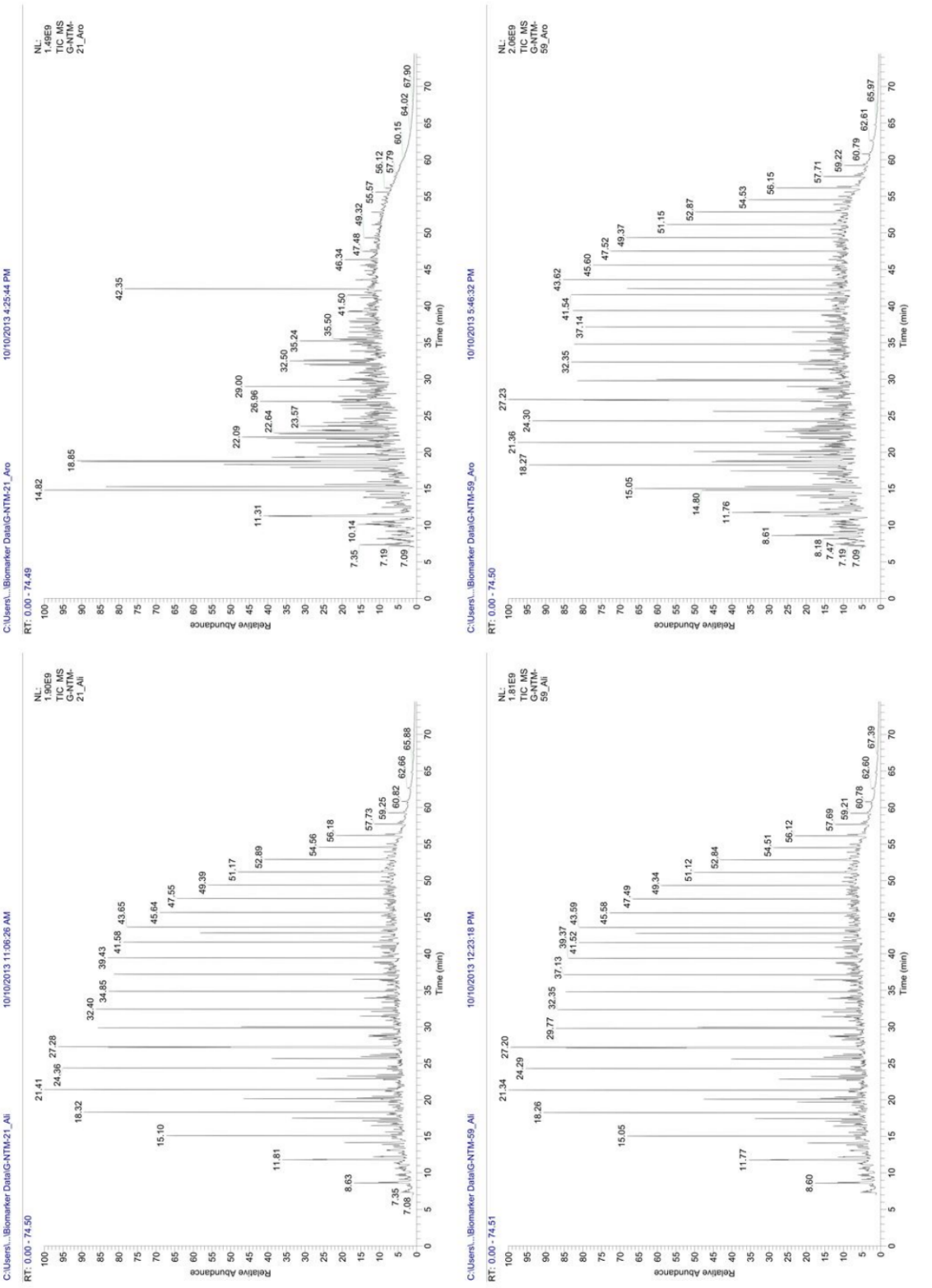
C:\Users\...\Biomarker Data\G-NTM-21_Aro
10/10/2013 4:25:44 PM
RT: 0.00 - 74.49
NL: 1.49E9 TIC MS G-NTM-21_Aro
Relative Abundance
Time (min)
C:\Users\...\Biomarker Data\G-NTM-59_Aro
10/10/2013 5:46:32 PM
RT: 0.00 - 74.50
NL: 2.06E9 TIC MS G-NTM-59_Aro
Relative Abundance
Time (min)
C:\Users\...\Biomarker Data\G-NTM-21_Ali
10/10/2013 11:06:26 AM
RT: 0.00 - 74.50
NL: 1.90E9 TIC MS G-NTM-21_Ali
Relative Abundance
Time (min)
C:\Users\...\Biomarker Data\G-NTM-59_Ali
10/10/2013 12:23:18 PM
RT: 0.00 - 74.51
NL: 1.81E9 TIC MS G-NTM-59_Ali
Relative Abundance
Time (min)

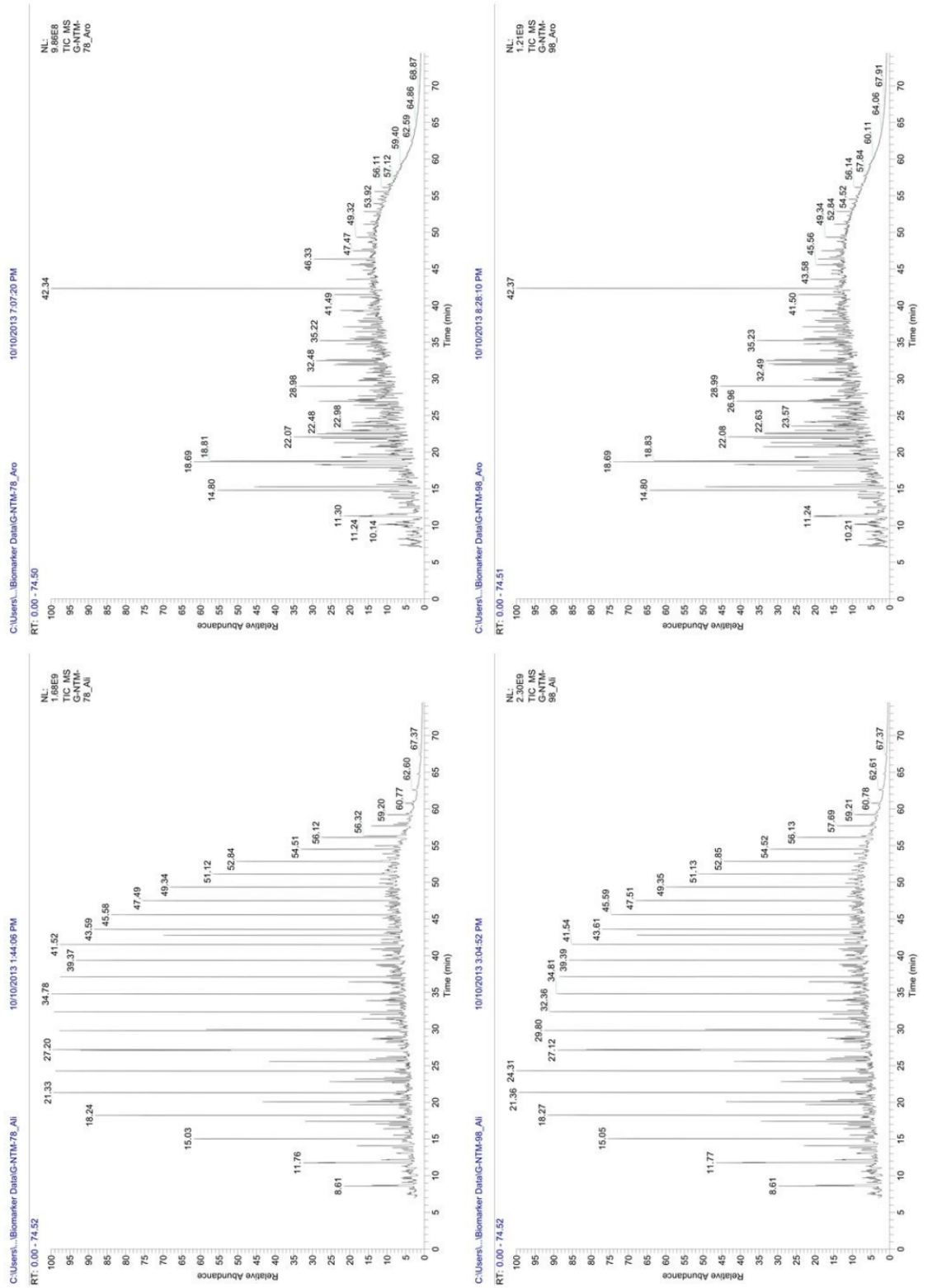
C:\Users\...\Biomarker Data\G-NTM-78_Ali
10/10/2013 11:44:06 PM
RT: 0.00 - 74.52
NL: 1.16E9 TIC MS G-NTM-78_Ali
C:\Users\...\Biomarker Data\G-NTM-78_Aro
10/10/2013 7:07:20 PM
RT: 0.00 - 74.50
NL: 9.66E8 TIC MS G-NTM-78_Aro
C:\Users\...\Biomarker Data\G-NTM-98_Ali
10/10/2013 3:04:52 PM
RT: 0.00 - 74.52
NL: 2.30E9 TIC MS G-NTM-98_Ali
C:\Users\...\Biomarker Data\G-NTM-98_Aro
10/10/2013 8:28:10 PM
RT: 0.00 - 74.51
NL: 1.21E9 TIC MS G-NTM-98_Aro
Relative Abundance
Time (min)

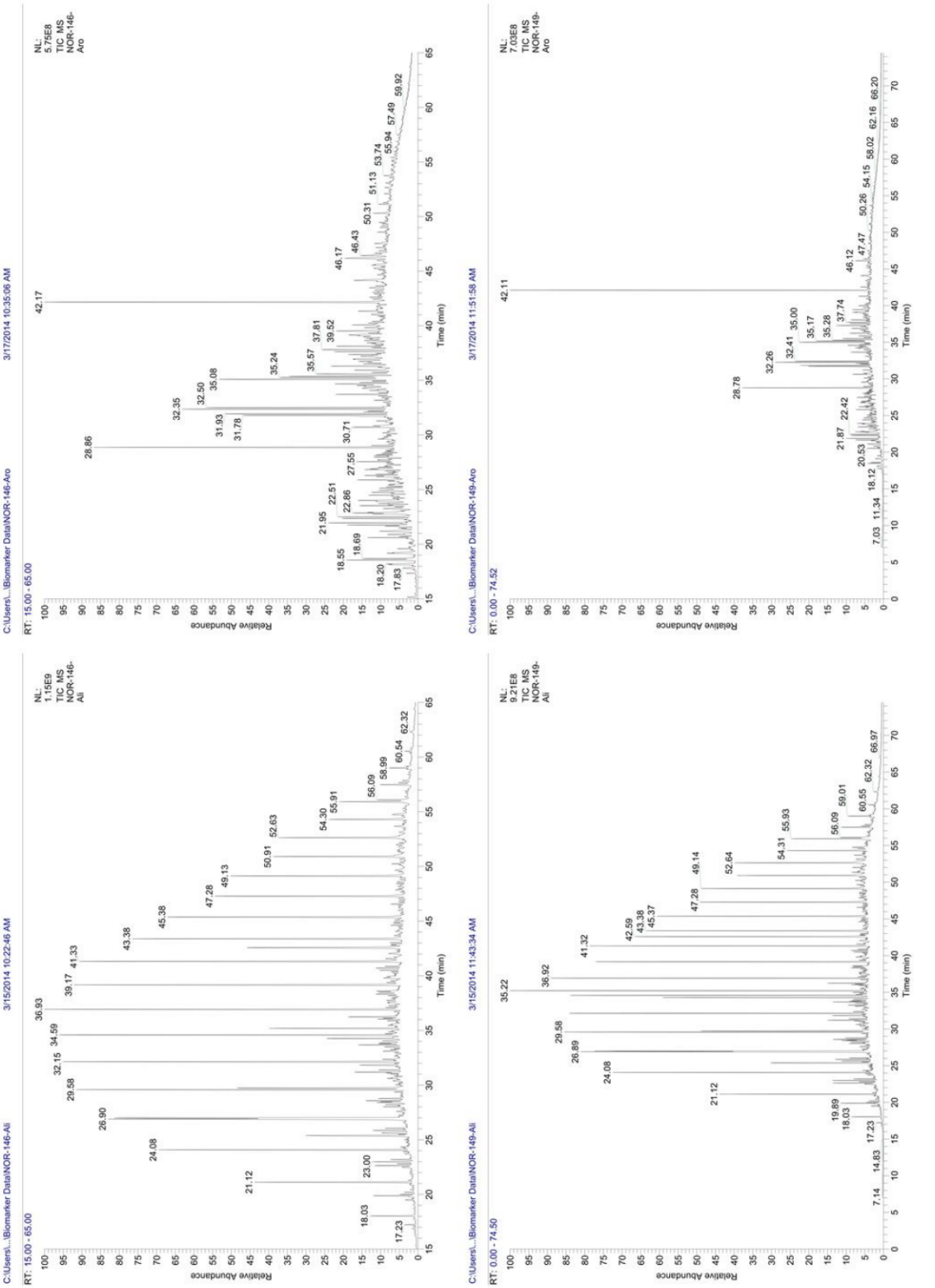
C:\Users\...\Biomarker Data\NOR-146-Ali
3/15/2014 10:22:46 AM
RT: 15.00 - 65.00
NL: 1.15E9 TIC MS NOR-146-Ali
Relative Abundance
Time (min)
C:\Users\...\Biomarker Data\NOR-146-Aro
3/17/2014 10:35:06 AM
RT: 15.00 - 65.00
NL: 5.75E8 TIC MS NOR-146-Aro
Relative Abundance
Time (min)
C:\Users\...\Biomarker Data\NOR-149-Ali
3/15/2014 11:43:34 AM
RT: 0.00 - 74.50
NL: 9.21E8 TIC MS NOR-149-Ali
Relative Abundance
Time (min)
C:\Users\...\Biomarker Data\NOR-149-Aro
3/17/2014 11:51:58 AM
RT: 0.00 - 74.52
NL: 7.03E8 TIC MS NOR-149-Aro
Relative Abundance
Time (min)

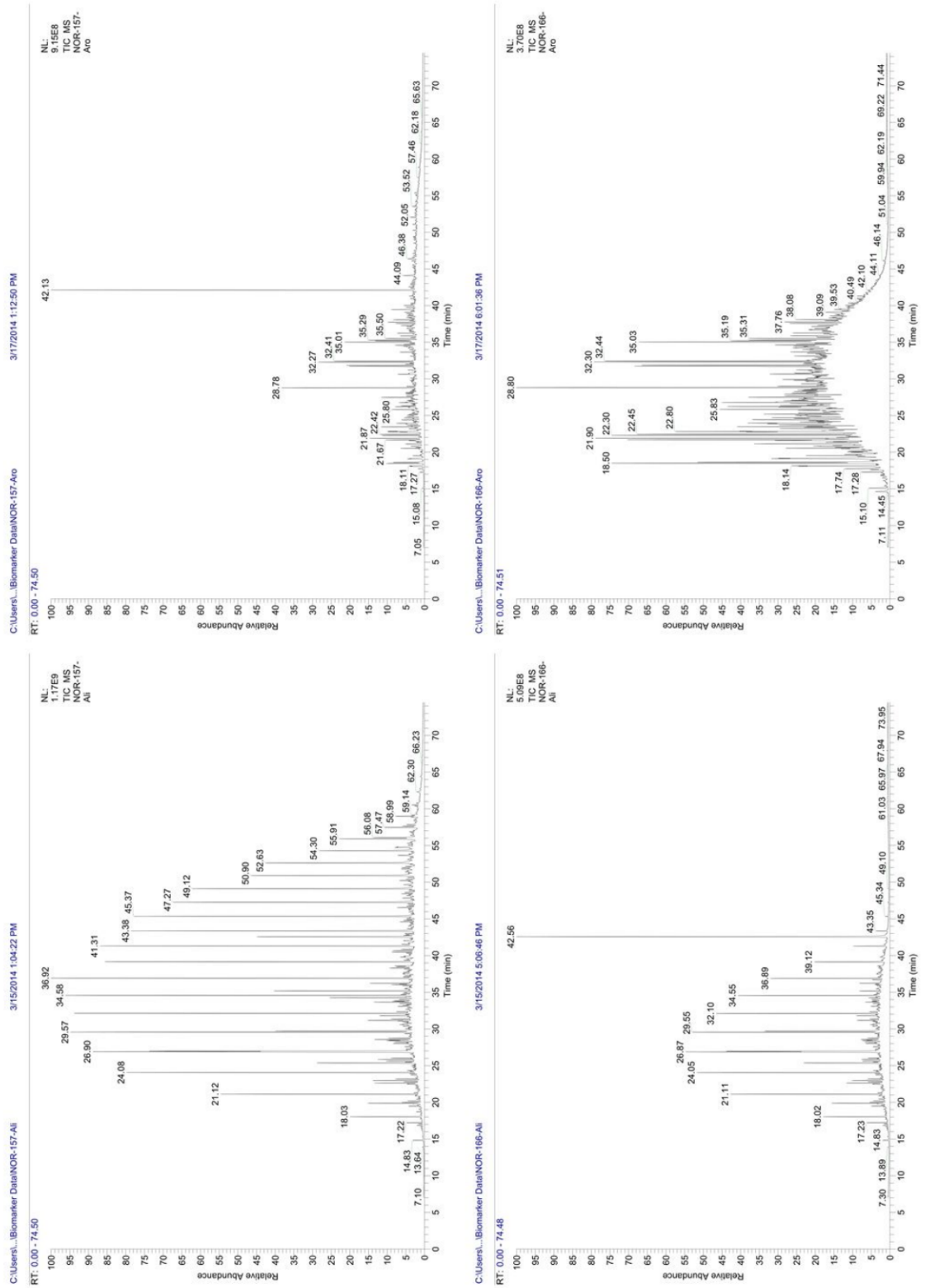
C:\Users\...\Biomarker Data\NOR-157-Aro
3/17/2014 1:12:50 PM
RT: 0.00 - 74.50
NL: 9.15E8 TIC MS NOR-157-Aro
Relative Abundance
Time (min)
C:\Users\...\Biomarker Data\NOR-166-Aro
3/17/2014 6:01:36 PM
RT: 0.00 - 74.51
NL: 3.70E8 TIC MS NOR-166-Aro
Relative Abundance
Time (min)
C:\Users\...\Biomarker Data\NOR-157-Ali
3/15/2014 1:04:22 PM
RT: 0.00 - 74.50
NL: 1.17E9 TIC MS NOR-157-Ali
Relative Abundance
Time (min)
C:\Users\...\Biomarker Data\NOR-166-Ali
3/15/2014 5:06:46 PM
RT: 0.00 - 74.48
NL: 5.09E8 TIC MS NOR-166-Ali
Relative Abundance
Time (min)

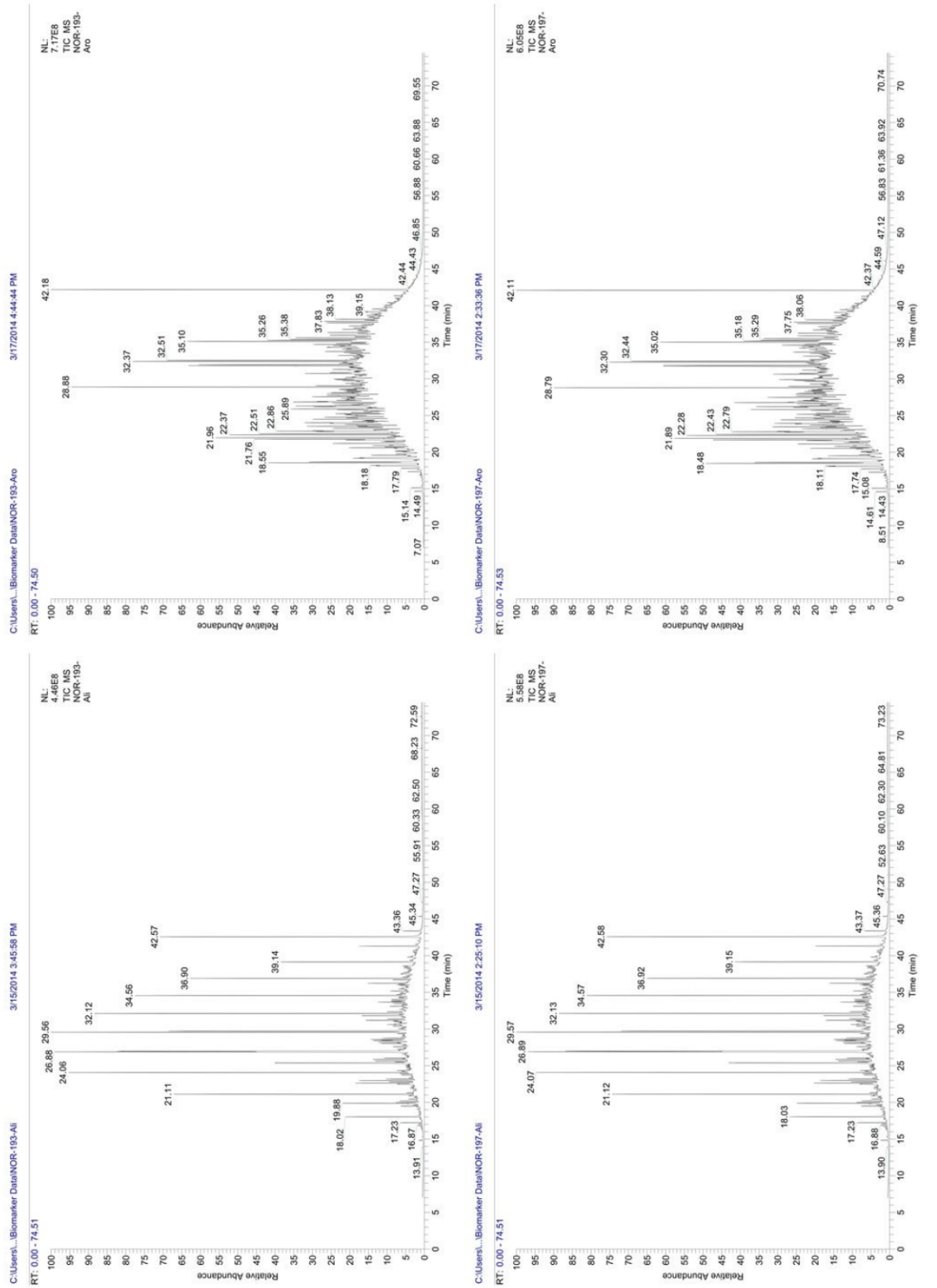
C:\Users\...\Biomarker Data\NOR-193-Ali
3/15/2014 3:45:58 PM
RT: 0.00 - 74.51
NL: 4.46E8 TIC MS NOR-193-Ali
Relative Abundance
Time (min)
C:\Users\...\Biomarker Data\NOR-193-Aro
3/17/2014 4:44:44 PM
RT: 0.00 - 74.50
NL: 7.17E8 TIC MS NOR-193-Aro
Relative Abundance
Time (min)
C:\Users\...\Biomarker Data\NOR-197-Ali
3/15/2014 2:25:10 PM
RT: 0.00 - 74.51
NL: 5.58E8 TIC MS NOR-197-Ali
Relative Abundance
Time (min)
C:\Users\...\Biomarker Data\NOR-197-Aro
3/17/2014 2:33:36 PM
RT: 0.00 - 74.53
NL: 6.05E8 TIC MS NOR-197-Aro
Relative Abundance
Time (min)

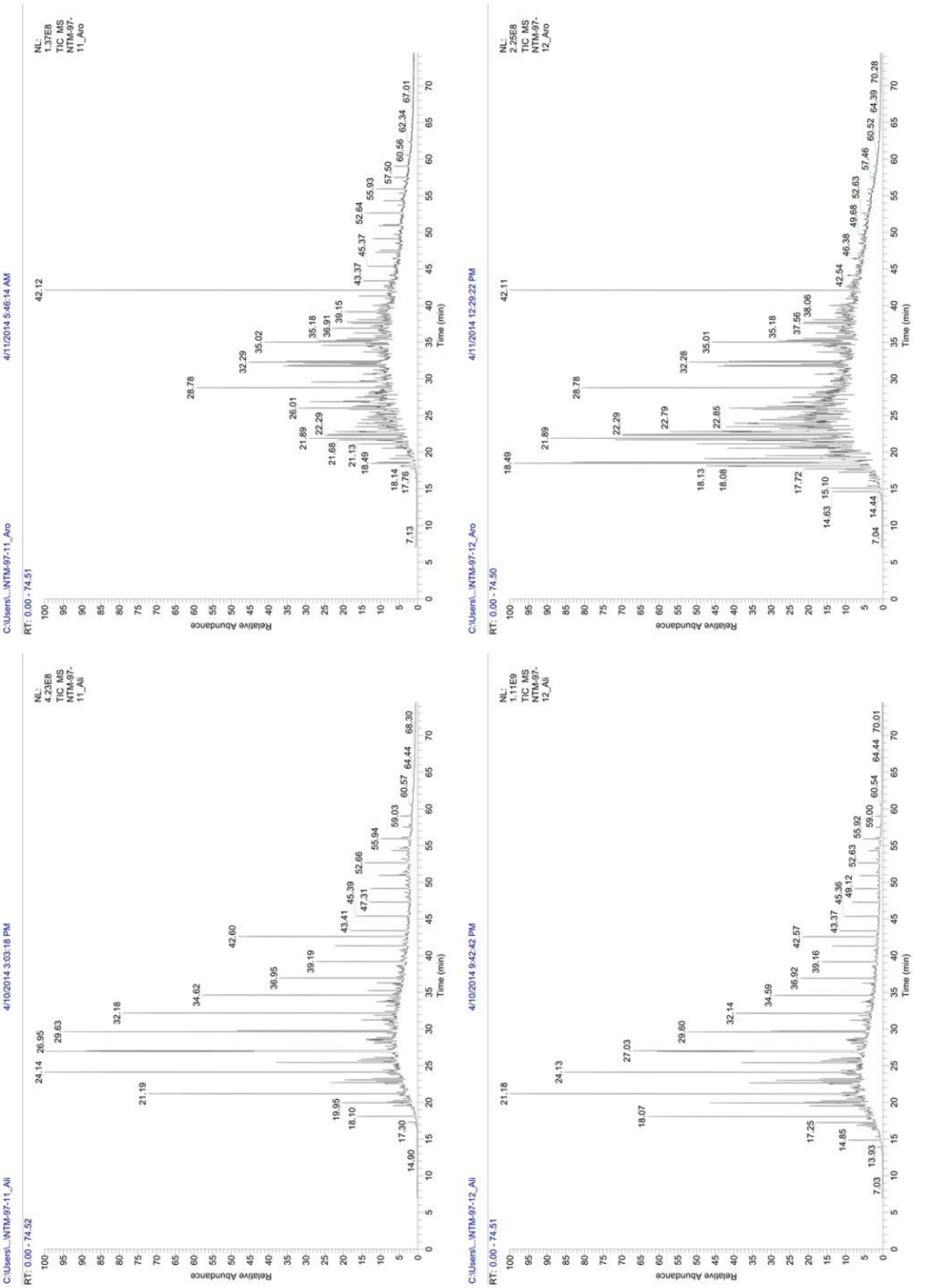
C:\Users\...\NTM-97-11_Aro
4/11/2014 5:46:14 AM
RT: 0.00 - 74.51
NL: 1.37E8 TIC MS NTM-97-11_Aro
Relative Abundance
Time (min)
C:\Users\...\NTM-97-12_Aro
4/11/2014 12:29:22 PM
RT: 0.00 - 74.50
NL: 2.25E8 TIC MS NTM-97-12_Aro
Relative Abundance
Time (min)
C:\Users\...\NTM-97-11_Ali
4/10/2014 3:03:18 PM
RT: 0.00 - 74.52
NL: 4.23E8 TIC MS NTM-97-11_Ali
Relative Abundance
Time (min)
C:\Users\...\NTM-97-12_Ali
4/10/2014 9:42:42 PM
RT: 0.00 - 74.51
NL: 1.11E9 TIC MS NTM-97-12_Ali
Relative Abundance
Time (min)

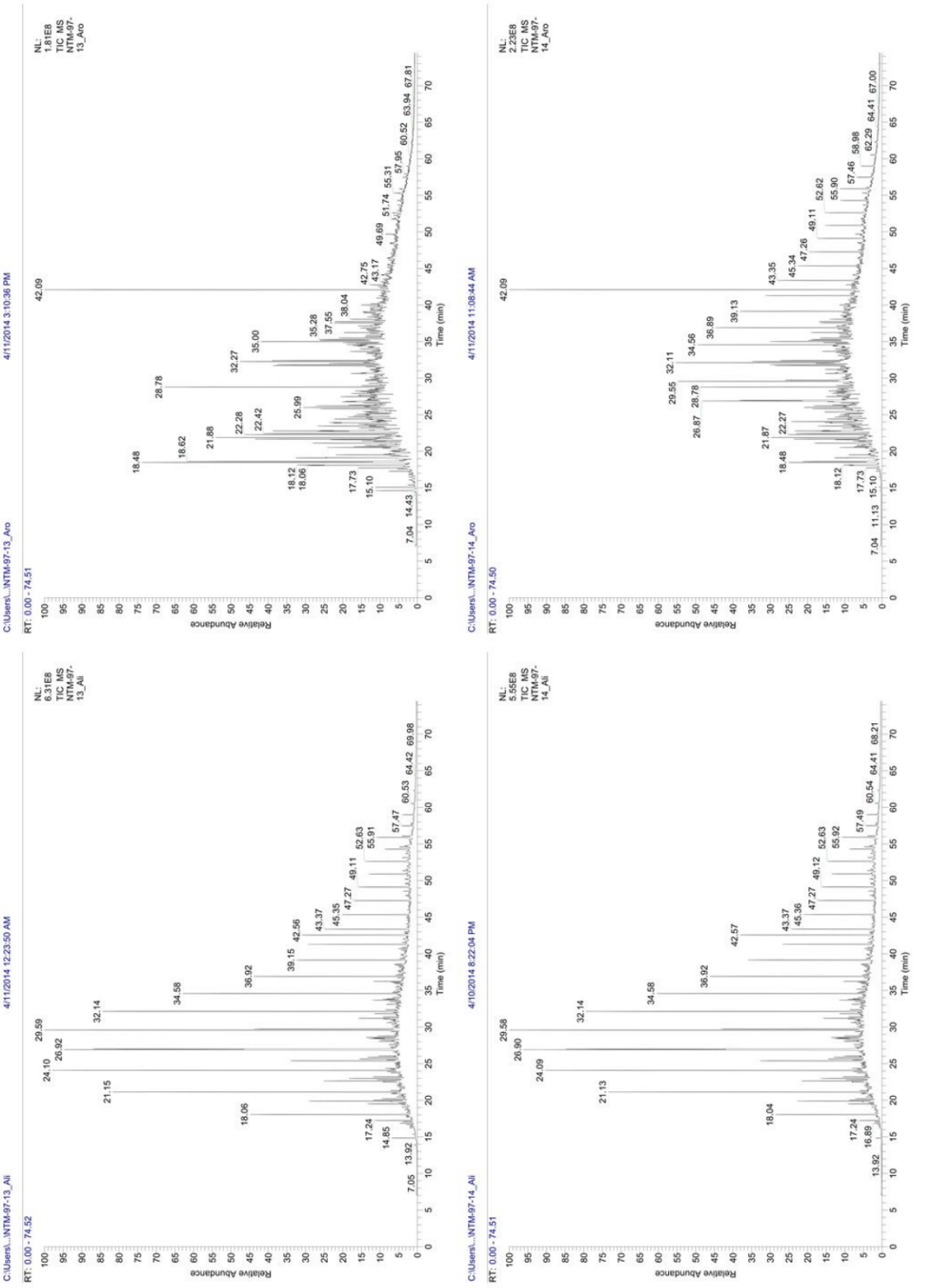
C:\Users\...\NTM-97-13_Ali
4/11/2014 12:23:50 AM
RT: 0.00 - 74.52
NL: 6.31E8 TIC MS NTM-97-13_Ali
C:\Users\...\NTM-97-13_Aro
4/11/2014 3:10:36 PM
RT: 0.00 - 74.51
NL: 1.51E8 TIC MS NTM-97-13_Aro
C:\Users\...\NTM-97-14_Ali
4/10/2014 8:22:04 PM
RT: 0.00 - 74.51
NL: 5.55E8 TIC MS NTM-97-14_Ali
C:\Users\...\NTM-97-14_Aro
4/11/2014 11:08:44 AM
RT: 0.00 - 74.50
NL: 2.23E8 TIC MS NTM-97-14_Aro
Relative Abundance
Time (min)

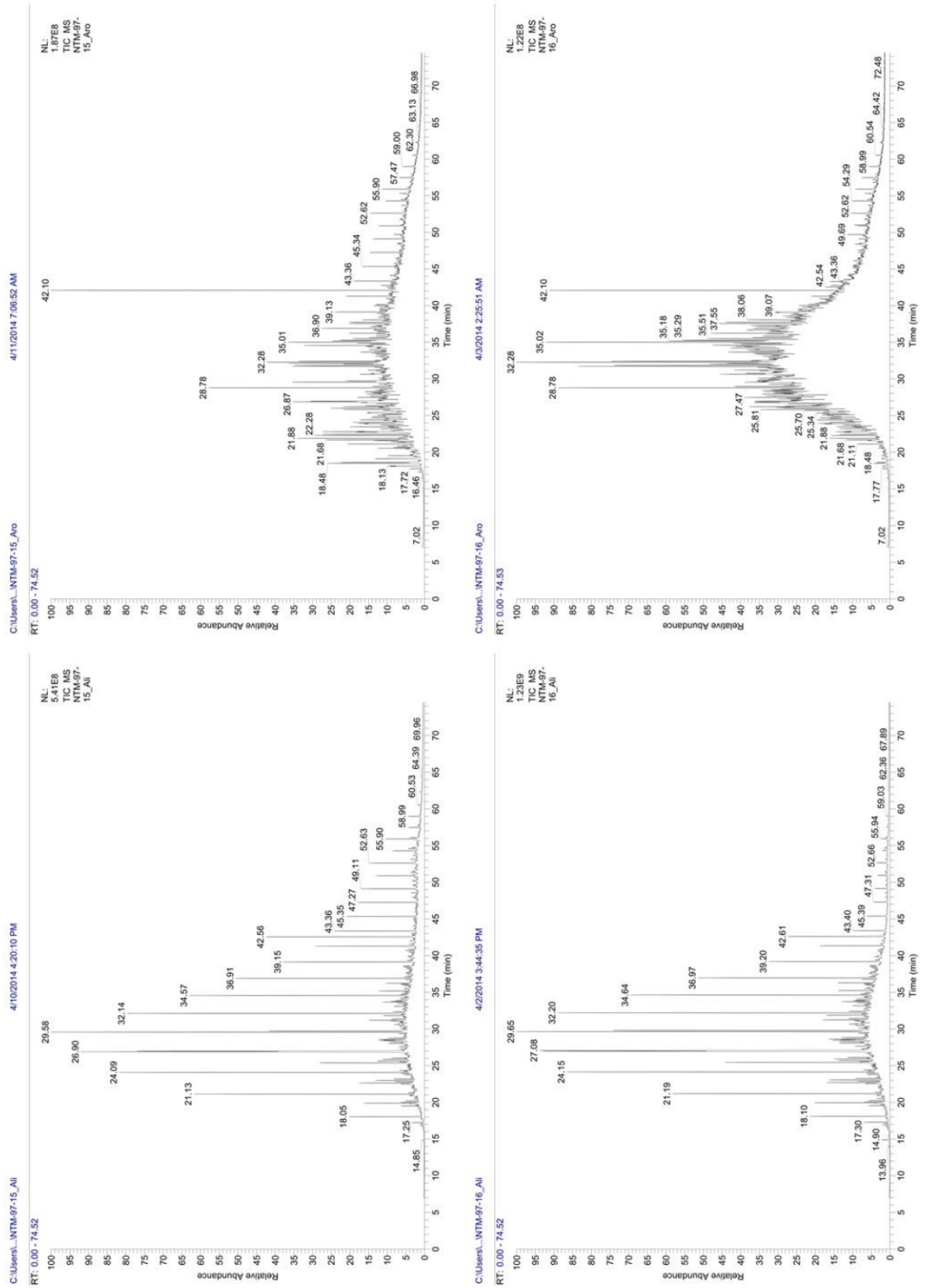
C:\Users\...\NTM-97-15_Ali
4/10/2014 4:20:10 PM
RT: 0.00 - 74.52
NL: 5.41E8 TIC MS NTM-97-15_Ali
C:\Users\...\NTM-97-15_Aro
4/11/2014 7:06:52 AM
RT: 0.00 - 74.52
NL: 1.87E8 TIC MS NTM-97-15_Aro
C:\Users\...\NTM-97-16_Ali
4/2/2014 3:44:35 PM
RT: 0.00 - 74.52
NL: 1.23E9 TIC MS NTM-97-16_Ali
C:\Users\...\NTM-97-16_Aro
4/3/2014 2:25:51 AM
RT: 0.00 - 74.53
NL: 1.22E8 TIC MS NTM-97-16_Aro
Relative Abundance
Time (min)

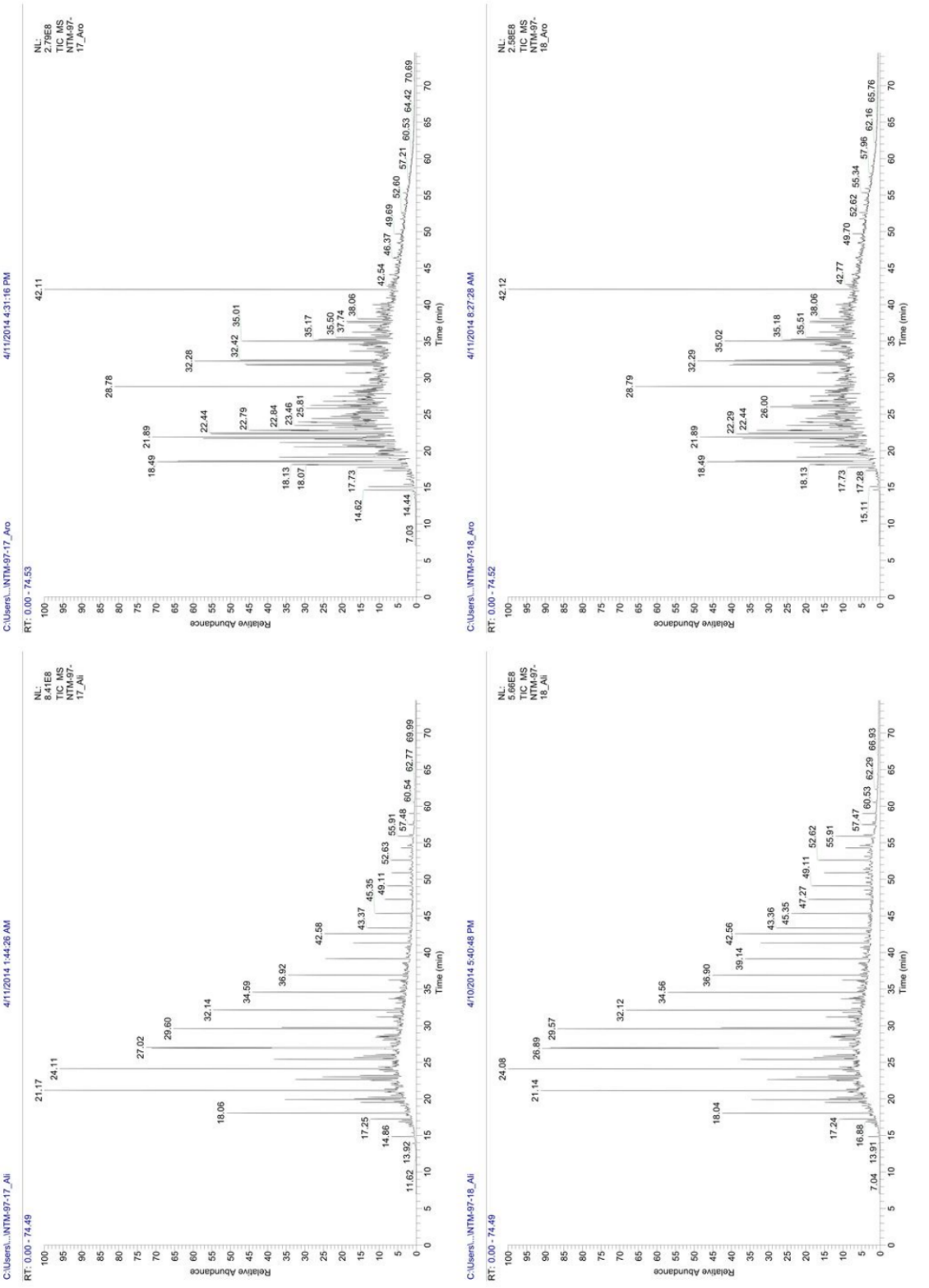
C:\Users\...\NTM-97-17_Ali
4/11/2014 1:44:26 AM
RT: 0.00 - 74.49
NL: 8.41E8 TIC MS NTM-97-17_Ali
C:\Users\...\NTM-97-17_Aro
4/11/2014 4:31:16 PM
RT: 0.00 - 74.53
NL: 2.79E8 TIC MS NTM-97-17_Aro
C:\Users\...\NTM-97-18_Ali
4/10/2014 5:40:48 PM
RT: 0.00 - 74.49
NL: 5.66E8 TIC MS NTM-97-18_Ali
C:\Users\...\NTM-97-18_Aro
4/11/2014 8:27:28 AM
RT: 0.00 - 74.52
NL: 2.58E8 TIC MS NTM-97-18_Aro
Relative Abundance
Time (min)

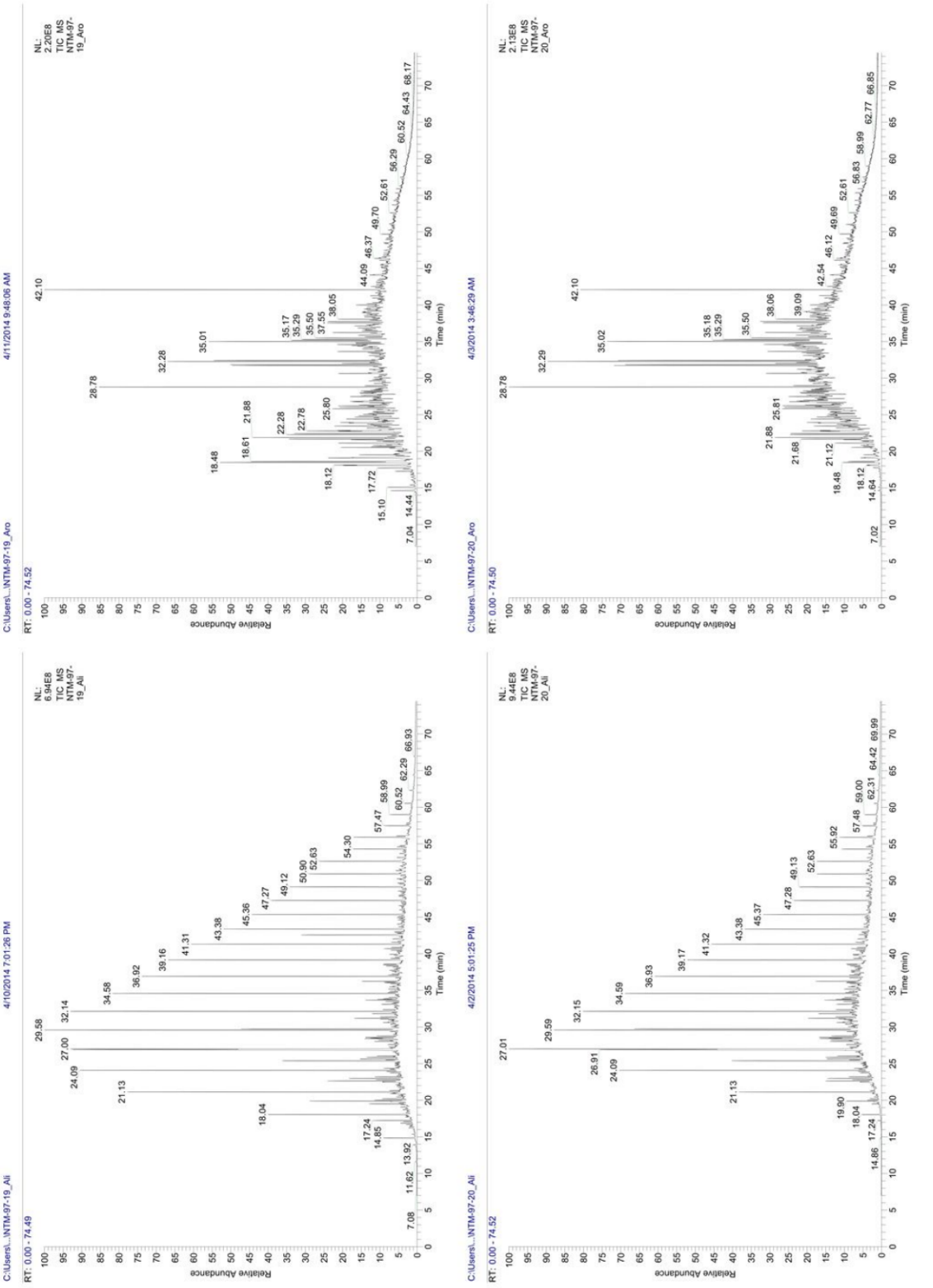
C:\Users\...\NTM-97-19_Ali
4/10/2014 7:01:26 PM
RT: 0.00 - 74.49
NL: 6.94E8 TIC MS NTM-97-19_Ali
Relative Abundance
Time (min)
C:\Users\...\NTM-97-19_Aro
4/11/2014 9:48:06 AM
RT: 0.00 - 74.52
NL: 2.20E8 TIC MS NTM-97-19_Aro
Relative Abundance
Time (min)
C:\Users\...\NTM-97-20_Ali
4/2/2014 5:01:25 PM
RT: 0.00 - 74.52
NL: 9.44E8 TIC MS NTM-97-20_Ali
Relative Abundance
Time (min)
C:\Users\...\NTM-97-20_Aro
4/3/2014 3:46:29 AM
RT: 0.00 - 74.50
NL: 2.13E8 TIC MS NTM-97-20_Aro
Relative Abundance
Time (min)

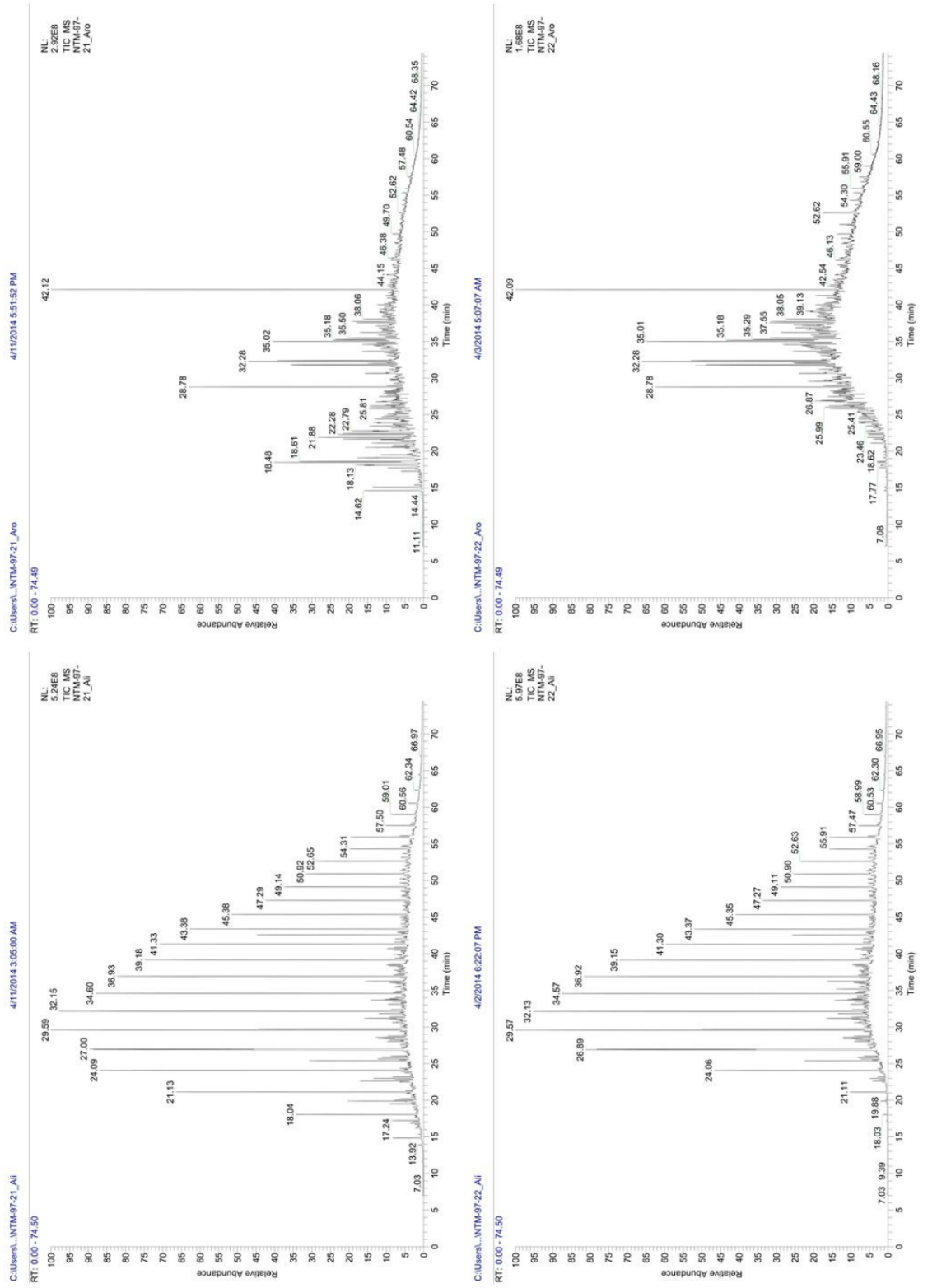
C:\Users\...\NTM-97-21_Ali
4/11/2014 3:05:00 AM
RT: 0.00 - 74.50
NL: 5.24E8 TIC MS NTM-97-21_Ali
C:\Users\...\NTM-97-21_Aro
4/11/2014 5:51:52 PM
RT: 0.00 - 74.49
NL: 2.92E8 TIC MS NTM-97-21_Aro
C:\Users\...\NTM-97-22_Ali
4/2/2014 6:22:07 PM
RT: 0.00 - 74.50
NL: 5.97E8 TIC MS NTM-97-22_Ali
C:\Users\...\NTM-97-22_Aro
4/3/2014 5:07:07 AM
RT: 0.00 - 74.49
NL: 1.68E8 TIC MS NTM-97-22_Aro
Relative Abundance
Time (min)

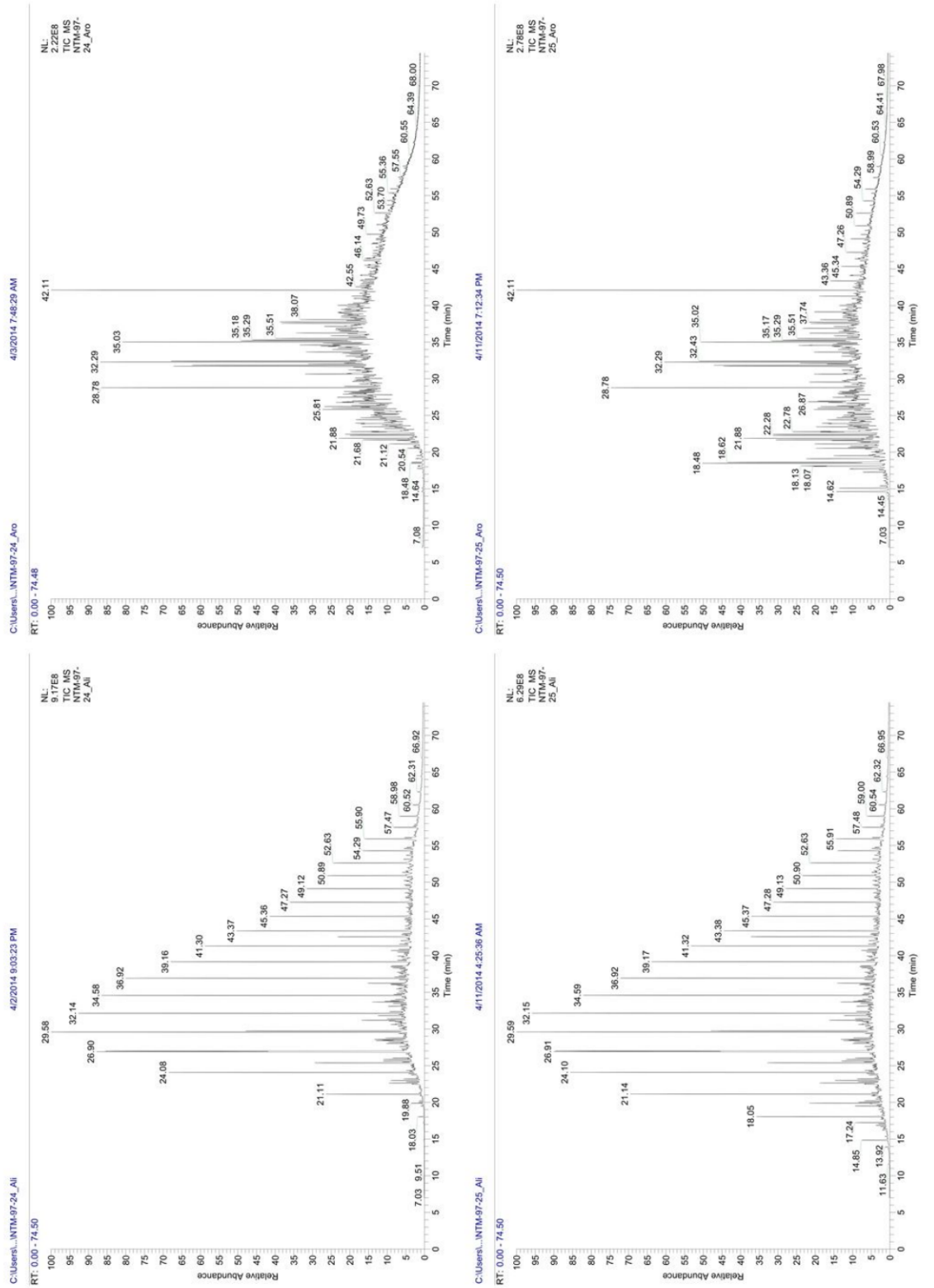
C:\Users\...\NTM-97-24_Ali
4/2/2014 9:03:23 PM
RT: 0.00 - 74.50
NL: 9.17E8 TIC MS NTM-97-24_Ali
C:\Users\...\NTM-97-24_Aro
4/3/2014 7:48:29 AM
RT: 0.00 - 74.48
NL: 2.72E8 TIC MS NTM-97-24_Aro
C:\Users\...\NTM-97-25_Ali
4/11/2014 4:25:36 AM
RT: 0.00 - 74.50
NL: 6.29E8 TIC MS NTM-97-25_Ali
C:\Users\...\NTM-97-25_Aro
4/11/2014 7:12:34 PM
RT: 0.00 - 74.50
NL: 2.78E8 TIC MS NTM-97-25_Aro
Relative Abundance
Time (min)

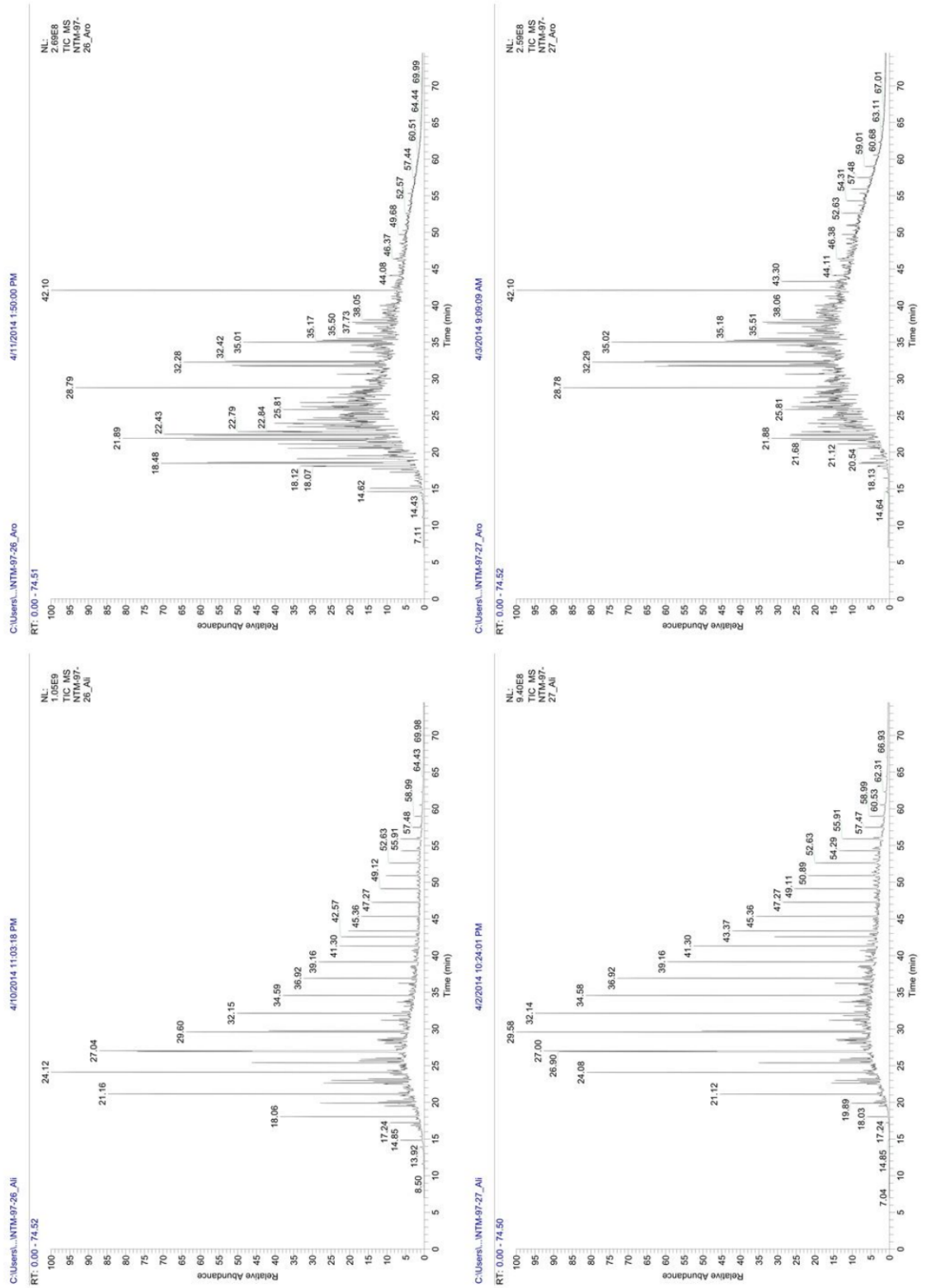
C:\Users\...\NTM-97-26_Ali
4/10/2014 11:03:18 PM
RT: 0.00 - 74.52
NL: 1.10E9 TIC MS NTM-97-26_Ali
C:\Users\...\NTM-97-26_Aro
4/11/2014 1:50:00 PM
RT: 0.00 - 74.51
NL: 2.66E8 TIC MS NTM-97-26_Aro
C:\Users\...\NTM-97-27_Ali
4/2/2014 10:24:01 PM
RT: 0.00 - 74.50
NL: 9.40E8 TIC MS NTM-97-27_Ali
C:\Users\...\NTM-97-27_Aro
4/3/2014 9:09:09 AM
RT: 0.00 - 74.52
NL: 2.59E8 TIC MS NTM-97-27_Aro
Relative Abundance
Time (min)

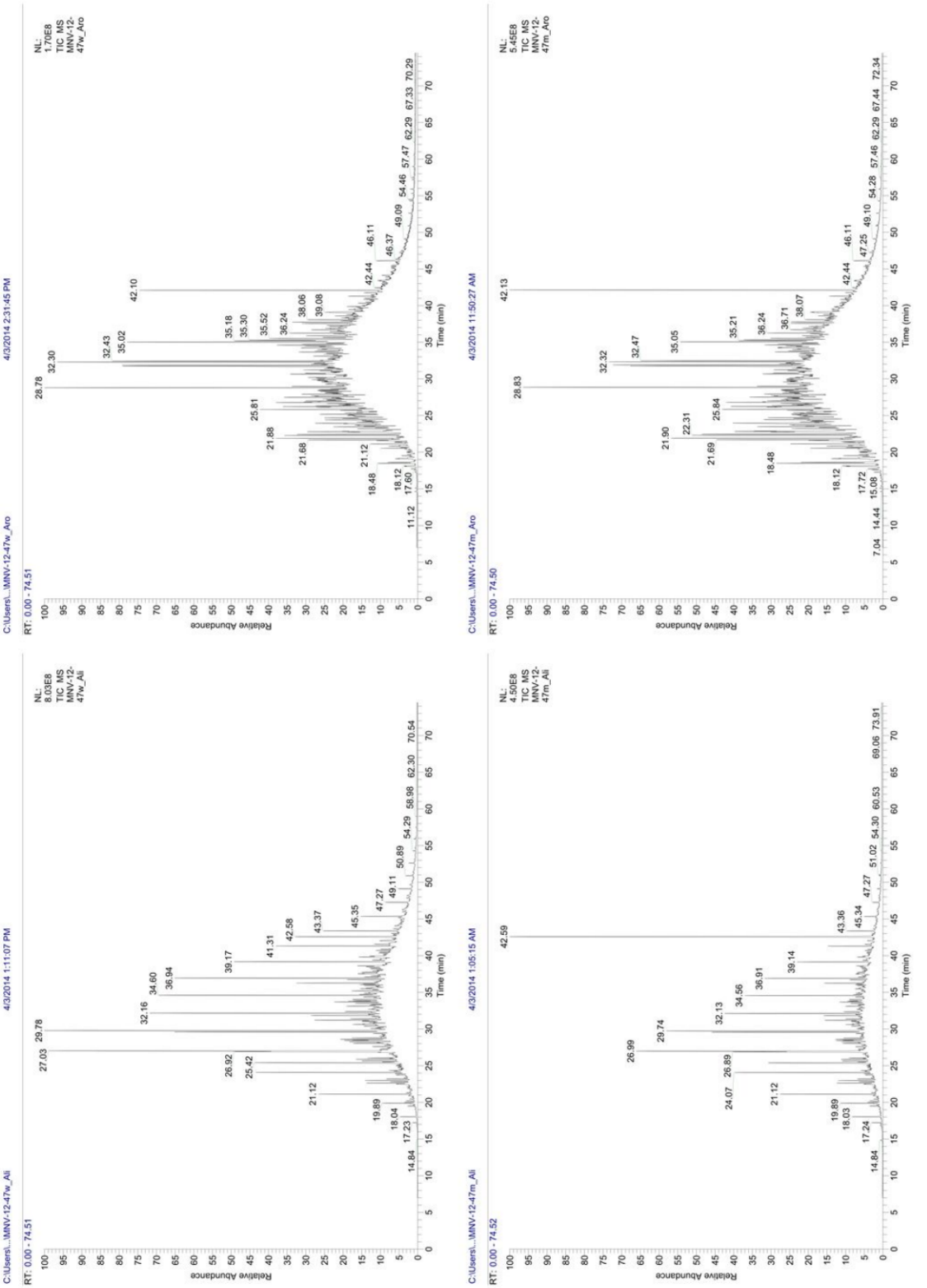
C:\Users\...\MNV-12-47w_Ali
4/3/2014 1:11:07 PM
RT: 0.00 - 74.51
NL: 8.03E8 TIC MS MNV-12-47w_Ali
C:\Users\...\MNV-12-47w_Aro
4/3/2014 2:31:45 PM
RT: 0.00 - 74.51
NL: 1.70E8 TIC MS MNV-12-47w_Aro
C:\Users\...\MNV-12-47m_Ali
4/3/2014 1:05:15 AM
RT: 0.00 - 74.52
NL: 4.50E8 TIC MS MNV-12-47m_Ali
C:\Users\...\MNV-12-47m_Aro
4/3/2014 11:50:27 AM
RT: 0.00 - 74.50
NL: 5.45E8 TIC MS MNV-12-47m_Aro
Relative Abundance
Time (min)

G-MNV-12 = Oel-Georgien

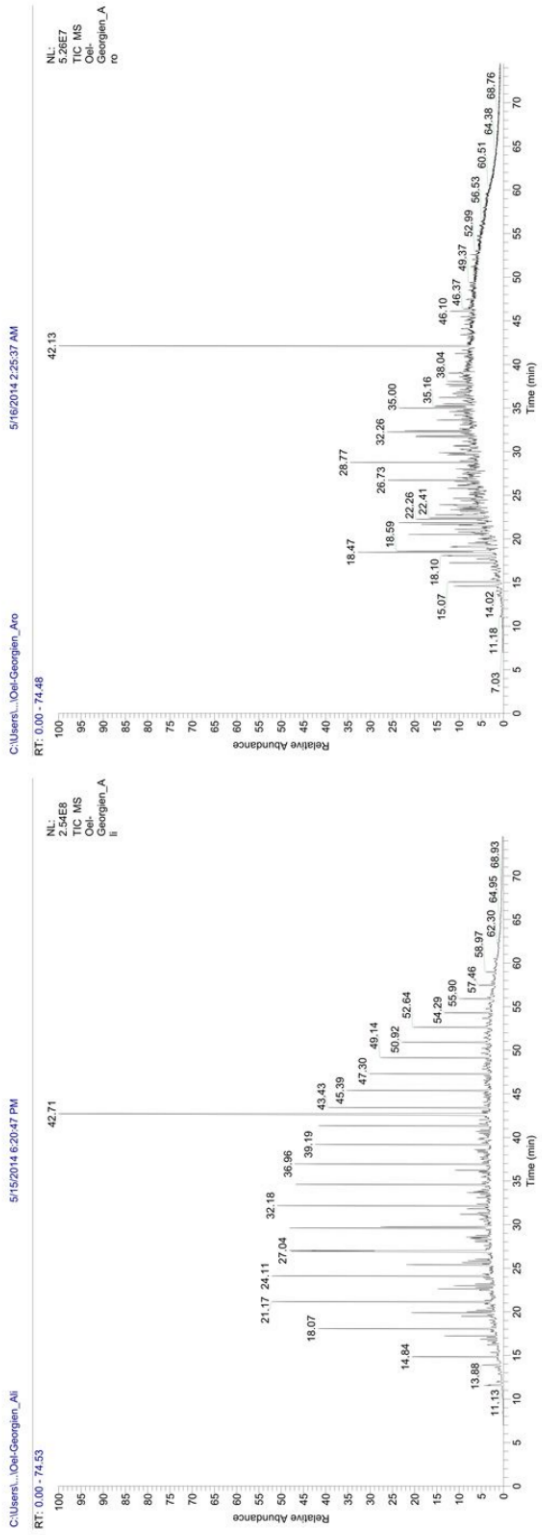

Appendix G: Carbonate Isotopy

Sample	Depth [m]	d18O/16O	Std. Dev.	d13C/12C	Std. Dev.
NOR-72-1	3625	-5.61	0.11	-5.00	0.06
NOR-72-4	3710	-7.18	0.07	-5.47	0.03
NOR-72-10	3745	-2.83	0.12	-15.61	0.04
NOR-72-16	3775	-8.25	0.08	-12.31	0.05
NOR-72-28	3835	-5.03	0.13	-1.75	0.08
NOR-72-44	3915	-5.26	0.11	-1.89	0.11
NOR-72-94	4165	-10.71	0.05	-5.80	0.09
NOR-72-107	4235	-4.96	0.15	-2.05	0.06
NOR-72-139	4400	-2.71	0.19	7.85	0.04
NOR-72-140	4405	-6.30	0.14	-1.93	0.10
NOR-72-143	4420	-6.10	0.12	2.56	0.07
NOR-72-146	4435	-5.86	0.14	-3.12	0.12
NOR-72-149	4450	-5.77	0.20	-1.76	0.09
NOR-72-157	4490	-4.58	0.37	1.08	0.06
NTM-97-3	2340	-4.55	0.06	-1.51	0.07
NTM-97-5	2350	-4.75	0.06	-0.90	0.07
NTM-97-7	2360	-4.96	0.07	-1.63	0.07
NTM-97-9	2370	-5.17	0.10	-0.99	0.06
NTM-97-10	2375	-4.95	0.11	-0.58	0.07
NTM-97-11	2440	-3.83	0.11	-7.34	0.07
NTM-97-12	2445	-3.99	0.17	-7.82	0.08
NTM-97-14	2455	-3.52	0.11	-3.77	0.06
NTM-97-16	2465	-3.71	0.16	-5.19	0.13
NTM-97-17	2470	-3.86	0.11	-6.69	0.09
NTM-97-18	2475	-4.14	0.13	-5.29	0.07
NTM-97-19	2515	-3.98	0.08	-0.13	0.08
NTM-97-21	2525	-4.62	0.11	-0.77	0.07
NTM-97-22	2530	-5.13	0.08	-0.86	0.05
NTM-97-24	2540	-5.61	0.07	-0.61	0.06
NTM-97-25	2545	-4.79	0.10	-0.02	0.03
NTM-97-26	2550	-4.83	0.16	-0.09	0.09
NTM-97-27	2555	-5.69	0.06	-0.69	0.07

Appendix H: 1-D Thermal Maturity Model Input

Input parameters, water depth and sediment-water-interface temperature trends

Name	Top	Base	Present Thickness	Eroded	Deposition Age from	Deposition Age to	Erosion Age from	Erosion Age to	Lithology
	m	m	m	m	Ma	Ma	Ma	Ma	Ma
Norio-72									
Miocene	0	3600	3600	500 / 0	23.30	5.30	5.30	0.00	SANDshaly
Upper Oligocene	3600	3790	190		28.10	23.30			SHALEsand
Lower Oligocene	3790	4500	710		33.90	28.10			SHALEsand
Upper Eocene	4500	4870	370		37.80	33.90			SHALEsand
Middle Eocene	4870	5020	150		40.00	37.80			Andesite
Ninotsminda-97									
Miocene	0	1460	1460	2000 / 800	23.30	5.30	5.30	0.00	SANDshaly
Upper Oligocene	1460	1650	190		28.10	23.30			SHALEsand
Lower Oligocene	1650	2360	710		33.90	28.10			SHALEsand
Upper Eocene	2360	2730	370		37.80	33.90			SHALEsand
Middle Eocene	2730	2880	150		40.00	37.80			Andesite

Age	Water Depth	SWI Temp.
m	Ma	°C
0.00	0	15.00
7.00	100	13.07
200.00	200	20.42

Physical properties assigned to lithotypes used for simulations

	Density	Initial Porosity	Min. Porosity	Compressibility Max	Compressibility Min	Thermal Conduct. at 20°C	Thermal Conduct. at 100°C	Heat Capacity at 20°C	Heat Capacity at 100°C	Permeability 5%por	Permeability 75%por	Permeability Sandst. Mod.	Permeability Multi-point M. key	Specific Surface Area	Scaling Factor	Anisotropy Factor Perm.	Anisotropy Factor Therm.Cond.
	kg/m³			(1E-7/kPa)		(W/m/K)		(kcal/kg/K)		(log mD)		(log mD)				(log)	unitless
SHALEsand	2674.0	0.57	0.05	9000.0	10	2.32	2.12	0.205	0.248	-4.50	0.00	0.00	none	1.00E+08	1	2.20	1.40
SANDshaly	2666.0	0.48	0.05	1400.0	10	2.78	2.37	0.190	0.226	-1.00	7.00	-4.00	PermSand4	1.00E+08	1	1.30	1.30
Andesite	x	x	x	x	x	3.20	2.90	0.20	0.22	x	x	x	x	x	x	x	x

Assumption:
Constant heat flow